NORTHWESTERN UNIVERSITY

Engineering bilayer membranes for nano- and microscale sensing

A DISSERTATION

SUBMITTED TO THE GRADUATE SCHOOL
IN PARTIAL FULFILLMENT OF THE REQUIREMENTS

for the degree

DOCTOR OF PHILOSOPHY

Field of Biomedical Engineering

By

Margrethe A. Boyd

EVANSTON, ILLINOIS

June 2022

ABSTRACT

Engineering bilayer membranes for nano- and microscale sensing

Margrethe A. Boyd

In environments ranging from natural ecosystems to living organisms, small molecule signals and nanoscale forces communicate important information regarding chemical contamination and pollution, pathogenesis, and physical stressors. As these stimuli are often well below detection limits for our own senses, we depend on biosensing technologies to monitor them. Many biosensors operate through direct molecular interactions with a target analyte, which can be sensitive to off-target molecules or to dilution and matrix effects in environmental or biological samples. Other stimuli, particularly mechanical forces, remain extremely difficult to monitor without highly specialized equipment. As a result, our ability to reliably and accurately detect biologically and technologically important signals in many contexts remains limited.

One way to introduce additional sensing features to these systems is to reintroduce a key component of many cellular biosensing mechanisms: the bilayer membrane. As the primary barrier between a cell and its environment, the membrane plays a critical role in signal transduction and information transfer, force response, and protection and containment of intracellular components. Membranes offer a unique sensing platform in that they can incorporate both hydrophobic, membrane-localized sensors as well as encapsulated aqueous sensors. Similarly, as bio-inspired structures, they can incorporate a range of naturally and synthetically derived components, ranging from amphiphiles to protein transporters, which can introduce additional functionality to the sensor as a whole.

In this dissertation, I discuss how synthetic membranes can be engineered to advance approaches to biosensing. I first focus on the development of membrane-based sensors for

mechanical force, exploring an optical method to monitor stretch and lipid uptake in a population of nanoscale sensors in response to a changing external environment. I then establish three approaches to lipid vesicle-based sensing with encapsulated aqueous sensors; I design these vesicle sensors with increasing complexity, encapsulating a chemical ion indicator, a transcription-based sensor, and a cell-free protein expression-based sensor. First, I establish a vesicle-based nanosensor for potassium ions. By encapsulating a fluorescent indicator for potassium, I show that dye encapsulation and incorporation of an ion-specific membrane transporter can improve specificity to an ion of interest and allow detection in the presence of live bacteria. Building upon this system, I next incorporate a transcription-based sensor which transcribes an RNA aptamer in the presence of magnesium. I incorporate nonspecific pores into the membrane and demonstrate that both pore concentration and the presence of the target molecule modulate sensor output. Finally, I encapsulate a cell-free protein expression-based sensor for a biologically important analyte, fluoride. I demonstrate function of the encapsulated riboswitch sensor and show how membrane composition can be changed to modulate sensitivity to externally added fluoride ions. I then deploy these sensors in real-world samples and demonstrate detection of fluoride in complex environments.

Through the incorporation of a variety of sensing strategies, this work highlights the ways in which synthetic membranes can be introduced and engineered to enhance sensing capabilities. These sensing strategies ultimately result in tradeoffs between sensitivity, specificity, and stability and allow the incorporation of a wide variety of sensor types, enabling the detection of both chemical and physical signals in new contexts.

ACKNOWLEDGEMENTS

I would not be writing this thesis if it weren't for many wonderful people in my life who helped me reach this point. To those of you who inspired my interest in science, who encouraged me to push beyond what I thought possible, and who supported me through every up and down of this chapter of my life, I share this accomplishment with you.

First and foremost, thank you to my advisor, Professor Neha Kamat, for serving as an incredible mentor during my time in graduate school. I have truly appreciated the amount of time, energy and thought that you have put into mentorship, and I am honored to have been one of the first few graduate students in the Kamat Lab. The way that you have led the lab, maintaining high expectations but with an incredible amount of empathy and kindness, has served as a model that I will forever take with me.

To the members of the Kamat Lab, past and present, thank you for helping me to become the scientist and the person I am today. To my undergraduates, Anna and Nora, thank you for your eagerness in lab and your patience in helping me learn how to be a better mentor.

To my thesis committee, Professors Julius Lucks, John Marko and Hao Zhang, thank you for your guidance and feedback throughout this journey. I truly appreciate the thoughtful input from each of you, and the culmination of this work is all the greater for it. To the many wonderful collaborators I have had the privilege of working with, thank you for sharing your expertise and enthusiasm on some incredibly cool projects.

Thank you to my undergraduate mentors, Dr. Matthew Herron and Dr. David Macaluso, for believing in me and for encouraging me early on in my scientific journey. You inspired my interest in research, helped me grow my scientific curiosity, and gave me incredible

opportunities to be a part of the broader scientific community, for which I am truly grateful. I would not have reached this point without your support and encouragement.

I have tried many times to come up with the words to adequately thank the friends and family who have been my rock during this journey, and I find that I always come up short. As such (and since I know I've told you all in person many times), I will keep this brief. To the friends, near and far, I cannot thank you enough for your kindness, your seemingly endless support, and most importantly for the incredible fun we've had over the years. You have made this experience for me, and it has been so wonderful being part of your journeys as well. A special thank you to Madi, who has been not only a best friend but a second sister to me. I am endlessly thankful for your love and kindness.

Thank you to my parents, who not only inspired my interest in science, but who taught me perseverance, resilience, and unconditional love - who have unwaveringly been my biggest supporters from day one. To my sister, one of the smartest, funniest people I know, who has taught me to live life to the fullest and who has never failed to both build me up and keep me grounded at the same time. To the Kinsey family, who have welcomed me with open arms.

Most importantly, thank you to Michael. Thank you for being the first to celebrate my successes, no matter how small, and the first to be there after the hard days along the way. Thank you for promising that I could do it until I finally believed it myself. For all the moments, large and small, and for those yet to come.

LIST OF ABBREVIATIONS

αHL	Alpha-hemolysin pore
1.05k	PEO_9-b-PBD_{12}
1.8k	PEO_{14}-b-PBD_{22}
3.5k	PEO_{24}-b-PBD_{46}
3OC6HSL	N-(3-oxo-hexanoyl)-L-homoserine lactone
AHL	Acylated Homoserine Lactone
aTc	Anhydrotetracycline
BDNF	Brain-derived neurotropic factor
BSA	Bovine Serum Albumin
C23DO	Catechol (2,3)-dioxygenase
CFPS	Cell-free Protein Synthesis
Chol	Cholesterol
CMC	Critical micelle concentration
COVID 19	Coronavirus disease 2019 (SARS-CoV-2)
Cy 5.5 PE	1,2-dioleoyl-sn-glycero-3-phosphoethanolamine-N-(Cyanine 5.5)
Cy 7 PE	1,2-dioleoyl-sn-glycero-3-phosphoethanolamine-N-(Cyanine 7)
DAPG	2,4-Diacetylphloroglucinol
DIC	Differential Interference Contrast
DLS	Dynamic Light Scattering
DMPC	1,2-dimyristoyl-sn-glycero-3-phosphocholine
DMSO	Dimethylsulfoxide

DOPC	1,2-dioleoyl-sn-glycero-3-phosphocholine
DOPE	1,2-dioleoyl-sn-glycero-3-phosphoethanolamine
DOPG	1,2-dioleoyl-sn-glycero-3-phospho-(1'-rac-glycerol)
DPhPG	1,2-diphytanoyl-sn-glycero-3-phosphocholine
Egg PC	L-α-phosphatidylcholine
FRET	Förster Resonance Energy Transfer
GUV	Giant unilamellar vesicle
HF	Hydrofluoric Acid
HPTS	8-Hydroxypyrene-1,3,6-trisulfonic acid trisodium salt
IPTG	Isopropyl β-D-1-thiogalactopyranoside
Laurdan GP	Laurdan Generalized Polarization
Liss-Rho PE	18:1 1,2-dioleoyl-sn-glycero-3-phosphoethanoamine-N-(lissamine rhodamine B sufonyl) (ammonium salt)
MilliQ	MilliQ Ultrapure Water
mRNA	Messenger RNA
MscL	Mechanosensitive Channel of Large Conductance
NBD PE	NBD-phosphoethanolamine, triethylammonium salt
NTPs	Nucleoside Triphosphates
OA	Oleic Acid
OA647	Ovalbumin-conjugated Alexafluor 647
PBFI	Potassium-binding benzofuran isophthalate
PBS	Phosphate-buffered Saline

PC	Phosphatidylcholine
PEG	Poly(ethylene glycol)
PEO-b-PBD	Poly(ethylene oxide)-b-poly(butadiene)
PFO	Perfringolysin O
POPC	1-palmitoyl-2-oleoyl-glycero-3-phosphocholine
SEC	Size Exclusion Chromatography
sfGFP	Superfolder green fluorescent protein
SNARE Protein	SNAP Receptor protein
SUV	Small unilamellar vesicle
TetR-mCherry	Fusion protein of TetR and mCherry fluorescent protein
TetR-sfGFP	Fusion protein of tetracycline repressor (TetR) and sfGFP

TABLE OF CONTENTS

LIST OF FIGURES

LIST OF TABLES

Chapter 1: Introduction

1.1 The bilayer membrane

Spatial segregation is a cornerstone feature of life.[1,2] The basic unit of life, the cell, is delineated spatially by a bilayer membrane composed primarily of lipids and proteins.[2-4] This membrane is the gate through which information enters and exits the cell, the enclosure within which vital cellular components are retained, and the dynamic envelope through which the cell can grow, divide, and migrate.[1,5-7] While the cellular membrane has long been recognized for its critical role as a cellular container, many mechanisms have been discovered by which the membrane itself can play a role in the regulation of cellular behavior and in the cell's ability to sense it's environment.[1-3,5-11] Many of these membrane features can be recapitulated in model membrane systems outside of a cellular context, allowing membrane properties – particularly the powerful ability control information transfer and molecular transport – to be harnessed for technological applications. These bio-inspired membranes can interface with or mimic biological systems, generate a chassis for aqueous cargo, and harness biological components like membrane proteins and transporters.[12] With a growing understanding of the importance of membranes in a biological context and an expanding body of research toward strategies to engineer model membranes for technological uses, bilayer membranes can ultimately serve as a powerful tool for the development of new platforms which allow us to tune environments on a molecular scale.

1.2 Biological membranes

At their most basic, bilayer membranes serve as a biological structure responsible for the spatial segregation of aqueous compartments.[2,4] In cells, these structures play a major role in retaining, protecting, and segregating molecular machinery, including nucleic acids and proteins, while creating a selectively permeable interface through which a cell can communicate with the surrounding environment. Through the incorporation of different types of amphiphiles, including phospholipids, fatty acids and amphiphilic proteins, cells tailor their membranes structurally and biophysically to meet specific needs – whether regulated by lipid packing, membrane strength, or spatial localization of biological molecules (**Figure 1.1**).[2,4,13,14] In addition, membranes are flexible and constantly evolving, with monomers that can move, insert and leave;[15] this allows membranes to respond to insult and to facilitate budding, tubulation, fission and fusion – processes which underly key cellular functions such as endo- and exocytosis, cellular division, and adaptation to changing environmental stressors.[14,15] A critical structure which delineates and modulates the cellular boundary, the bilayer membrane plays key roles in cellular communication, growth and division, and, ultimately, in cell survival.

While well known for its spatially segregating features, the cellular membrane has a significant role beyond that of a container for the cellular milieu: it serves as a major gate through which information enters and exits the cell. As the primary boundary delineating the cell from the surrounding environment, the membrane is the first barrier through which many physical and chemical signals are encountered.[4] Membranes can fuse to endocytose intra- or extracellularly-derived, cargo-carrying compartments, can transport and maintain gradients of molecular targets through the incorporation of specific membrane proteins, and can even generate specific regions that localize proteins and other biomolecules to serve as an organizer

for signaling systems or serve as signaling elements themselves.[13,14] The semipermeability, amphiphilicity and structural organization of the membrane facilitate these features,[4] allowing the cell to probe its environment and respond accordingly.

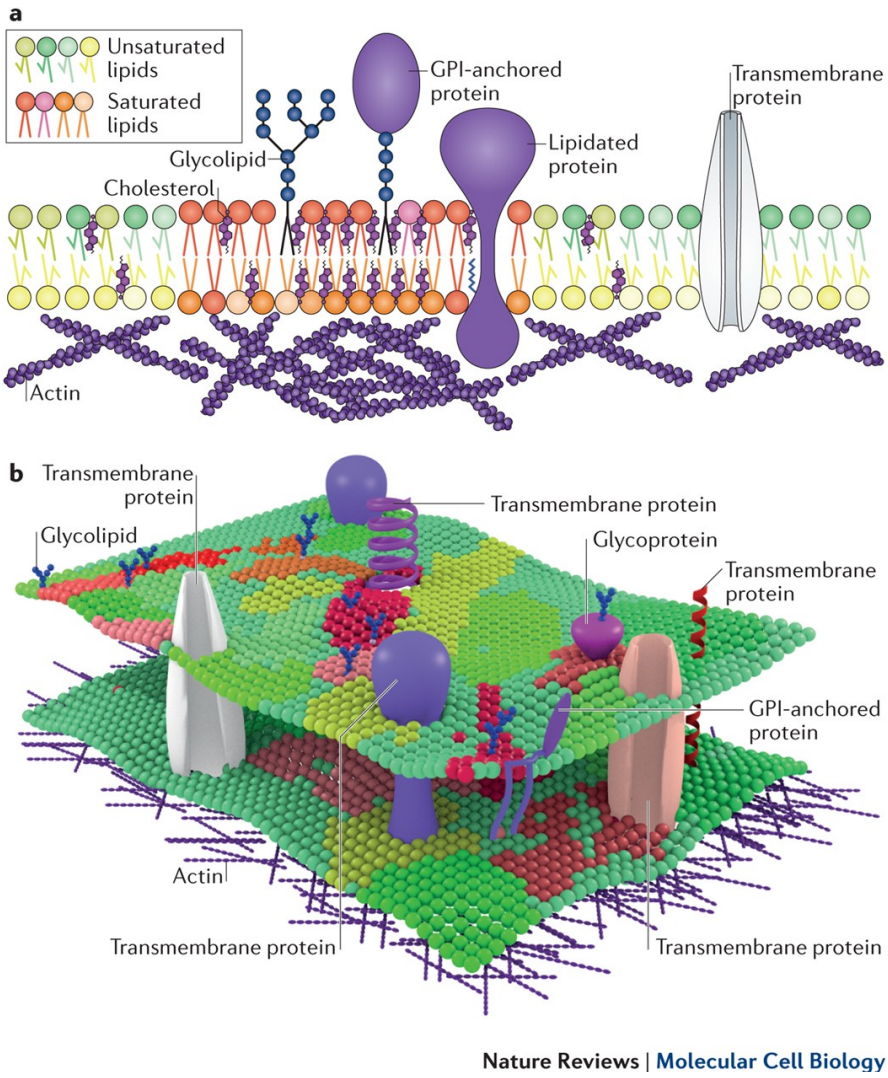

Figure 1.1 Biological membrane organization. A. Biological membranes are composed of a dynamic mixture of saturated and unsaturated phospholipids, sterols, associated proteins and cytoskeletal contacts. These components organize laterally into domains, which form regions of specific physical properties based on their lipid, sterol and protein composition. **B.** Lateral complexity is maintained in three-dimensions, with specific lipids and proteins localizing to form

regions with varying physical and biochemical properties. Reprinted, with permission, from reference [13].

In order to regulate the interface between the cell and its environment, biological membranes are complex, dynamic structures.[14,16] This feature allows a wide range of physical and biochemical properties to arise from membrane composition alone, but also makes the membrane particularly difficult to define and characterize.[13] Membrane composition varies between cell type - and even between organelles within a single cell - and can change dramatically as forces and biochemical processes act upon the membrane.[15] Lateral organization within a single membrane can arise and dissipate on short timescales, and lipid homeostasis can be regulated biochemically to modulate membrane properties in response to changing external conditions.[13,15] Due to the intricacies of membrane biophysics and biochemistry in biological systems, membranes have been extracted from a cellular context to generate model systems which recapitulate certain features of cellular membranes in a more defined system.[17] These model membranes provide a platform which can be harnessed to not only better understand biological systems but to engineer membranes for new applications.

1.3 Model membranes harness membrane features for engineered uses

1.3.1 Forming model membranes

In contrast to the complex structures that are cellular membranes, model membranes are bio-inspired structures in which a limited number of amphiphiles are assembled into higher order morphologies from scratch in a laboratory setting.[17] They consist of a much smaller subset of amphiphilic components and are generated through the principles of self-assembly by mixing

amphiphilic molecules in aqueous solution.[18] Assembly of model membranes in a laboratory can often be achieved using relatively straightforward methods and various techniques can be used to control features of the final lipid structure, for example to encapsulate molecular cargo or to form membranes of various sizes or lamellarity.[17,19] Membranes can be formed into different types of assemblies, including supported lipid bilayers,[20] black lipid membranes,[21] and lipid or polymer vesicles,[19] which exhibit distinct structural and compositional features. These platforms can then be used to probe different features of the membrane, ranging from mechanical robustness to protein insertion and activity.[17,20-22] By taking advantage of the ability of amphiphiles to self-assemble and by incorporating methods to manipulate their final structure and properties, model membranes provide a simplified method by which we can explore the processes of assembly and ultimately engineer membranes to exhibit specific characteristics.

1.3.2 Using model membranes to understand biological membranes

Once formed, model membranes have a wide variety of uses. One important application of model membranes is to isolate properties of biological membranes. Although the exact composition of cellular membranes varies between cell type, membrane location, and specific membrane function, there are certain amphiphiles that are generally present in high abundance in biological membranes.[2,13,15] Phospholipids and cholesterol are two types of amphiphilic molecules that make up a large portion of many cellular membranes,[2] and as such they are often incorporated into model membranes.[13] Certain structural and biophysical features of biological membranes can be recapitulated in these model systems by combining different types of phospholipids with varying amounts of cholesterol, providing a simplified platform with which to probe the biophysical properties of the membrane itself.[17] In particular, it can be difficult to

isolate changes within the bilayer from the effect of other cellular processes, as the presence and activity of structural components such as cytoskeletal adhesions and membrane proteins can make it nearly impossible to distinguish the response of the bilayer itself.[13] Model membranes eliminate many of these confounding variables by allowing a high degree of control over membrane composition and by removing non-membranous cellular components. Although the precise composition of cellular membranes remains difficult to attain in these model systems,[2] incorporation of a simplified version can offer a sufficient platform to probe many of the properties of the membrane in the absence of cellular effects.

Model systems allow us to explore features of naturally derived membranes, however they can also allow us to go beyond what is possible in biological systems by introducing synthetic amphiphiles. In particular, diblock and triblock co-polymers with hydrophobic and hydrophilic segments have been of significant interest in model membrane systems.[23-25] Polymers can impart new properties onto the membrane, such as increased elasticity and reduced permeability,[25] and can also be used to improve technologically relevant features such as biocompatibility and circulation time.[23,24,26] Polymers and other synthetic amphiphiles can offer a unique opportunity to engineer membrane features as they can be chemically synthesized to contain different segment lengths, segment chemistries, and numbers of segments.[27,28] These polymers can subsequently be incorporated into lipid and cholesterol bilayers to form hybrid membranes which exhibit some of the advantageous features of each, integrating the ability of biological amphiphiles to interact with membrane proteins with the increased robustness and biocompatibility of polymer components.[24] Model systems can therefore be a powerful platform with which we can engineer and explore membrane behaviors beyond what is found in nature.

1.3.3 Technological applications of model membranes

Due to their tunability and biocompatibility, model membranes have proven to be a useful platform for the development of nanoscale technologies. One field in which this has been especially important is in cargo delivery for medical applications. Liposomes, or lipid vesicles, have been of particular interest for these applications as they can transport both lipophilic and aqueous molecules either within the membrane or the vesicle lumen, respectively.[29] Liposomes have provided a biomimetic scaffold which can improve the solubility of drugs, prevent degradation and rapid clearance of cargo, prolong release, target to specified locations, and provide an additional mechanism of cellular uptake (**Figure 1.2**).[29,30] The membrane can be engineered to not only carry drug molecules through the body but to modulate interactions with cells, creating "stealth particles" with favorable pharmacokinetics.[30] These types of liposomal platforms have led to notable successes; one well-known example of this type of therapeutic is the liposomal formulation of Doxil, a chemotherapy agent consisting of the drug doxorubicin encapsulated within a PEGylated liposome. Encapsulation resulted in fewer side effects than the free-drug form and showed improved efficacy in the treatment of sarcoma, ovarian cancer, breast cancer and multiple myeloma.[31] More recently, the incredible success of the mRNA-based COVID-19 vaccines has highlighted the power of lipid-nanoparticle-based cargo delivery to address emerging global health concerns.[32] Based on the demonstrated feasibility of this type of lipid-based nucleic acid vaccine, it is likely that future efforts to develop membrane-based delivery platforms will continue to expand, focusing on diversifying the targets for this type of therapy to address a range of diseases.

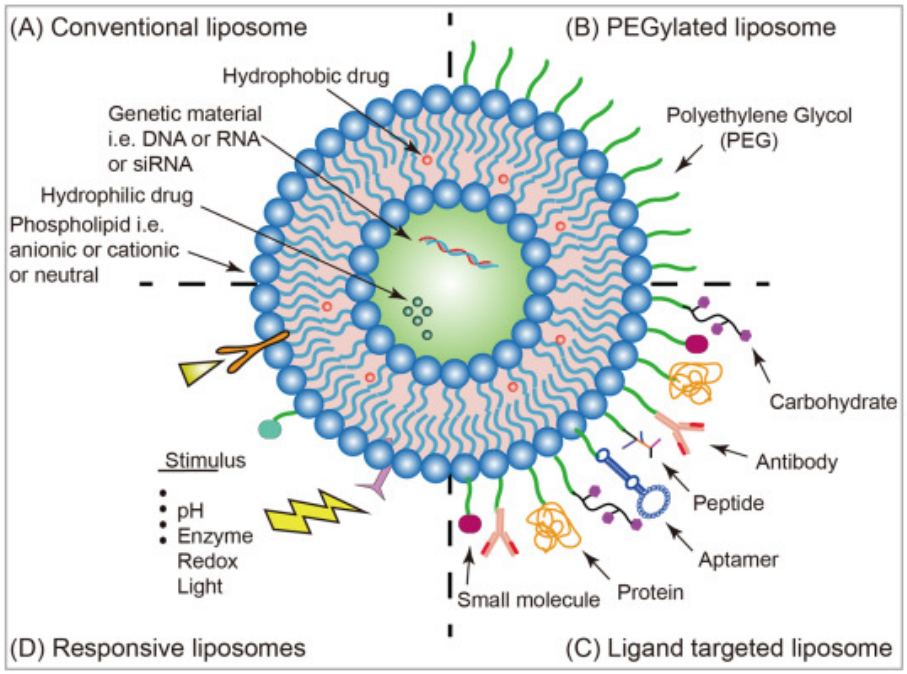

Figure 1.2 Liposome functionalization. Liposomes can be functionalized through a variety of membrane engineering strategies for their use in technological applications. **A.** Liposomal membranes composed of phospholipids and other amphiphiles can contain hydrophobic drugs, while the aqueous interior of vesicles can contain genetic material and hydrophilic drugs. **B**. Liposomes can contain PEGylated lipids to create 'stealth' particles which exhibit improved pharmacokinetics. **C**. Surface conjugation allows targeting moieties to be incorporated into liposome membranes to target liposomes to specific locations and modulate interactions with live cells. **D**. Stimuli-responsive molecules can be incorporated into model membranes to introduce new functionality into liposomal systems. Reprinted, with permission, from reference [33].

Beyond cargo delivery, model membranes can be harnessed for applications in the fields of synthetic biology and biomanufacturing. With the emergence of cell-free protein expression systems and improved genetic manipulation techniques, biological processes that occur within the cell can be harnessed for engineered behaviors in an *in vitro* context, re-directing transcription and translation processes to respond to certain stimuli or to produce specific

molecular products.[34,35] Model membranes can be introduced to these systems to compartmentalize cell-free expression or enzymatic reactions to spatially segregate these processes as microscale bioreactors.[36] Not only does this assembly have implications in the evolution of life and the development of artificial cells,[12] it can allow the separation of toxic intermediates or incompatible reactions,[37,38] can reduce the effects of dilution and sample contamination,[38] and can introduce active membrane features to enhance sensing.[39] Membranes can also be added to cell-free protein expression systems to improve the expression of membrane proteins and to directly generate lipid-protein nanoparticles.[22,40] Model membranes can ultimately reintroduce features that were lost in the removal from the cellular environment, allowing greater complexity and serving as a biomimetic interface between engineered reactions and the surrounding environment.

Model membranes allow the advantageous features of bilayer membranes to be engineered for a wide array of specific uses – whether that is to explore membrane biophysical properties and their effect on biomolecular interactions or to engineer biomimetic drug delivery vehicles with improved biocompatibility and circulation time. These advances in membrane engineering for technological uses have highlighted the many ways in which membranes can be incorporated into new types of platforms and have generated an array of strategies to accomplish this. Despite the diversity of technologies that have been demonstrated using model membranes, however, we have yet to fully realize their capabilities toward applied platforms. In particular, bilayer membranes have yet to be fully harnessed for their ability to control information transfer toward the development of biosensors for environmental signals.

1.4 Scope of thesis

In this thesis, I am to incorporate aspects of the approaches described above in order to harness bilayer membranes to advance biosensing technologies. Inspired by the critical role that the plasma membrane plays in cellular biosensing, I demonstrate that the recapitulation of membranes into nanoscale and microscale sensors can serve as a platform by which sensing can be modulated through biologically inspired mechanisms. Certain features explored in the process of developing liposomes to suit the applications described above have allowed the expansion of membrane engineering strategies that are similarly well suited for these biosensing applications, including methods to enhance biocompatibility, control membrane elasticity, permeability and cross-membrane transport, and encapsulate of a wide range of lipophilic and hydrophilic molecules. Here, I focus on the use of model membrane systems for two primary goals: first, for the exploration of forces within the membrane itself, and second, to develop sensing platforms that harness membrane features for the improved detection of small molecules.

This thesis is composed of eight chapters. **Chapter 2** discusses the thermodynamic principles of membrane self-assembly, which underly all future studies discussed in this thesis. Membrane amphiphiles and membrane composition are a particular focus, especially the ways in which they govern membrane self-assembly to form bilayer vesicles and how the resulting bilayer properties are altered depending on the specific amphiphiles located within the membrane. To determine the effect of these changes on our specific membrane compositions, we use micropipette aspiration to probe these properties and to establish the effect of membrane modifications on global membrane features, specifically membrane elasticity.

Chapter 3 introduces an optical approach to monitor physical force using a set of membrane-localized fluorescent probes. Through the combinatorial use of two types of spatially distinct membrane dyes, we show that osmotically induced membrane stretching can be monitored across a population of membranes. This is facilitated by localization of probes both to the lipid headgroups, reporting stretch and increases in inter-lipid distances within the hydrophilic portion of the membrane, and to the hydrophobic membrane core, monitoring hydration of the membrane under induced force. We show that these probes can be used to monitor and differentiate processes occurring in the bilayer under tension, with a focus on tension-induced lipid uptake.

We next focus on the development of sensors incorporating encapsulated components within the vesicle interior. **Chapter 4** provides an overview of the state of the field of a specific type of vesicle-based biosensors, those described as artificial cells, with a particular focus on genetically encoded sensors. Here, we motivate the need for improved biosensing technologies, and present ways in which membranes have been used to advance and modulate cell-free sensing strategies to develop microscale biosensors. We then present our outlooks for the field of artificial cell-based biosensing and highlight areas of research that may greatly improve vesicle-based sensing technologies.

Chapters 5, 6 and 7 present the development of encapsulated sensors with varying membrane gating strategies and increasing levels of complexity.

Chapter 5 discusses the development of a sensor which improves the specificity of an encapsulated chemical ion indicator for potassium by introducing target-analyte-specific

membrane gating. We incorporate a potassium-specific membrane transporter, a bacterially derived ionophore called Valinomycin, into vesicle membranes to provide a mechanism by which molecular import can be modulated. Upon encapsulation inside of bilayer membranes, we show that a fluorescent indicator for potassium exhibits significantly higher specificity to potassium over off-target responses to sodium and calcium ions, both of which are similarly present in biological systems. We observed that sensor responses were reversible to a degree upon the removal of potassium from the environment, however time to detection was increased in the system overall. This nanoscale sensor retained improved specificity and an ability to detect changes in potassium concentrations, even when deployed into cultures of live bacteria.

Chapter 6 describes the development of an encapsulated transcription-based sensor that is initiated through the external addition of magnesium ions, which enter the vesicle through nonspecific membrane pores. A first step toward the development of a cell-free protein expression-based sensor, we first show that transcription reactions can be encapsulated and initiated inside of bilayer vesicles. We explore various types of sensor readouts, including strand displacement and aptamer-dye outputs, and demonstrate variable compatibility with vesicle-based platforms. We show that sensor responses are modulated both by the presence or absence of magnesium as well as the concentration of pores in the membrane, indicating that both analyte presence and degree of membrane permeability can be harnessed to tune sensor responses to an analyte.

Chapter 7 introduces a cell-free protein expression-based sensor for fluoride. We encapsulate a fluoride-responsive riboswitch, which exhibits a conformational change that allows

transcription to occur in the presence of fluoride. To our knowledge, this work is the first demonstration of a transcriptionally regulated riboswitch encapsulated inside vesicle membranes. We show that the riboswitch can function within vesicles and can respond to increasing concentrations of fluoride added to the vesicle exterior. Fluoride is relatively membrane permeable, and as such this platform didn't require the addition of membrane transporters; we show that membrane composition can be engineered to tune membrane permeability and subsequently the response of the sensor to external fluoride. By incorporating both fluorescent and colorimetric readouts, we demonstrate that multiple output types can be detected with vesicle platforms. Finally, we highlight how these sensors can be deployed in samples by showing that encapsulation protects encapsulated sensors from degradation by complex samples while allowing the sensor to detect and respond to fluoride in real-world water samples.

Chapter 8 summarizes the studies presented in this thesis and discusses future directions for membrane-based sensors. In addition, this chapter presents a discussion of some of the tradeoffs that occur due to encapsulation and indicates areas of research that may help to mitigate these challenges in the future. We conclude by highlighting how the various strategies employed in each chapter may ultimately be combined in new ways to broaden the library of analytes that can be detected.

Chapter 2: Membrane Biophysics

2.1 Membrane amphiphiles self-assemble into bilayer membranes

2.1.1 Amphiphilic molecules

In engineering membranes for specific applications, it is first important to understand how membranes form and how the composition of these membranes can impact features of the resulting bilayer. Membrane formation is rooted in the amphiphilic character of membrane monomers, which can include phospholipids, fatty acids, sterols, and non-natural amphiphiles.[2] These amphiphiles are defined by their chemical composition and, broadly, consist of both a hydrophobic component and a hydrophilic component. As biological systems are generally heavily water-based, this chemical difference creates a single molecule with two very different interactions with the surrounding environment. The hydrophilic portion, often referred to as the hydrophilic 'head,' interacts favorably with surrounding water molecules due to its polar nature. In contrast, the nonpolar, hydrophobic 'tails' repel water, instead preferring to interact with other hydrophobic groups. This phenomenon creates a driving force for amphiphiles to interact with one another, known as membrane self-assembly.[2,18,41,42]

The structure of these associating amphiphiles can vary; lipids and fatty acids can consist of different types of charged and uncharged headgroups, varying lengths and degrees of unsaturation of tail groups, and different numbers of hydrophobic tails.[2] Non-lipid amphiphiles such as sterols and synthetic polymers can also be incorporated into self-assembled membranes, and the resulting properties and behaviors of the membrane vary drastically based on the specific monomers it is composed of (**Figure 2.1**).[2,23] In cellular systems, different types of amphiphiles

can be used to generate structural organization in the membrane and to adjust the properties of the membrane based on desired function.[2,3,13] Outside of the cell, membrane self-assembly allows bilayer membranes to be formed in the lab for a wide range of uses, and facilitates changes to membrane composition in order to modulate membrane characteristics for a number of applications.[12]

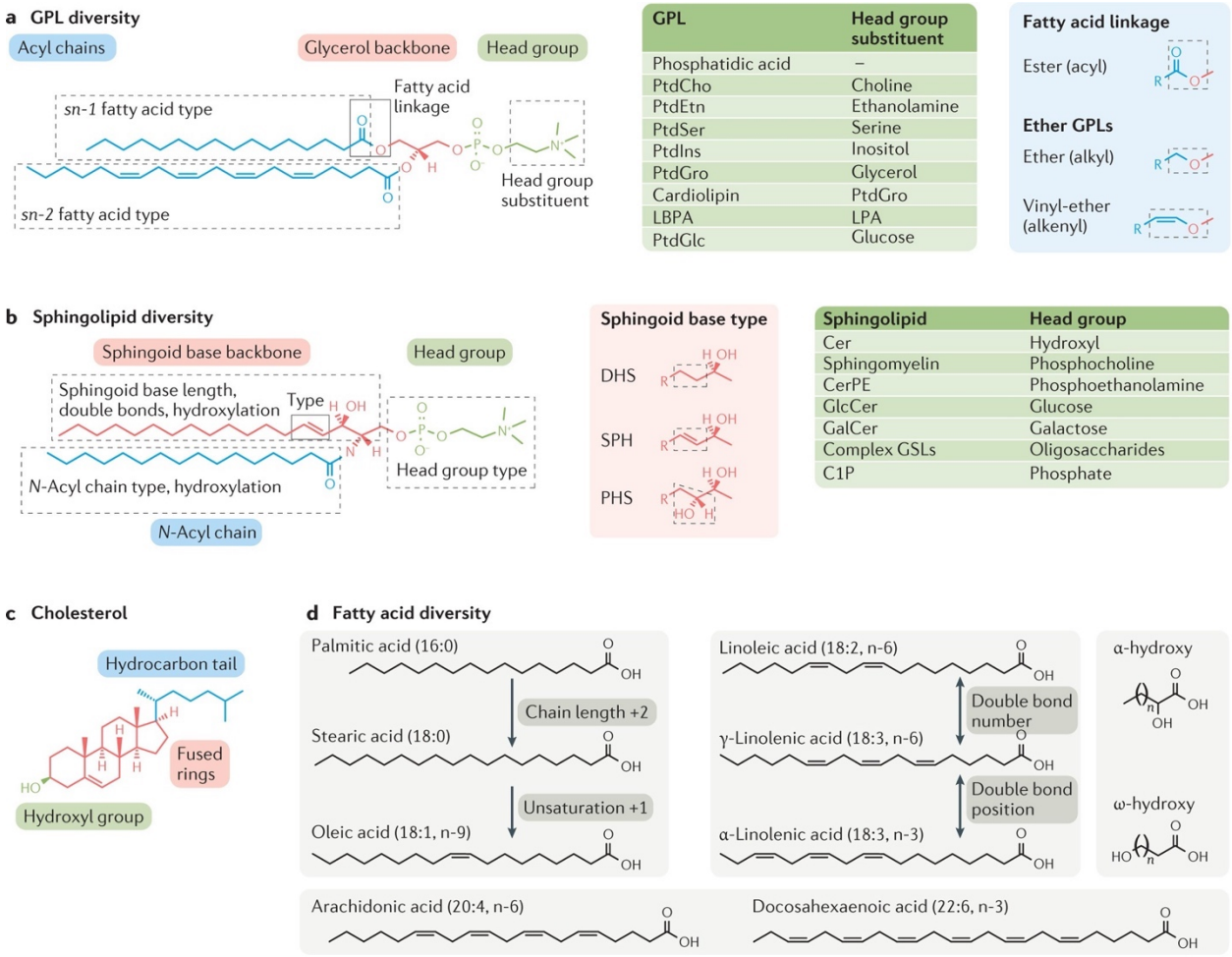

Figure 2.1 Amphiphilic structure and chemical diversity of common lipids. Biological and model membranes can contain a variety of amphiphiles, including lipids, sterols, and fatty acids. **A**. Glycerophospholipids (GPLs) are a major structural component of many cellular and model membranes. Variations can arise in the acyl chains, particularly acyl chain saturation, as well as the fatty acid linkage and headgroup moiety. **B**. Sphingolipids, which interact with sterols in the

membrane, exhibit similar chemical diversity. **C.** Cholesterol, a key sterol in biological membranes. **D**. Fatty acids exhibit diversity in their chain length as well as the location and degree of unsaturation. Adapted and reprinted, with permission, from reference [2].

2.1.2 Self-assembly and aggregate formation

The assembly of model membranes, and amphiphile self-assembly in general, is a thermodynamically driven process by which bilayers form. Membrane assembly begins due to the drive for amphiphilic monomers to aggregate in solution as a result of the hydrophobic effect.[18,41-43] In the presence of water, the bulk aqueous solvent interacts unfavorably with the hydrophobic tail of the amphiphile, driving hydrophobic segments to associate with each other rather than the surrounding water molecules.[18,41] This aggregation of amphiphiles to form a more highly ordered structure would generally be energetically unfavorable, however it is thought that the hydrophobic effect arises to dissipate ordered structures formed by water molecules in the presence of hydrophobic molecules.[41] Hydrophilic headgroups, on the other hand, interact favorably with water, driving organization of amphiphiles with headgroups facing the water interface. In this formation, the hydrophilic heads play an important role in stabilizing the overall structure through their interactions with surrounding water molecules.[18,42] This results in an interfacial energy between the hydrophobic core and the hydrophilic heads and water.[18] In order to decrease this interfacial energy, it becomes energetically favorable for the monomers to form aggregated higher order structures, thereby decreasing the total interfacial area.[28]

As amphiphilic monomers associate in solution, the total free energy of this process can be described as a sum of the interaction energy of forming a micelle, $N\Delta\mu_{micelle}$, and the energy of self-assembly, ΔG_{agg}:[18,27,28,41-53]

$$\Delta G_{total} = N\Delta\mu_{micelle} + \Delta G_{agg} = 0 \quad \textbf{(2.1)}$$

The entropy of self-association is unfavorable ($\Delta G_{agg} > 0$), meaning that $\Delta\mu_{micelle}$ must be negative to overcome this barrier; this is largely a result of the hydrophobic effect as described above.[41] When present in sufficiently low concentrations, monomers associate and dissociate rapidly as interaction energies are not significant enough to overcome the unfavorable barrier of self-association to form large aggregates.[41] At some *N* number of monomers, however, this balance shifts and aggregates grow into larger structures. The critical micelle concentration, or CMC, describes the concentration at which significant aggregation begins,[18,41,42] given as the point at which the number of monomers free in solution is equal to the number associated into micelles.[41,53] The CMC can be described as:[41-43,54]

$$C_{CMC} \sim e^{\frac{\Delta\mu_{micelle}}{kT}} \quad \textbf{(2.2)}$$

As is evident from equation 2.2, the interaction energy of micelle formation dictates the concentration at which aggregation occurs – a property which depends strongly on the molecular architecture of the amphiphiles involved.[28,41,43]

2.1.3 Aggregate growth and morphology

As aggregates continue to grow, the unfavorable interactions between hydrophobic chains and water are reduced. This effect is not infinite, however, as the reduced enthalpic

penalty from hydrophobic/hydrophilic interactions comes at the cost of an increased entropic penalty for single chains.[18,41,43] As more amphiphiles assemble, both the hydrophobic and hydrophilic segments are forced into closer proximity, leading to unfavorable intermolecular interactions. At some critical point, the energetic benefit of aggregation will no longer surpass the energetic penalty of chain interactions; the final vesicle morphology will arise as a result of the thermodynamic interplay between these phenomena.[45] There are two types of forces that play a key role in this process: attractive interactions arising from the hydrophobic effect and interfacial tension, and repulsive interactions caused by steric and electrostatic interactions between headgroups and between hydrophobic tails.[18,41,50] The attractive interactions discussed above initiate aggregation, however final aggregate morphology is dictated by the repulsive interactions that begin to dominate as molecular packing increases.

As a result of increased molecular packing, the relative area per headgroup, a_0, decreases, and headgroups begin to repel one another due to steric interactions while hydrophobic chains begin to stretch and compress.[50,51] The degree to which each of these forces affect amphiphile assembly and morphology can be understood through the packing parameter:[28,42,43,50,53]

$$p = \frac{v}{a_0 l_c} \quad \textbf{(2.3)}$$

where v is the volume of the hydrophobic segment, a_0 is the area of the hydrophilic headgroup, and l_c is the length of the hydrophobic segment. The packing parameter can be used to understand amphiphile shape and predict how it will impact final aggregate morphology (**Figure 2.2**). For example, amphiphiles with a packing parameter of ½ < p < 1 will tend to form bilayer

vesicles or flexible lamellae, amphiphiles with $p < 1/3$ will tend to form spherical micelles, and those in between will form cylindrical rods.[42,54] Amphiphiles with $p > 1$ can likewise form inverted micellar structures.[43,53] This relationship indicates that packing parameter and hydrophobic volume fraction increase simultaneously, as there is a more significant effect of hydrophobic chain stretching compared to headgroup repulsion. The inverse is also true, with a more significant contribution of hydrophilic head repulsion as the hydrophilic volume fraction increases.[45] This relationship between hydrophilic and hydrophobic segment volume ultimately impacts final aggregate morphology by dictating the structure with the minimum free energy.[28,42,43,50,53,54]

The final structures resulting from amphiphile self-assembly are ultimately dictated by these thermodynamically regulated interactions, which can be recapitulated in the lab to form membranes with various shapes and compositions. By understanding the attractive forces of the hydrophobic effect and interfacial tension and the repulsive forces caused by intermolecular electrostatic and steric interactions of hydrophilic headgroups and hydrophobic chains, a better understanding of bilayer membrane dynamics can be gained. Importantly, the properties of amphiphiles themselves can be explored to generate a range of morphologies and physical properties. Although the principles of self-assembly remain consistent across amphiphiles, the nature of the amphiphiles involved has a significant effect the resulting properties of the final structure - not only final shape, but membrane organization, membrane permeability, and the response of membranes to force.

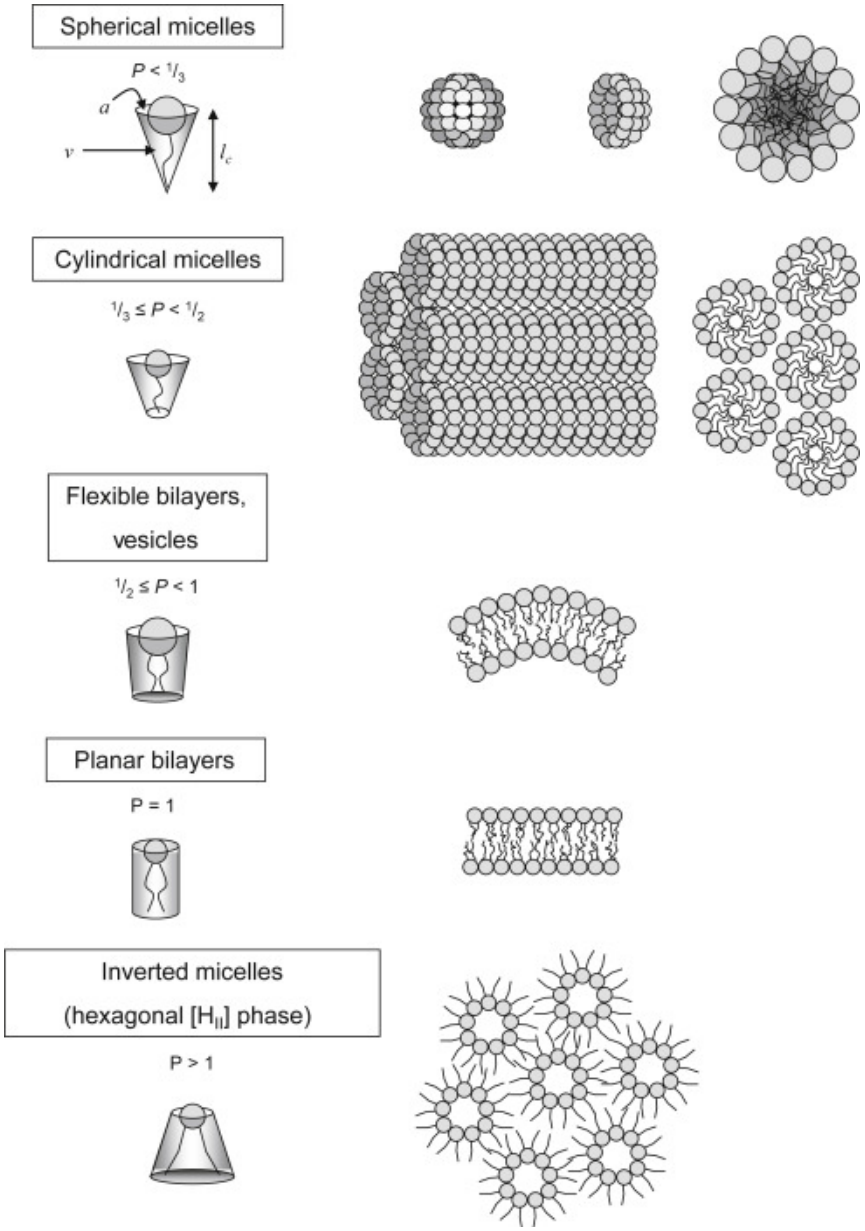

Figure 2.2 Lipid packing parameter and resulting morphology. Lipid packing parameter, $p = v/a_o l_c$ affects the self-assembly of amphiphiles into higher order structures by dictating equilibrium morphology. As packing parameter increases, resulting aggregates exhibit greater hydrophobic character, resulting in the transition from micelle → bilayer → inverted micelle with greater values of p. Reprinted, with permission, reference [55].

2.2 Membrane composition and membrane biophysical properties

While the thermodynamic principles underlying membrane self-assembly are relatively straightforward, membranes can be complex, dynamic structures. Biological membranes incorporate a diverse set of lipids and amphiphiles into their various membranes, and lipid homeostasis is a tightly-regulated process that has significant implications in proper cellular function.[2] This is largely due to the fact that a wide range of physical and biochemical properties arise from the specific composition membranes, and maintaining these compositions is key for the regulation of a broad set of membrane physicochemical properties, including charge, curvature, bending rigidity, elasticity, membrane thickness, lipid packing, fluidity, and phase separation (**Figure 2.3**).[2,3,13,14,56,57] These properties can, in turn, have a significant impact on membrane-specific behaviors, for example fusion and fission, lateral organization into lipid domains and lipid rafts, and modulation of membrane protein behaviors.[2,3,13]

Many of these membrane features can be maintained and recapitulated in model membranes, which serve as an important platform to build membrane-based systems with specific characteristics.[13] With this consideration in mind, specific membrane features can be imparted upon vesicle platforms in order to adjust their behaviors through the membrane alone – a feature which is particularly important for the development of membrane based-sensors, which rely on cross-membrane transport and signaling.[12] Whether regulating membrane organization, adjusting permeability to control access to the vesicle interior, or allowing the detection and dissipation of physical force, membrane composition is a key handle by which membrane properties can be engineered within bilayer systems to enhance sensing capabilities.

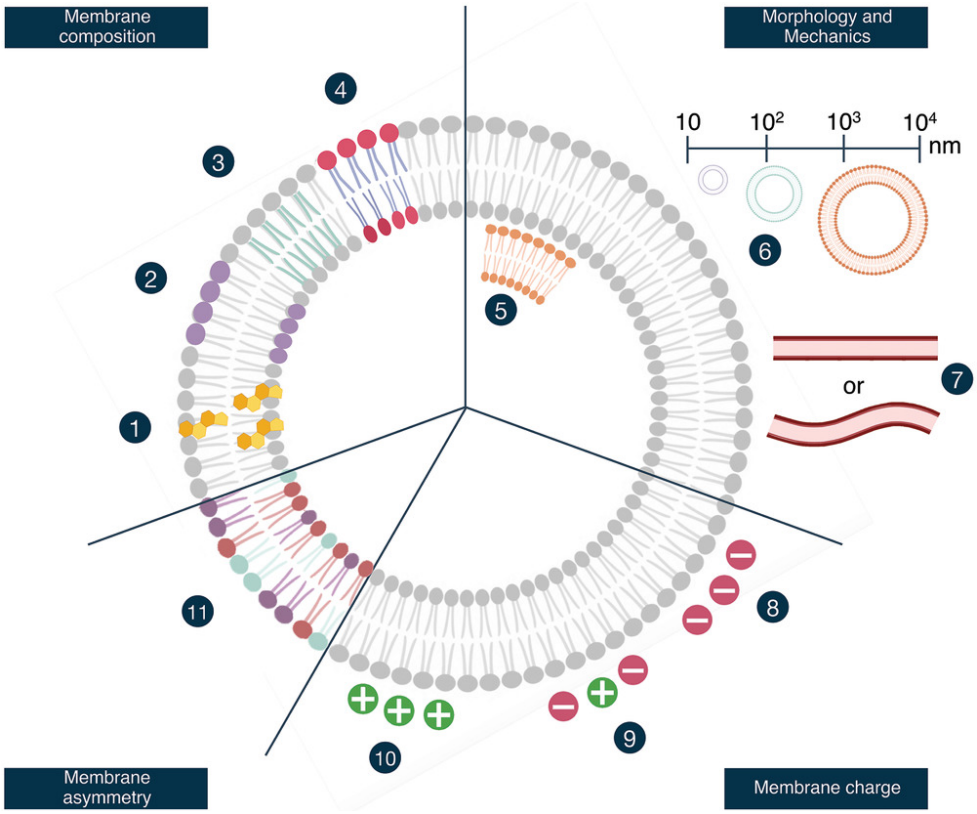

Figure 2.3 Membrane composition regulates membrane physicochemical properties. Membrane composition affects a variety of membrane properties. Membranes can incorporate sterols (1), and lipids with varying headgroups and tail lengths and unsaturations (2-4). These compositional changes impact the resulting lamellarity (5), size (6) and curvature of the assembled structure, as discussed above. Headgroup identity can affect resulting charge (8-10), which can regulate interactions with other membranes and biomolecules such as proteins and nucleic acids. Lipid mixing can result in membranes with varied compositions and asymmetries both laterally and between leaflets (11). Reprinted, with permission, from reference [58].

2.2.1 Lipid rafts and lateral membrane organization

On a large scale, membrane composition plays a major role in the spatial organization of membrane components by generating distinct regions in the bilayer composed of lipids of different phases. This lipid domain, or lipid "raft," formation is transient and can occur on a

range of length scales, generating nano- and microscale assemblies that can sequester lipids and proteins.[13,59] Rafts in cellular systems are thought to play a key role in a number of biological processes and pathologies, including immune signaling, modulation of host-pathogen interactions, cancer development and progression, and development of atherosclerosis.[13,59] More generally, however, this spatial organization can create regions within the membrane that organize transmembrane proteins and which exhibit different physical and mechanical properties.[3,59-61] Although establishing lipid domains in living cells has been difficult due to their complexity, small size, and short lifetimes,[3,13] phase separation has been observed in model membrane systems,[2,3,13,60] indicating that features of the lipid makeup itself can drive these large-scale remodeling forces.

Model membranes have been particularly useful for probing the liquid-liquid phase separation seen in raft formation, which generally arises from the presence of a liquid disordered (L_d) phase and a liquid ordered (L_o) phase.[60,61] This phase separation is largely thought to be due to interactions between saturated lipids and cholesterol driving them to segregate from unsaturated, more fluid lipids. In particular, sphingolipids interact strongly with cholesterol, show more potential for hydrogen bonding, and generally have longer and more saturated tails.[2,13,59] This is thought to result in the formation of more highly ordered, cholesterol-rich domains, which can incorporate other phospholipids with more saturated tails. Cholesterol-lipid interactions also force lipid tails into more extended conformations, increasing membrane order and thickness.[57,60,62] The resulting height differences between more ordered, “stretched” lipid tails and more fluid, unsaturated tails which exist in the remainder of the membrane are thought to drive hydrophobic mismatches within the membrane, which are minimized through self-

association of lipids of the same thickness and saturation.[3,13,60] Here, the simple modulation of membrane composition alone can result in large-scale reorganization of membranes, even in the absence of other cellular features.

2.2.2 Membrane permeability

Membrane composition also plays an important role in regulating membrane permeability. A unique feature of bilayer membranes is their semipermeability; lipid membranes are impermeable to large, charged or polar solutes due to an inability for these molecules to pass through the hydrophobic region of the membrane,[57,63] while small, neutral molecules, some ionic salts, hydrogen ions, and water generally pass through the bilayer passively.[63,64] As a result, although biological membranes incorporate a diverse set of membrane transporters to actively transport small molecules across the membrane, certain solutes can also cross the bilayer in a permeability-mediated process to enter the cell or vesicle nonspecifically.[63] The degree to which these molecules permeate the bilayer depends significantly on the lipid makeup of the membrane and can be significantly impacted by the presence of specific amphiphiles like cholesterol, fatty acids, and non-natural amphiphiles.[57,59,62-68]

The first major consideration in membrane permeability, particularly with regard to biological membranes, is cholesterol content and lipid packing. Sterols play a key role in regulating mechanical stiffness as they simultaneously make the membrane more fluid but also thicker and more tightly packed, which reduces permeability to solutes and water alike.[63] A similar effect is observed with saturated versus unsaturated lipids, where increased lipid packing and thickness of saturated lipids results in reduced permeability compared to more fluid,

unsaturated lipids.[63,69] The hydration of the membrane, or relative penetration of the membrane by water molecules, can serve as an indicator of this effect, where higher degrees of unsaturation in the lipids of the bilayer and lower levels of cholesterol allow formation of defects through which water and solutes can travel.[69] Importantly, however, membrane permeability dictated by lipid and cholesterol packing also depends significantly on temperature, which can affect the lipid organization and phase.[63] By altering the physical space between lipids in the membrane, cholesterol and saturated lipids can ultimately regulate the permeability of the bilayer to a number of molecules.

In addition to cholesterol, other amphiphiles can be inserted into the bilayer to modulate permeability. Fatty acids, which exhibit a conical shape due to their single hydrophobic chain, can insert into the bilayer and disrupt membrane integrity and packing.[65-67] This effect has been previously used to induce higher degrees of permeability in membranes for drug delivery.[66] A similar effect is observed with the incorporation of PEG-grafted lipids, which are often incorporated into liposome-based drug delivery systems. These lipids have been shown to not only reduce clearance *in vivo* by shielding the liposome surface from immune cell recognition, but to increase membrane permeability – a phenomenon which is thought to be caused by increased lateral pressure in the membrane due to steric interactions between PEG molecules.[26] Synthetic diblock or triblock copolymers can also be incorporated into the membrane to either reduce or increase permeability, depending on the specific polymer and its relative concentration.[19,24] These synthetic molecules can be added to model membranes during vesicle formation, imparting increased mechanical robustness thickness.[24,25] While tradeoffs ultimately arise between the desired function of membrane additives and their resulting impact on

membrane integrity, both naturally derived and synthetic amphiphiles can provide an additional handle by which permeability can be regulated.

2.2.3 Membrane bending, stretching, and response to force

In addition to lateral organization and membrane permeability, membrane composition plays a role in modulating the physical responses of the bilayer in response to force.[3] The response of the cellular membrane to force has been implicated in intracellular trafficking, mechanosensation, endo- and exocytosis, and cell migration and division.[6-8,70] Some of these physical features of the membrane are dictated by the structure of the amphiphiles within the membrane, for example membrane curvature and bending stiffness, which arise largely as an intrinsic feature due to the specific shapes of the amphiphiles within the bilayer.[3,8] Bending stiffness is similarly impacted by the presence of membrane proteins, or, in living cells, cytoskeletal contacts,[8,11] and can be an important factor influencing protein function and conformational changes.[3,8] The physical properties of the bilayer and the proteins embedded within them can also be impacted by forces within the bilayer, including transverse forces, which arise due to thickness mismatches, line tension at the interface of different height domains, and lateral “compressive” pressures.[3] By adjusting the lipid composition of the membrane, these features can be exaggerated or minimized to affect membrane properties and bilayer behaviors.

For both model and cellular membranes, there are not only intrinsic forces within the membrane but external forces that must be mitigated to avoid lysis or rupture. Perhaps the most important of these from a technological standpoint are forces that induce membrane tension. Membrane tension is generated by lateral stretching of the bilayer and a subsequent increase in

inter-lipid distances.[3,11] The increase in space between lipid molecules results in more contact between water and the hydrophobic portions of the membrane, a change which is unfavorable and results in the drive for lipids to pull together, generating tension.[3,5] Membrane tension is encountered often for vesicles or cells exposed to varying external solute concentrations, which results in osmotic pressure and swelling that stretches the membrane outward and can eventually lead to rupture.[3,9] The ability of a membrane to adapt to this force and to accommodate the resulting stretching of the bilayer is rooted in its elasticity. Membrane elasticity describes the resistance of the membrane to deformation in various directions, and plays a role in responses to shear deformation, bending, and stretching.[3] Composition also plays a significant role in membrane elasticity; for example, lipid membranes are relatively weak, only accommodating an areal expansion of about 3-5% before rupture,[5] while polymer membranes are significantly more elastic and robust to lysis.[24,25] This ability of membranes to accommodate lateral stretch is therefore an important consideration in many systems in which tension-inducing forces will be encountered.

2.3 Measuring membrane elasticity using micropipette aspiration

*Portions of this section adapted from the following publication:

Jacobs, M. L., Boyd, M. A., Kamat, N. P. Diblock copolymers enhance folding of a mechanosensitive membrane protein during cell-free expression. *PNAS,* 116 (10) 4031-4036, 2019. DOI: 10.1073/pnas.1814775116

In order to develop membrane-based sensors, our goal was to incorporate membranes of varying compositions to impart new functionality and to improve sensor stability. Aqueous sensors are expected to experience changing solute conditions and osmotic pressures in the process of biosensing, and we aimed to introduce membranes to cell-free protein expression systems, which have high salt concentrations and proteins present. In addition, vesicle-based sensors can be formed through multiple preparation methods, which may affect membrane mechanical properties through the presence of residual oils. Therefore, we sought to explore the ways in which composition, formation method and cell-free expression affect membrane elasticity. To assess the elasticity and robustness of our model vesicle systems, we set out to characterize membranes of varying compositions to determine their apparent area expansion modulus, K_{app}. Compared to the area expansion modulus, K_A, the apparent expansion modulus does not account for thermal undulations during bilayer stretching, but still allows a comparison of membrane stretch in response to a specified force in the high-tension regime.[26,71,72] For these studies we chose to focus simply on elasticity rather than on the contributions of bending or shear forces.[71] To assess this, we conducted micropipette aspiration on vesicle membranes.

2.3.1 Theory of micropipette aspiration

Micropipette aspiration is a technique which uses the application of pressure to a membrane through a micron-scale pipette, allowing high resolution exploration of membrane expansion and elastic reversibility.[73] In micropipette studies, a large vesicle on the scale of ~10-100 μm is aspirated into a ~1-5 μm diameter pipette. As a controlled suction pressure is applied, the membrane expands into the pipette, generating a lateral tension across the membrane (**Figure 2.4 A & B**). Analysis of the length of the membrane aspirated into the pipette allows an

estimation of areal expansion of the vesicle membrane, which can be used to generate a stress/strain curve establishing the area expansion modulus of the membrane.[71-74]

The tension in the membrane under applied pressure can be described by the Law of Laplace:[75]

$$\tau = \frac{PR}{2} \quad \textbf{(2.4)}$$

During aspiration, a controlled suction pressure, ΔP_p, is applied to the membrane using a pipette of radius R_p, on a vesicle of initial radius R_0. The tension in the membrane balances the pressure generated inside the spherical vesicle, and the projection of the membrane into the pipette increases. The resulting tension can be calculated through the Laplace law as:[71,73,75]

$$\tau = \frac{\Delta P_p R_p}{2(1-\frac{R_p}{R_0})} \quad \textbf{(2.5)}$$

To establish K_{app} for a vesicle membrane, the pressure-induced tension is compared to the extent of membrane stretching. The resulting change in area can be described as:[71]

$$\Delta A = 2\pi R_p \Delta L \left(1 - \frac{R_p}{R_0}\right) \quad \textbf{(2.6)}$$

where the initial area is defined as:

$$A_0 = 4\pi {R_v}^2 \quad \textbf{(2.7)}$$

The areal strain is then found by taking the change in area over the initial area,

$$strain = dA/A_0 \quad \textbf{(2.8)}$$

As the vesicle is aspirated with increasing suction pressure applied, the induced tension is plotted against this measured areal strain. The slope of this stress-strain curve gives the apparent area elastic modulus, or K_{app}, of the membrane.[71-75]

2.3.2 Micropipette aspiration of blended membranes

We assessed membranes composed of varying mol% of lipids, polymers and cholesterol, as well as membranes prepared through double emulsion vesicle formation and electroformation. We similarly assessed membranes that were 1) in sucrose buffer, 2) in cell-free protein expression buffer with no protein expressed, and 3) in cell-free protein expression buffer with the expression of a small membrane protein, crcB. These results serve as a first step towards future studies assessing nanosensors and microsensors with varying membrane compositions and in the presence of cell-free protein expression systems.

Materials and Methods

Chemicals

DOPC (18:1 (Δ9) 1,2-dioleyoyl-sn-glycero-3-phosphocholine, 25 mg/mL), POPC (1-palmitoyl-2-oleoyl-glycero-3-phosphocholine), Cholesterol, Cy 5.5 PE (1,2-dioleoyl-sn-glycero-3-phosphoethanolamine-N-(Cyanine 5.5), and Cy 7 PE (1,2-dioleoyl-sn-glycero-3-phosphoethanolamine-N-(Cyanine 7) were obtained from Avanti Polar Lipids, Inc. Laurdan (6-Dodecanoyl-N,N-dimethyl-2-naphthylamine, 176.8 mg/mL) was obtained from Invitrogen. 1.8k polymer (PEO_{14}-b-PBD_{22}) was obtained from PolymerSource. PURExpress 2.0 was obtained from Cosmo Bio USA. crcB-RFP plasmid was a gift from the Lucks lab.

Vesicle formation & protein expression

Vesicles of varying composition were formed either through electroformation in sucrose buffer or through double emulsion. Briefly, electroformed vesicles were formed using the Nanion Vesicle Prep Pro by drying down lipids onto a conductive glass slide, adding 280 mOsm sucrose to the top of the lipid film, and running the standard formation protocol. Double emulsion liposomes were formed according to established protocols as follows: amphiphiles were dried onto the side of a glass vial, placed in a vacuum oven for >3 hours, and dissolved in BioUltra Mineral Oil at 80ºC for 1 hour with occasional vortexing. Inner solution with sucrose was vortexed into amphiphile/oil mixtures for 30 seconds to form an emulsion. Emulsions were layered onto 200 μL of outer solution containing equimolar glucose and allowed to equilibrate for ~5 minutes. Vesicles were centrifuged into outer solution at 18,000 rcf for 15 minutes, following which the vesicle pellet was collected and resuspended in fresh outer solution. For vesicles in the presence of cell-free protein expression, inner solution contained 800 mmol/kg sucrose to match the osmolarity of PUREfrex reactions (815 mmol/kg). 10 μL vesicles were added to fully assembled PUREfrex reactions: 10 μL Solution I, 1 μL Solution II, 2 μL Solution III, with either 0 nM or 0.25 nM DNA and MilliQ Ultrapure water to a final volume of 20 μL. Plasmid stock: 100 ng/μL (48 nM). Plasmid pWT083, crcB-mRFP. Vesicles and PUREfrex reactions were incubated for 3 hours at 37ºC to allow protein expression to occur.

Micropipette aspiration

Vesicles were aspirated in equiosmolar PBS using a custom-made coverglass holder. Coverglass was blocked with 1 wt% BSA in water for >20 minutes before vesicles were added,

then rinsed 3x with PBS. Borosilicate pipettes were filled with a PBS solution with 1 wt% BSA and connected to an aspiration station mounted on the side of a Nikon inverted microscope, equipped with a manometer, Validyne pressure transducer (model DP 15-32, Validyne Engineering Corp), digital pressure read-outs, and micromanipulators (model WR-6, Narishige). Suction pressure was applied via a syringe connected to the manometer. GUVs were picked up by a micropipette and suction was applied in ~1 cm H_2O increments, allowing for 5s of equilibration before subsequent aspiration steps. Images were taken using DIC and Cy 3 (ex: 545 nm, em: 620 nm) filters and were analyzed in *Fiji* software[76] to measure vesicle diameter and membrane extension, which were then used to calculate the average apparent area expansion modulus, K_{app}, of each population of vesicles.

2.3.3 Results and discussion

Membranes were assessed under two sets of conditions. First, electroformed vesicles of varying compositions were assessed to determine the effect of adding membrane dyes, polymers, and cholesterol to the membrane of DOPC lipid vesicles. DOPC vesicles exhibited an apparent elastic modulus of ~200 dyne/cm, consistent with results in literature.[73] The addition of increasing concentrations of diblock copolymer (1.8k MW PEO_{14}-b-PBD_{22}, hereafter referred to as 1.8k) reduced K_{app} as polymer content increased, as expected,[77] resulting in a pure polymer K_{app} of ~80 dyne/cm. The addition of even 10 mol% 1.8k polymer was observed to significantly reduce elasticity compared to DOPC lipid alone, indicating that low concentrations of polymer can be added to lipid membranes to enhance their elasticity, and therefore to likely enhance robustness to changing osmotic conditions. The addition of membrane dyes to the membrane, in this case 0.1 mol% of each Cy 5.5 PE and Cy 7 PE as well as 0.5 mol% Laurdan, is similarly

sufficient to reduce the apparent area expansion modulus significantly – a shift which is important to consider when incorporating small concentrations of dyes to monitor membrane properties. Finally, the addition of 50% cholesterol to the membrane significantly increased apparent elastic modulus, indicating increased stiffness, as expected.[63] Measured area expansion moduli were significantly different than DOPC for all membrane compositions (**Figure 2.4 C**).

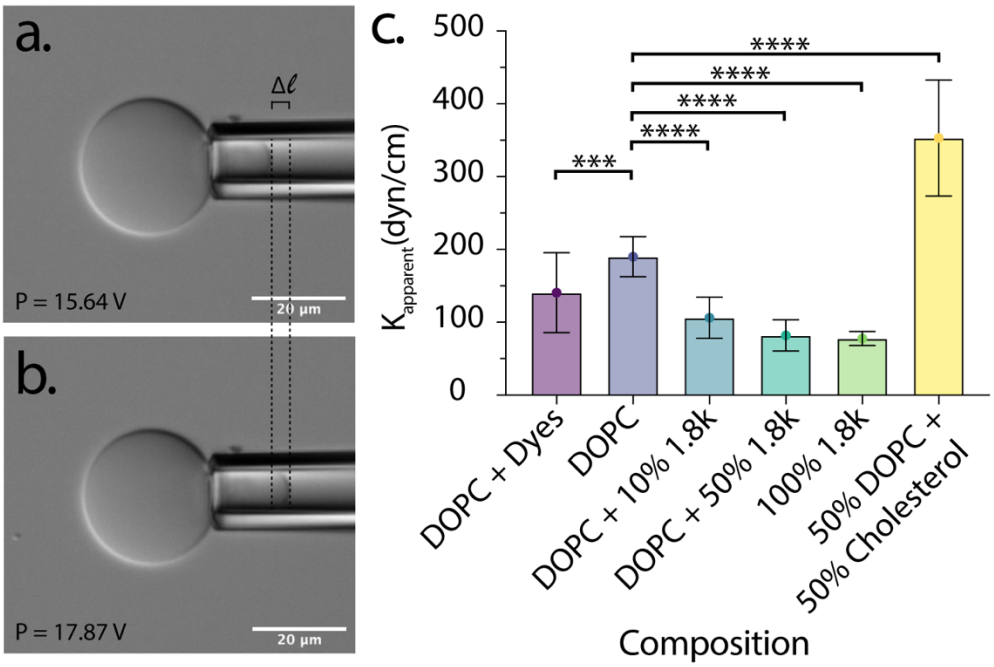

Figure 2.4 Area expansion moduli of electroformed vesicles. Micropipette analysis of a DOPC lipid vesicle under lower (**A**) and higher (**B**) pressure. ΔL and ΔP can then be used to estimate membrane area expansion modulus. Scale = 20 μm **C.** Apparent area elastic modulus, $K_{apparent}$, of vesicles with varying membrane compositions formed via electroformation. The addition of either membrane dyes or diblock copolymer reduces area expansion moduli significantly compared to pure DOPC lipid membranes. In contrast, the addition of 50 mol% cholesterol significantly increases area expansion modulus. N > 15 vesicles analyzed per composition, black bars represent mean and standard deviation. *** $p \leq 0.0004$; **** $p < 0.0001$; One-Way ANOVA and Dunnett Multiple Comparisons Test.

Our next goal was to assess membranes under the conditions expected for vesicle sensors in the presence of cell-free protein expression reactions. In order to encapsulate cell-free reactions for sensing applications, vesicles are often formed using water-in-oil emulsion techniques due to the higher resulting encapsulation efficiency of large biomolecules.[78] This technique is generally used with a 2:1 molar ratio of cholesterol and POPC lipid for cell-free expression studies. Unfortunately, this technique requires the incorporation of mineral oil into the lipid/oil mixture, and is known to result in residual oil in the membrane following vesicle isolation.[79,80] To better characterize the impact of mineral oil and emulsion formation techniques on our resulting membranes, we first set out to compare the K_{app} of pure POPC lipid vesicles prepared using emulsion compared to electroformation techniques to assess whether there is a change in elasticity due to residual oil in the membrane. We did not observe a significant difference in average membrane K_{app} for POPC vesicles formed via either emulsion or electroformation, although the spread of area expansion moduli was larger for emulsion-templated vesicles, consistent with some variations in membrane composition due to residual mineral oil (**Figure 2.5 A**).

We next wanted to compare vesicle membranes with a highly controlled membrane composition, formed via electroformation, in the presence of cell-free protein expression buffers either with or without the expression of a small membrane protein, crcB. CrcB is a small, four transmembrane domain protein which serves as a fluoride transporter in bacteria.[81] We observed no significant differences in K_{app} between populations of POPC vesicles in sucrose (emulsion and electroformed POPC) compared to those in PURExpress buffers with or without the expression of an RFP-tagged crcB protein, indicating that 1) the presence of cell-free buffers does not have

a major impact on membrane properties, and 2) this effect is not changed as a membrane protein is expressed and inserted into the membrane (**Figure 2.5 A**). Although membrane properties were not observed to vary significantly, crcB-RFP could be observed to be localized to the vesicle membrane (**Figure 2.5 B & C**). This localized fluorescence was not observed in the absence of crcB-RFP, as indicated by micrograph overlays of DIC and Cy3 filters for POPC – crcB (**Figure 2.5 D**) and POPC + crcB (**Figure 2.5 E**).

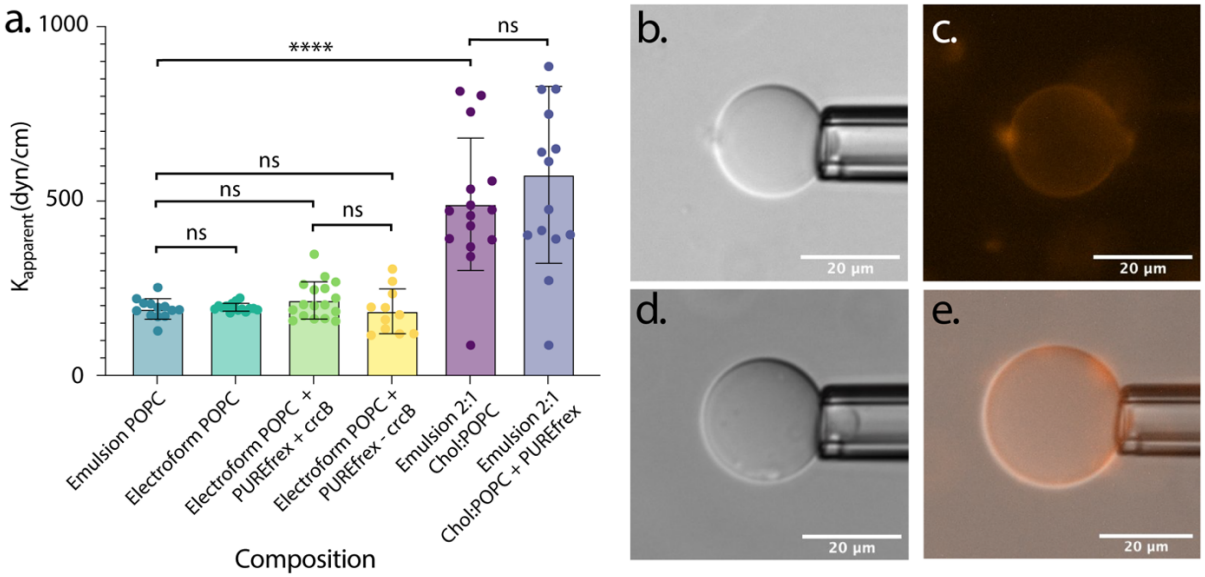

Figure 2.5 Area expansion moduli of emulsion templated vesicles with expressed protein. A. $K_{apparent}$ values for various membrane compositions prepared either via electroformation or emulsion with or without cell-free expression buffers and protein expression present. No significant differences were observed between POPC conditions or between 2:1 Chol:POPC conditions. ns $p > 0.999$; **** $p < 0.0001$; One-Way ANOVA and Dunnett's Multiple Comparisons Test. DIC (**B**) and Cy 3 (**C**) micrographs of a POPC vesicle with crcB-RFP inserted into the membrane. Scale = 20 µm. DIC/Cy3 overlay micrographs of POPC vesicles in PURExfrex buffer without crcB DNA (no protein expression), **D**, or with 0.25 nM crcB-RFP DNA (with protein expression), **E**, show localization of RFP fluorescence only in the presence of crcB-RFP DNA. Scale = 20 µm.

Finally, we wanted to assess the properties of a commonly used composition for emulsion-templated vesicles: a 2:1 ratio of cholesterol:POPC lipid. Importantly, this composition has been the most commonly used to encapsulate cell-free expression systems to generate artificial cell-like constructs.[38,82-85] We were unable to directly compare this composition to electroformed vesicles, as electroformation does not accommodate such high concentrations of cholesterol. Similarly, we were unable to explore the expression of crcB using this composition as crcB insertion is impeded by the presence of cholesterol in membranes (**Figure 2.6 A & B**). Despite these limitations, we assessed the K_{app} of 2:1 Cholesterol:POPC membranes prepared in sucrose buffer versus in the presence of PURExpress buffers used for cell-free protein expression (**Figure 2.5 A**). We observed a significant increase in K_{app} compared to POPC vesicles for both populations of vesicles, as expected for the addition of cholesterol; this increase was slightly higher than in electroformed vesicles with 50% cholesterol shown in Figure 2.3 C, consistent with the presence of additional cholesterol. We also observed a larger spread in area expansion moduli, likely due to variability in cholesterol and mineral oil content between individual liposomes using this method. We did not observe a significant difference between these vesicles prepared in sucrose compared to those in PURExpress buffer, however, indicating that the presence of cell-free expression components does not significantly impact membrane properties. As we aim to encapsulate these systems later, this result supports our hypothesis that cell-free protein expression systems will be compatible with this membrane composition.

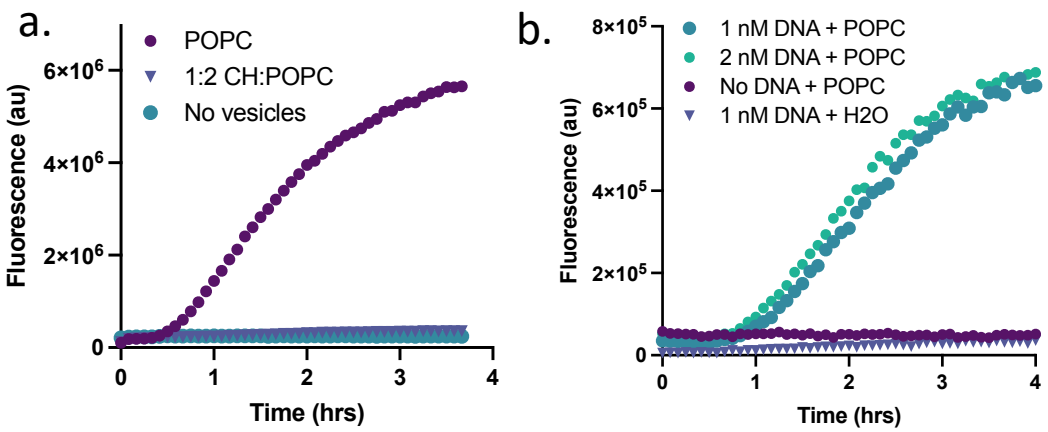

Figure 2.6 Expression of crcB into membranes in bulk conditions. A. crcB does not express in the absence of vesicle membranes or in the presence of cholesterol-containing membranes. **B**. crcB expresses well at 1 nM and 2 nM DNA concentration into POPC membranes but does not express in the absence of vesicles. Little background is observed in the absence of DNA.

Taken together, these results indicate that membrane properties can be modulated by altering membrane composition, particularly by incorporating diblock copolymers or cholesterol into the membrane. These membrane properties do not vary significantly depending on vesicle formation method, specifically electroformation or double emulsion methods, and they do not vary significantly in the presence of the variety of small molecules present in cell-free protein expression buffers. Finally, area expansion moduli remain consistent following the expression and localization of a small membrane protein, crcB, indicating that these membranes are compatible with and robust to cell-free protein expression reactions.

2.4 Conclusions

In considering membrane formation and properties, the individual lipids and other amphiphiles within the membrane exhibit considerable influence on the final features of the

resulting structure. Membrane composition plays a number of important roles in cellular processes, however it is a key factor by which membranes can be regulated independently from contributions from other cellular components or biomolecules. Amphiphiles themselves play a critical role in not only assembling into bilayer membranes but in modulating their structure, which can laterally organize membrane components and can regulate which molecules can and cannot pass through the membrane. The shape of each amphiphile dictates morphology of these assemblies as well as certain intrinsic features, such as bending and stiffness. Finally, the nature of these amphiphiles can modulate the response of the overall structure to external force, imparting a significant change to elasticity and robustness. These impacts are seen not only in cellular systems but in relatively minimal model membranes, and as such the composition of model membranes can serve as an important handle by which features of the membrane can be modulated.

Towards applying model membranes for technological uses, and particularly towards their use in nano- and microscale sensors, these features provide opportunities to regulate intermolecular interactions, to better contain and protect encapsulated components, and to create robust compartments that can travel through complex environments with improved stability. By understanding the ways in which membranes can be engineered to control these parameters, we can introduce new functionality to sensors which incorporate bilayer membranes – both naturally-inspired and synthetic. Perhaps more importantly, we can anticipate tradeoffs in permeability, organization and stability that arise in multi-component membranes and which may have a significant impact on processes requiring tightly regulated conditions, such as cell-free protein expression.

Chapter 3: Sensing forces and lipid uptake in synthetic vesicle membranes through the combinatorial use of optical dyes

3.1 Foreword

An important feature of bilayer membranes is their ability to change dynamically over time. As a cohesive structure composed of amphiphilic monomers, bilayer membranes can stretch, bend, and compress, and monomers can diffuse laterally. In addition, when under force, lipid membranes can take up or expel additional lipids to accommodate these forces and avoid rupture. In using membranes to design new types of vesicle-based sensors, it would therefore be highly beneficial to first understand the response of the membrane to various forces that might be encountered in a sensing application. In particular, it would be useful to understand the response of bilayer membranes to changing osmotic conditions – a scenario likely to be encountered in sample-based sensing applications.

While various techniques exist to assess membranes under force, including micropipette aspiration and optical tweezers, these strategies are invasive and require physical contact with the membrane. These approaches can be highly sensitive, however they are limited by their inability to assess membranes in bulk and the requirement for a physical interface with the membrane. For this reason, we first sought to develop an optical method to assess the changes in bilayer membranes under force, specifically membrane tension, and to characterize the effect of these forces on subsequent amphiphile uptake. This chapter was adapted from the following publication:

Boyd, M. A. & Kamat, N. P. Visualizing Tension and Growth in Model Membranes Using Optical Dyes. *Biophys J* 115, 1307-1315, doi:10.1016/j.bpj.2018.08.021 (2018).

Publication was featured by the *Biophysical Journal

3.2 Introduction

Mechanical properties of the bilayer membrane play a vital role in information transfer in cells, driving complex behaviors independent of biochemical processes.[6,7,11] Membrane tension, in particular, is increasingly thought to regulate a variety of cellular processes, including opening stretch-activated ion channels,[86,87] localizing membrane components through phase segregation and changes in curvature,[88-92] and changing the dynamics of cytoskeletal polymerization,[11,93,94] all of which subsequently influence cellular growth and motility.[5,7,10,70,95,96] Despite growing evidence for tension as an important regulator of cellular behavior, the mechanism by which cells sense and respond to membrane tension remains largely unknown.

Recent evidence suggests that simple physical principles may play an important role in guiding how the membrane initially responds to tension.[9] Membrane tension, which refers to the force needed to stretch the membrane in-plane,[97] has been observed to result in four primary responses in cellular and model membranes: membrane stretching, membrane rupture, membrane reservoir depletion, and insertion of additional lipids into the bilayer.[98] These responses indicate an important relationship between membrane tension and lipid exchange. In support of this idea, recent observations in both model and cellular systems have suggested that the lipid bilayer maintains a constant lipid density.[6,9] This guiding physical principle could help explain cellular processes such as surface area regulation during cell migration and synapse fusion.[5,6,99,100] In order to uncover the nature of this relationship and to explore its role in other biophysical membrane processes, it would be useful to monitor changes in membrane surface area and tension in real time.

A roadblock in the path to understanding the interplay between membrane strain and surface area is the lack of a reliable quantization method that measures both simultaneously. Traditional methods to measure physical membrane changes, like optical tweezers and micropipette aspiration, involve direct manipulation of the membrane, where an applied force can be used to analyze changes in membrane properties.[74,101-105] These methods often require a single cell or vesicle to be analyzed at a time. Importantly, they are unable to spatially resolve differences in mechanical properties that may emerge across a single membrane. Optical probes can serve as force sensors, and provide a useful route to monitor cellular dynamics in that they allow the non-mechanical examination of particles at both the individual and population level.[106,107] Another useful feature of optical probes is that they can monitor different structural components (ex. located at the interface or interior of a system) in order to provide spatially distinct information, which can then be integrated to gain a better idea of the response of the system as a whole. Despite these distinct advantages, the use of optical dyes to measure strain in membranes and polymeric materials has been limited.[108-110]

Here, we introduce the combinatorial use of two types of optical probes that are localized to distinct regions of a bilayer membrane to monitor membrane dynamics under tension. Using lipid vesicles as a simple model cellular system, we induce membrane tension through subjection to osmotic pressure. We then use these probes to observe a process that is expected to be important in tension sensation, namely the enhanced uptake of lipids by membranes under tension. Finally, we demonstrate the compatibility of our selected probes with microscopy techniques, which allows us to optically track changes in membrane tension and surface area during lipid uptake on a single vesicle level.

3.3 Materials & Methods

Chemicals

DOPC (18:1 (Δ9) 1,2-dioleyoyl-sn-glycero-3-phosphocholine, 25 mg/mL), Cy 5.5 PE (1,2-dioleoyl-sn-glycero-3-phosphoethanolamine-N-(Cyanine 5.5), Cy 7 PE (1,2-dioleoyl-sn-glycero-3-phosphoethanolamine-N-(Cyanine 7), and Lissamine-Rhodamine PE (18:1 1,2-dioleoyl-sn-glycero-3-phosphoethanoamine-N-(lissamine rhodamine B sufonyl) (ammonium salt) stock solutions in chloroform were obtained from Avanti Polar Lipids Inc., Alabaster, AL. NBD PE (NBD-phosphoethanolamine, triethylammonium salt) and Calcein dye were obtained from Thermo Fischer, Waltham, MA. Laurdan (6-Dodecanoyl-N,N-dimethyl-2-naphthylamine, 176.8 mg/mL) was obtained from Invitrogen (Thermo Fischer, Waltham, MA). Phosphate-buffered Saline (PBS) and sucrose were obtained from Sigma Aldrich, St. Louis, MO.

Vesicle Preparation

Small unilamellar vesicles were prepared through the thin film hydration method. 20 mM DOPC in chloroform was mixed with either 0.5 mol% Laurdan and/or 0.1 mol% FRET dye pairs (FRET pairs: Cy5.5/Cy7, Lissamine-Rhodamine/NBD). For each FRET pair a standard curve was generated by adding 0.025, 0.05, 0.1, 0.125, 0.175 and 0.2 mol% of each dye pair to DOPC. Films were dried down to a uniform film on the inside of a glass vial. DOPC in chloroform was also dried down with no dye addition to generate unlabeled films for Calcein assays. Film dehydration was followed by evaporation under vacuum for 5 hours. Evaporated films were hydrated with 1000 mOsm PBS for at least 2 hours at 60ºC, followed by brief vortexing and extrusion through 30, 50, 100 or 400 nm polycarbonate filters (Avanti Polar Lipids, Inc.) to 7

passes. For calcein leakage studies, unlabeled DOPC films were hydrated in 1000 mOsm PBS with 20 mM Calcein dye, extruded, and purified through a size exclusion column to remove unencapsulated dye. A 1000 mOsm PBS running buffer was used to maintain vesicle osmolality. Giant unilamellar vesicles (GUVs) were prepared through electroformation using the Nan]i[on Vesicle Prep Pro (Nanion Technologies, GmbH). 40 µL of 5 mM DOPC films with incorporated dyes were dried on to the conductive side of the Nan]i[on slides. A medium O-ring was coated with microscope grease and placed around the dried film. 200 µL 285 mOsm sucrose was added inside of the O-ring, and the second conductive slide was placed over top. The standard vesicle prep protocol was run for 120 minutes. A GUV standard curve was also generated through electroformation by adding 0.025, 0.05, 0.1, 0.125, 0.175 and 0.2 mol% of each dye pair to DOPC GUV films.

Fluorescence Spectroscopy

Spectroscopic measurements were gathered using a Cary Eclipse Fluorescence Spectrophotometer (Agilent Technologies, Santa Clara, CA). Full emission spectra were obtained for Laurdan (**Figure 3.1 A**), NBD PE/Lissamine-Rhodamine PE FRET and Cy 5.5/Cy 7 FRET (**Figure 3.2 A & B**). FRET emission spectra were obtained by exciting the dye pair at the donor excitation wavelength and measuring emission intensity across both the donor and acceptor ranges. Spectra were used to determine maximum emission wavelengths for subsequent kinetic scans. Laurdan fluorescence was excited at 350 nm and emission was measured at 439 and 483 nm. NBD PE/Lissamine-Rhodamine PE FRET fluorescence was excited at 463 nm and emission was measured at 517 and 590 nm. Cy 5.5 PE/Cy 7 PE FRET fluorescence was excited at 675 nm and emission was measured at 713 and 775 nm. Calcein fluorescence was excited at

495 nm and emission was measured at 515 nm. Membrane hydration level was analyzed by calculating the change in generalized fluorescence polarization (GP) of Laurdan (**Figure 3.1 B**) through the following formula as characterized by Gratton et al.:[111]

$$GP = (I_{439} - I_{483})/(I_{439} + I_{483}) \quad \textbf{(3.1)}$$

Vesicles under tension were compared to isotonic controls to eliminate the effect of dilution on fluorescent signal (**Figure 3.1 C**).

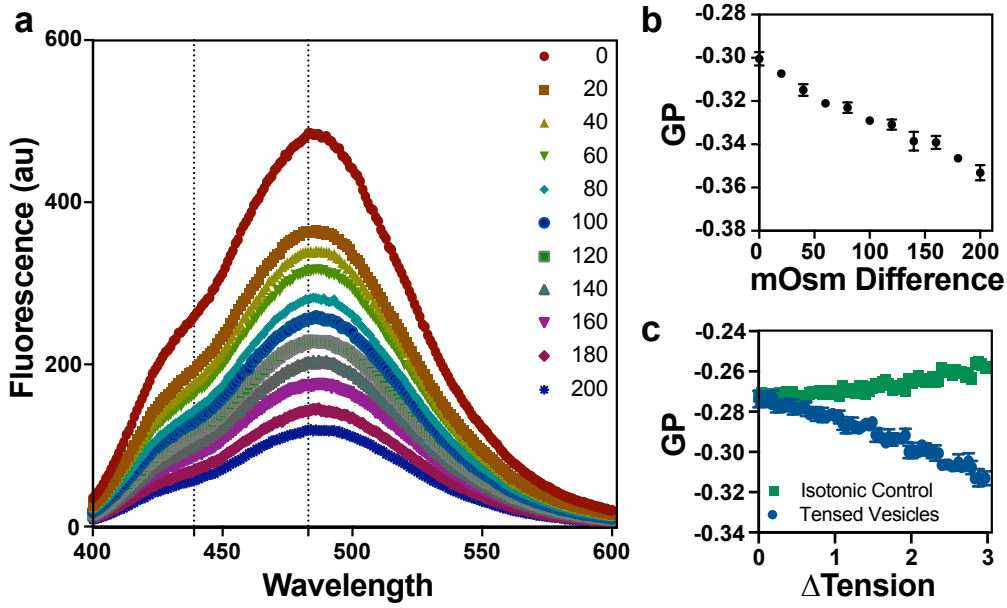

Figure 3.1 Changes in Laurdan emission spectra as induced tension increases. A. Representative full Laurdan emission spectra indicating fluorescence shifts over an osmolarity difference of 200 mOsm (285 to 85 mOsm). Each curve shows the full spectrum for a given osmolarity difference as marked in the legend. Dotted lines indicate the wavelengths used to calculate GP values (439 nm, 483 nm). **B.** Representative GP values calculated from the spectra in A. **C.** To control for the effects of dilution (as shown by the intensity decrease in A) tensed samples were compared to GP values for isotonic control samples.

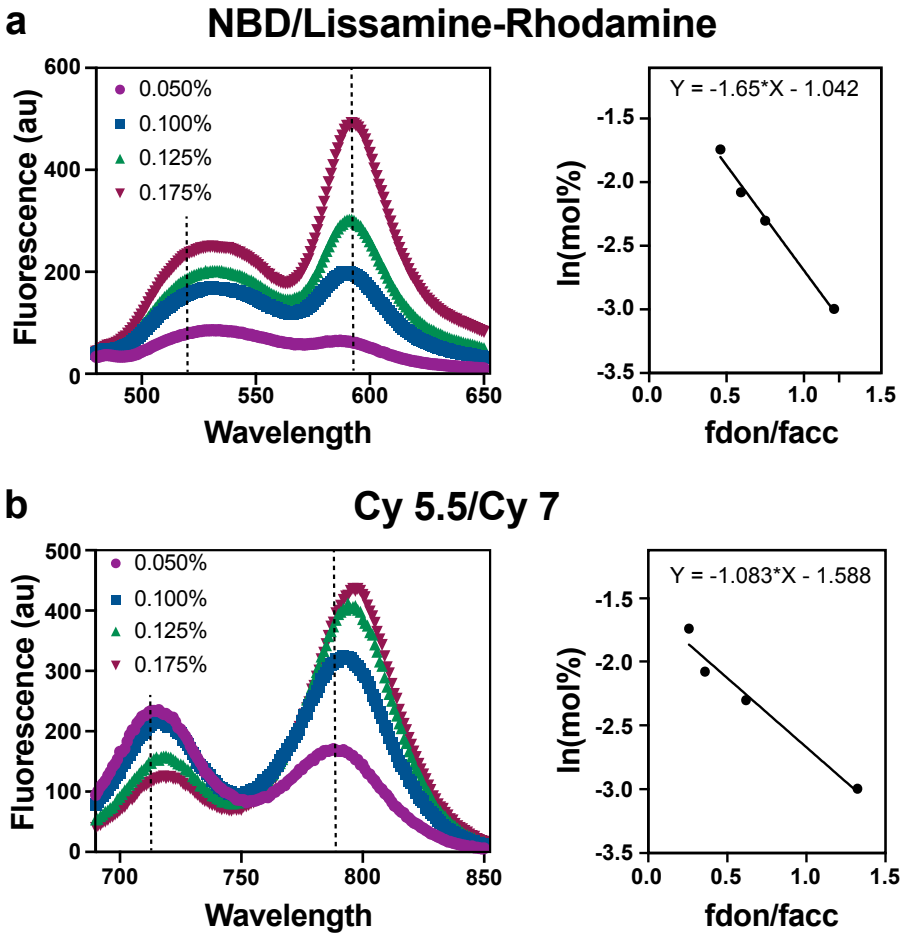

Figure 3.2 FRET spectra for various dye concentrations. A. Representative spectra of four mol% concentrations of NBD/Lissamine-Rhodamine FRET pairs and the subsequent standard curve generated from these spectra. The first peak represents the donor emission, and the second peak represents the acceptor emission. Dotted lines indicate the wavelengths at which FRET ratios were calculated for the standard curve and for experimental results reported in the article (517 nm, 590 nm). **B.** Representative spectra of four mol% concentrations of Cy5.5/Cy7 FRET pairs and the subsequent standard curve generated from these spectra. Dotted lines similarly indicate the wavelengths at which FRET ratios were calculated (713 nm, 780 nm). For both FRET pairs, standard curve equations were used to calculate surface area changes from fluorescence data.

Forster Resonance Energy Transfer (FRET) ratios were generated by taking the fluorescence of the donor molecule over the fluorescence of the acceptor molecule, as:

$$\text{FRET efficiency} = f_{donor} / f_{acceptor} \quad \textbf{(3.2)}$$

FRET fluorescence intensities were compared to standard curve samples to translate changes in fluorescence intensities into surface area calculations. Changes in surface area (ΔSA) reflect the changes in lipid density (**Figure 3.2**):

$$\Delta SA = (\text{mol\% dye}_{init}/\text{mol\% dye}_{final})_{exp} - (\text{mol\% dye}_{init}/\text{mol\% dye}_{final})_{control} \quad \textbf{(3.3)}$$

Osmotic Swelling of Vesicles

To confirm the ability of Laurdan and FRET dyes to report changes in membrane tension and surface area respectively, dye-labelled vesicles were exposed to hypotonic conditions induced by dilution with DI H_2O. Dilutions were carried out sequentially by 50 mOsm increments with DI H_2O additions every 2 minutes over an osmolality difference of 750 mOsm. To generate higher tensions, films were originally hydrated in 1444 mOsm PBS. It is important to note that sample volume limitations in these experiments prohibited us from obtaining the same total degree of the expected induced tension for each vesicle population, as, according to the LaPlace Law, smaller vesicles experience significantly less tension due to a given change in osmolality compared to larger vesicles. Isotonic controls were generated by exposing vesicles to isotonically matched PBS at the same rate as hypertonic studies. A relative value for the induced tension was calculated as:

$$T \approx (r \cdot \Delta P)/2 \quad \textbf{(3.4)}$$

where ΔP is the osmotic pressure resulting from the induced osmotic differential and r is the estimated radius after extrusion. ΔP was estimated from change in molarity as:

$$\Delta P = \Delta M \cdot RT \quad \textbf{(3.5)}$$

where R is the ideal gas constant and T is the temperature in Kelvin. The change in osmolality for PBS was calibrated with an osmometer, and was found to be related to ΔM as $\Delta\ \mathrm{mOsm/kg} = 0.00007\ \Delta M$. Vesicles swell under osmotic pressure, therefore areal expansion was determined through FRET-based observations of surface area changes. Surface area was observed to increase linearly by 0.4% per 50 mOsm change. The resulting radius changes were incorporated into calculations of estimated tension.

Response to Excess Lipid

To explore the response of Laurdan and FRET dyes during the uptake of excess lipid, oleic acid micelles were added to tensed and untensed vesicles. An oleic acid micelle stock solution was prepared with 100 mM oleic acid in 100 mM NaOH. Vesicles were diluted to an osmolality difference of 300 mOsm in 50 mOsm increments as described above, at which point oleic acid micelles were added at a ratio of 1:1 vesicles:micelles. Fluorescence was monitored for 20 minutes. An equivalent volume of NaOH was added without micelles to a control population of tensed vesicles to determine the effect of NaOH alone.

Microscopy

GUVs were observed under the microscope to analyze fluorescence changes over time. Glass bottomed Lab-Tek® II microscope chambers (Thermo Fischer, Waltham, MA) were prepared by blocking with 150 µL Bovine Serum Albumin (1 mg/mL in PBS) for 5 minutes,

followed by a 3X rinse with 285 mOsm PBS. Chambers were filled with 150 uL of 285 mOsm PBS. 1 µL of 1 mM GUVs in an equiosmolar solution of sucrose was added and mixed thoroughly by pipetting up and down. For dilutions, a syringe pump was used to add 350 µL DI H_2O to the chamber at a rate of 0.25 mL/min. Laurdan fluorescence was observed for 30 min after dilution with this volume. For surface area assays, 1 µL OA micelles in NaOH were added to vesicles and fluorescence of the donor and acceptor was monitored for 30 minutes. To minimize photobleaching of both types of dyes, images were taken every 2 minutes at 5% light intensity. Laurdan was excited at 350 ± 25 nm and emission was measured at 445 ± 15 and 525 ± 25 nm. NBD and Rhodamine-Lissamine were excited at 470 ± 20 nm and emission was measured at 525 ± 25 nm for NBD and 620 ± 30 nm for Rhodamine-Lissamine. Cy 5.5 and Cy 7 were excited at 650 ± 22.5 nm and emission was measured at 720 ± 30 nm for Cy 5.5 and 810 ± 45 nm for Cy 7. All microscopy work was done on a Nikon Ti2 Microscope.

FRET and Laurdan analysis of Microscopy Data

All image analysis was done through Nikon VIS software. FRET and Laurdan general analysis protocols were created to select regions of interest localized to the membrane for fluorescence analysis. Frames were subjected to rolling ball correction (radius = 1.95 µm) and local contrast correction (size = 25, power = 10%) for background subtraction. Regions of interest were selected for intensity between 131 and 1638, size (in µm) between 8.62 and 24.49, and circularity between 0 and 0.16. These parameters were set manually, and analyzed the entire frame for the selection of vesicle membranes specifically. The parameters returned by the software include intensity of each frame for each region as well as the ratio of $f_{donor}/f_{acceptor}$ for each FRET pair. Laurdan GP was calculated manually based off

fluorescence intensities. Experimental populations were compared to control populations in which no tension was induced and no micelles were added, as differential photobleaching of the dyes leads to decreasing ratio over time. For this reason, changing FRET and GP values are reported as a relative value compared to this control, where, for each frame:

$$\text{Relative FRET} = \text{avg experimental } f_{donor}/f_{acceptor} - \text{avg control } f_{donor}/f_{acceptor} \quad \textbf{(3.6)}$$

$$\text{Relative GP} = \text{average experimental GP} - \text{average control GP} \quad \textbf{(3.7)}$$

As with SUVs, standard curve samples of GUVs with FRET dyes were analyzed to calibrate fluorescence ratio as a function of known dye concentration for FRET studies.

3.4 Results and Discussion

3.4.1 Laurdan dyes report changes in membrane tension

Membranes under tension stretch, which can lead to changes in both the chemical and physical properties of the bilayer. For example, a stretched membrane will allow water molecules to enter the hydrophobic interior (**Figure 3.3 A**), changing the chemical environment of the membrane. Simultaneously, the average distance between membrane lipids also increases, changing the physical properties of the membrane (**Figure 3.3 B**). By incorporating optical probes into a membrane that respond to both types of membrane changes, we hypothesized that we could optically track changes in membrane tension.

Laurdan is a polarity-sensitive, amphiphilic fluorophore that is nonpolar and can be incorporated into the hydrophobic region of a bilayer membrane.[112] When excited by incident

light, the molecule undergoes a dramatic charge separation, creating a strong dipole. Dipole coupling between Laurdan and nearby water molecules in the hydrophobic region of the bilayer results in a large Stokes shift, viewed as a red-shift in the emission spectrum in polar solvents (**Figure 3.3 A**).[112,113] Laurdan has been used previously to monitor changes in membrane bending, hydration, and domain formation, the first two of which can indicate changing membrane tension in single-lipid systems.[112-114] Given the relationship between these processes, we wanted to explore the capability of Laurdan to report changes in membrane tension through shifts in fluorescence.

We prepared model membrane vesicles composed of DOPC containing 0.5 mol% Laurdan within the hydrophobic core of the membrane. Vesicles were prepared and extruded through polycarbonate filters resulting in vesicles with an average diameter of 100 nm. This method has been well characterized to result in relatively homogenous populations of vesicles with an error of about ± 10 nm.[115] The hydration-induced emission shift of Laurdan can be quantitatively reported through a ratiometric method by calculating the generalized polarization, or GP, using Equation 3.1.[111,112] This value decreases as Laurdan is exposed to increasingly polar environments, such as nearby water in the hydrophobic region of the bilayer. We applied membrane tension by subjecting each population of vesicles to increasing osmotic pressure at a constant rate of 25 mOsm per minute and monitored the resulting change in GP value using a fluorimeter.

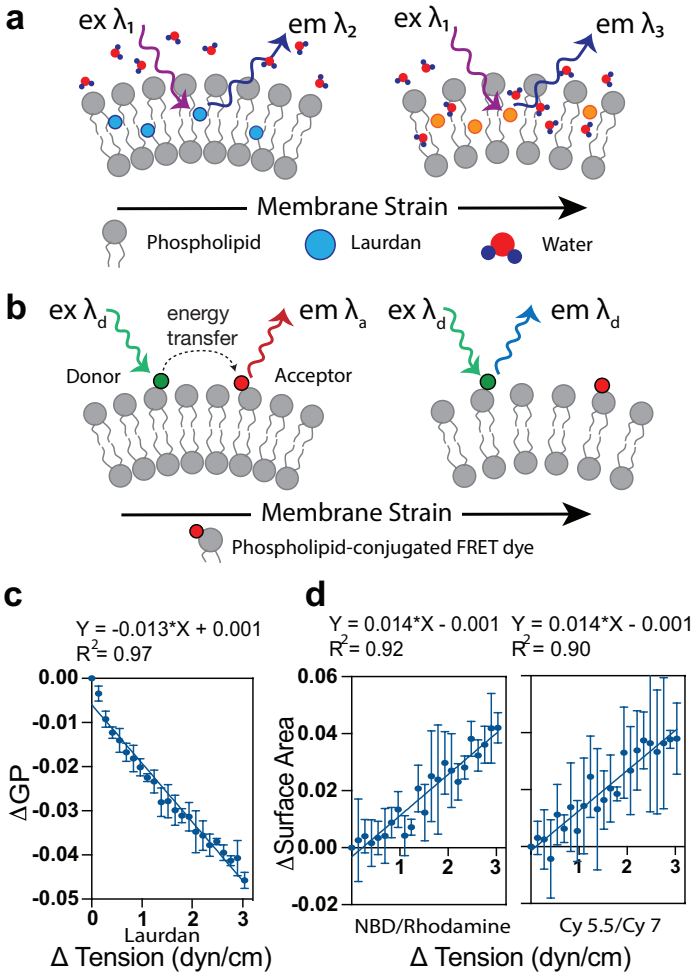

Figure 3.3. Laurdan dyes and FRET pairs report changes in membrane tension in response to osmotic pressure. Schematic of the behavior of encapsulated Laurdan **A.** and phospholipid-labeled FRET-probes **B.** in a bilayer membrane under osmotic stress. Changes in membrane hydration and lipid density that accompany membrane stretching are expected to shift the fluorescence of Laurdan and FRET efficiency between lipid-conjugated dyes, respectively. **C.** 100 nm vesicles containing Laurdan exhibit a linear change in GP between 0 to 3 dyn/cm. ΔGP reflects the GP value in tensed vesicles with respect to initial GP values. **D.** 100 nm vesicles with lipid-conjugated FRET dyes report linear increases in relative surface area as vesicles swell under osmotic pressure. Surface area changes were calculated from a standard curve (**Figure 3.2**). Similar slopes between GP and both FRET responses indicate similarly scaled responses to tension. n= 3 samples of SUV vesicles; error bars represent standard deviation.

We observed linearly decreasing GP values with increased osmotic pressure (**Figure 3.3 C**). These results agree with those reported by Zhang et al., who observed a decrease in GP value as small unilamellar vesicles were exposed to increasing osmotic differentials.[113] By expanding this analysis to explicitly determine the relationship between GP value and membrane tension, we can better assess the suitability of Laurdan fluorescence as a probe for membrane tension. Osmotic pressure is directly proportional to induced tension, and scales as $T \approx r \cdot \Delta P/2$ (Equation 3.4), where r is the vesicle radius and P is the osmotic pressure.[113] We observed that GP values decreased relatively linearly with increasing membrane tension. This result was consistent for vesicles of various sizes, supporting the candidacy of Laurdan as a membrane tension probe (**Figure 3.4 A**). Importantly, the slope of this curve is highly dependent on vesicle size, which we attribute to the higher curvature and greater change in area per lipid for smaller vesicles that occurs for a given osmotic pressure change.[113,116] As a result, the rate of change in GP value with applied tension increases as the average vesicle size decreases (**Figure 3.4 B**).

We next examined the range of tensions that could be reliably detected with Laurdan by examining the linear range of ΔGP versus tension and analyzing content leakage as tension increased. When vesicles were exposed to increasing levels of osmotic pressure, the GP response was initially linear as expected. As tension surpassed 6 dyn/cm, however, a plateau in GP value was observed (**Figure 3.4 C**). At these higher tensions, samples are diluted in a large volume of either PBS or DI H_2O, so it is likely that the Laurdan signal/noise ratio is low (~0.7 mM Laurdan) in the final solution. We normalized experimental populations to isotonic controls to adjust for this change as well as any other light scattering effects. We also explored the effect of membrane lysis on Laurdan fluorescence. The lytic tension of DOPC vesicles has been reported

to be 9.9 ± 2.6 dyn/cm, so it is likely that vesicle lysis also contributes to the plateau in GP values we observe.[117] Lipid vesicles relieve high levels of osmotically induced membrane tension through a process of pore formation, intravesicular solute release, and membrane resealing.[89,118-120] This lytic process is expected to result in the release of some degree of membrane tension, and subsequent shifts in Laurdan fluorescence would not be expected to precisely report the total change in membrane tension from the initial unstressed state of the vesicle. To determine the tension at which vesicle lysis begins, we performed a content leakage assay by encapsulating calcein, a self-quenching fluorescent dye. Increasing levels of content leakage were observed at tensions above 1.75 dyn/cm, indicating that membrane pore formation and tension release occurs above this threshold tension in our system (**Figure 3.4 D**). Interestingly, a slight shift in the slope of ΔGP versus tension (**Figure 3.3 C**) can also be observed around this tension, indicating membrane relaxation is accompanied by shifts in Laurdan fluorescence. Together, these studies identify the range over which Laurdan GP values can be used to reliably track changes in membrane tension.

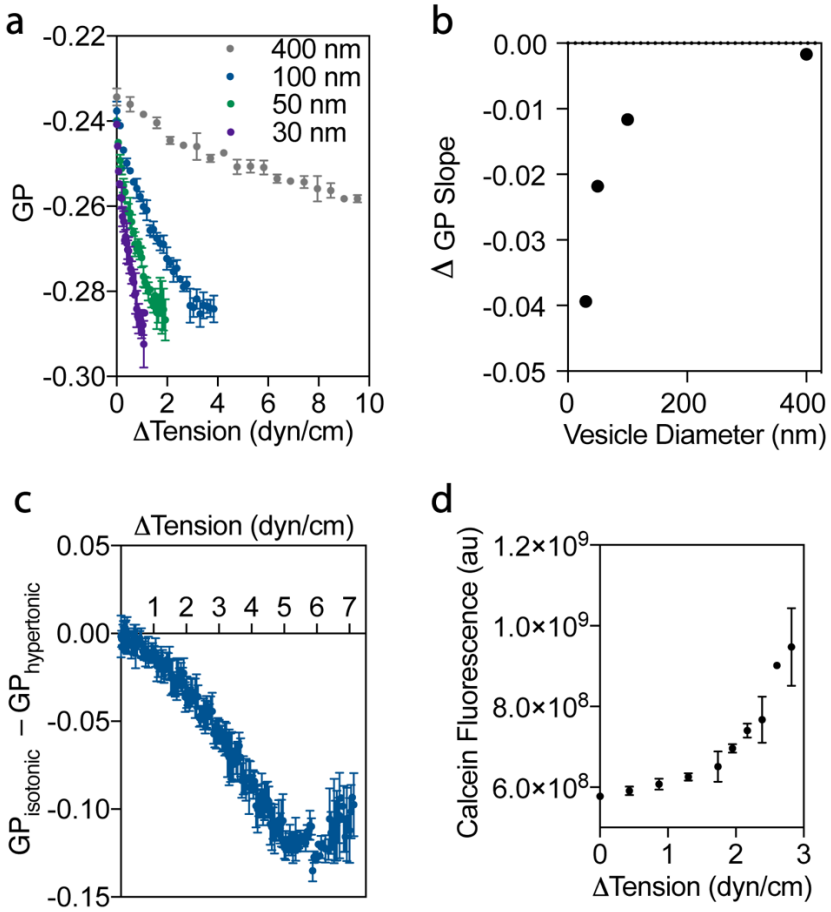

Figure 3.4 Characterization of GP value and tension. A. The GP value of Laurdan encapsulated in vesicle membranes of different sizes decreases as osmotically-induced tension increases. *n=3* samples of SUV vesicles, error bars represent standard deviation. **B.** As vesicle size increases, the magnitude of the changes in Laurdan GP value for a given tension change decrease. We expect this effect is due to the fact that larger vesicles have lower initial bending curvature and subsequent changes in membrane tension result in more gradual separation of hydrophilic head groups in comparison to small-diameter vesicles, indicating that membrane curvature strongly impacts Laurdan fluorescence. **C.** The relative GP of Laurdan in 100 nm vesicles is shown with respect to isotonic controls across a wider range of membrane tension. GP fluorescence shifts are relatively linear until 5 dyn/cm is reached, at which point fluorescence plateaus. *n= 3* samples of SUV vesicles; error bars represent standard deviation. **D.** Content release assays using self-quenching calcein dye indicate observable increases in content release from vesicles with induced membrane tensions above 1.5 dyn/cm. Content release likely

correlates to the initiation of the lytic process, which relieves some degree of tension through pore formation, content leakage, and membrane resealing. *n = 3* samples of SUV vesicles, error bars represent standard deviation.

3.4.2 FRET dyes report changes in membrane surface area under tension

As membranes stretch under tension, the distance between bilayer lipids should increase. In order to confirm that the optical changes in GP value were due to membrane tension, we turned to a second optical method that would allow us to monitor the areal expansion of vesicle membranes under osmotic pressure (**Figure 3.3 B**). We incorporated lipid-conjugated Förster Resonance Energy Transfer (FRET) dye pairs, which convey information about changes in inter-probe distance.[121] FRET describes the nonradiative transfer of energy from an excited fluorescent donor molecule to a corresponding acceptor molecule.[121,122] FRET between two fluorescently tagged phospholipids can therefore be used to monitor real-time changes in membrane surface area.[121,123] While FRET between phospholipid-labeled dyes has traditionally been used to measure large changes in membrane surface area that accompany the uptake of unlabeled lipid molecules into a vesicle membrane,[123] we hypothesized that this technique could also report small changes in inter-probe distance due to stretching of the lipid membrane (**Figure 3.3 B**).

We prepared DOPC vesicles containing varying amounts of lipid conjugated to donor (NBD-PE) and acceptor (Rhodamine-Lissamine-PE) dyes and measured the FRET efficiency as a function of dye concentration to generate a standard curve (**Figure 3.2**). This curve was then used to calibrate changes in FRET efficiency to changes in membrane surface area during osmotic swelling. We observed a small linear increase in membrane surface area as tension

increased, which was observed to be similar in rate to the Laurdan GP response (**Figure 3.3 C & D**). We then examined whether this response was reproducible with a second FRET pair. Near IR FRET pairs are less commonly used, but have excitation spectra that do not overlap with the Laurdan emission spectrum. This feature is attractive for our application as it would allow simultaneous measurement of both Laurdan and FRET probes with minimal co-excitation. Both sets of FRET pairs reported a similar change in membrane surface area in response to applied tension, as is shown in the slopes of both curves (**Figure 3.3 D**). These optical measurements illustrate the ability of FRET pairs to report minor spatial changes in the lipid density of vesicle membranes, allowing the detection of processes as subtle as osmotic swelling. Similarly, these results show that linear changes in Laurdan GP values correspond roughly with changes in surface area, indicating that in combination, both types of optical probes can provide a more detailed view of membrane tension and corresponding surface area changes.

A further benefit of our FRET-based quantification of areal expansion is that it allows us to estimate the vesicle size as osmotic pressure increases. Because our estimation of tension from the LaPlace law is dependent on vesicle radius, the values of membrane tension reported in our study were calculated using FRET-derived data to account for changes in vesicle radius. Additionally, areal expansion data allows us to estimate the elastic modulus of our vesicles. Based on the relationship between surface area changes (which can be converted to membrane strain) and tension presented in Figure 3.3, we calculate an elastic modulus of 70 dyne/cm. Reported values of DOPC elasticity range from 63 to 340 dyne/cm depending on the type of buffer used for hydration.[73,124,125] Our estimate of elastic modulus falls within this range, supporting the quantitative capability of our optical approach.

3.4.3 Laurdan and FRET dyes can be used simultaneously to observe tension-mediated membrane growth.

We next wondered if these two distinct optical methods could be used to address an important question in membrane tension studies, namely: does lipid uptake relieve membrane tension? One approach to answering this question is to determine if membranes under tension take up more lipid than their less-tensed counterparts. Model membrane systems provide an opportunity to isolate the tension-growth relationship from biochemical contributions, such as protein-mediated lipid transport, and are therefore well suited to this type of study.

In order to observe fluorescent responses to the uptake of excess lipid, we added oleic acid micelles to tensed and untensed vesicles (**Figure 3.5**). Oleic acid micelles insert spontaneously into phospholipid membranes, driven through hydrophobic interactions,[126] and are therefore expected to lead to some level of membrane growth even in the absence of tension. Figure 3.5A provides an experimental schematic illustrating the two phases of these experiments: (1) first, a tension-inducing regime is initiated in which vesicles were exposed to a hypo-osmotic or isotonic solution, (2) followed by the addition of excess lipid in the form of oleic acid micelles. We monitored both Laurdan GP and FRET efficiency in vesicle membranes to determine if they could concurrently report changes in membrane tension and membrane surface area that accompany micelle uptake in tensed vesicles. Laurdan GP values changed during both membrane tension and micelle exposure. As membrane tension increased in Laurdan-labeled vesicles, GP values decreased as expected (**Figure 3.5 B, blue**). Upon the addition of micelles, GP values were observed to recover to a degree in tensed vesicle populations. In contrast, the

addition of an NaOH solution used to prepare the micelles did not lead to recovery, indicating that the change in GP values during micelle uptake was due to the interaction of oleate with the vesicle membrane.

Non-tensed control vesicles also demonstrated an increase in GP value upon micelle addition as expected, though this increase was slower and of a smaller magnitude (**Figure 3.5 B, green**). Our observations of this control population indicate that the introduction of oleic micelles to the membrane contributes to the change in GP value, likely due to a chemical shift in the membrane. We therefore attribute the partial recovery of Laurdan GP values in experimental populations to a combination of tension relief, changing chemical composition in the membrane and relaxation time of the membrane.

We next examined how membrane surface area changed in response to micelle addition. Exposure to osmotic pressure led to small increases in the FRET-determined surface area as vesicles swelled, as previously discussed. When micelles were added to both tensed and un-tensed vesicle populations, a higher rate of micelle uptake was observed in tensed vesicles (**Figure 3.5 C**). After fitting the initial uptake phase through an exponential association model in MATLAB, we obtained growth rates of $k = 1.097/\text{min}$ for tensed vesicles and $k = 0.928/\text{min}$ for untensed vesicles. Tensed vesicles also exhibited a greater total change in surface area in comparison to isotonic controls. Our results with phospholipid vesicles agree with studies of monoacyl fatty acid vesicles, which have also been shown to uptake fatty acid micelles under tension in model systems.[127] These results indicate that tensed vesicles uptake excess lipid at a faster rate, incorporating micelles more quickly and in greater amounts. Further, our results support the idea that the addition of excess lipid mitigates applied membrane tension.

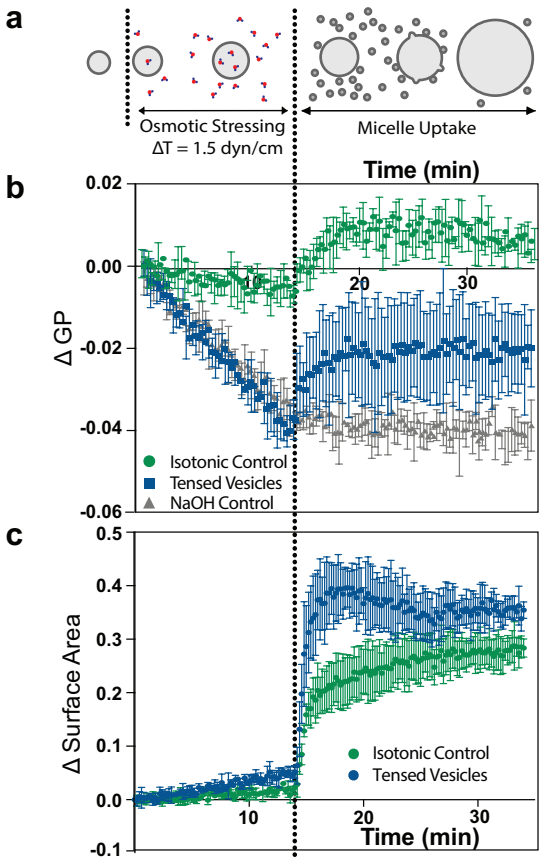

Figure 3.5 Response of Laurdan and FRET fluorescence in osmotically stressed vesicles before and after addition of oleic acid micelles. A. Experimental schematic indicating the tension inducing regime through hypotonic stress from t=0 to t=14 min, followed by the micelle uptake regime from t=14 to t=36 min. **B.** Laurdan-labeled vesicles under osmotic tension exhibit linearly decreasing GP values as vesicles are exposed to hypo-osmotic solutions, followed by a partial recovery of GP value following oleate micelle addition. Vesicles subjected to an isotonic control (green) or the NaOH buffer used to prepare micelles (grey) are shown in comparison. **C.** The effect of osmotically induced membrane tension on membrane surface area was explored with FRET (NBD/Rhodamine)-labeled vesicles. Tensed vesicles showed a higher rate of surface area increase than non-tensed vesicles during the initial phase of micelle uptake (k = 1.097/min and k=0.928/min respectively), as well as a greater total surface area change. *n= 3* SUV vesicle samples; error bars represent standard deviation.

3.4.4 Optical probes enable single-vesicle studies with microscopy

A major advantage of optical methods is their potential compatibility with microscopy techniques, which allows the visualization of spectral changes in fluorescent molecules with high spatial resolution and on a single particle level. We therefore set out to investigate whether probes used in the current study could be used to visualize membrane tension and membrane surface area changes on a single vesicle level. DOPC giant unilamellar vesicles (GUVs) with Laurdan and Cy 5.5/Cy7 FRET dyes were formed via electroformation in 300 mOsm sucrose. We used ratiometric microscopy by installing band-pass filter sets into an inverted fluorescent microscope, which enabled the detection of light in distinct spectral regions. This allowed quantification of both the spectral shift of Laurdan molecules and the relative FRET efficiency of the two FRET pairs used in this study. As shown in Figure 3.6 A, fluorescence from all probes is localized to the membrane in each population of GUVs.

GUVs were observed under the microscope during the processes of dilution or micelle addition. Samples were either diluted in water or micelles were added between minutes 1 and 5 to impose membrane tension or membrane growth, respectively. We calculated GP values from observed spectral shifts in Laurdan, and observed that Laurdan GP decreased with increasing tension in populations exposed to osmotic stress (**Figure 3.6 B**). The changes in GP observed via microscopy were similar in scale to those observed in SUVs. A standard curve was also generated (**Figure 3.7**).

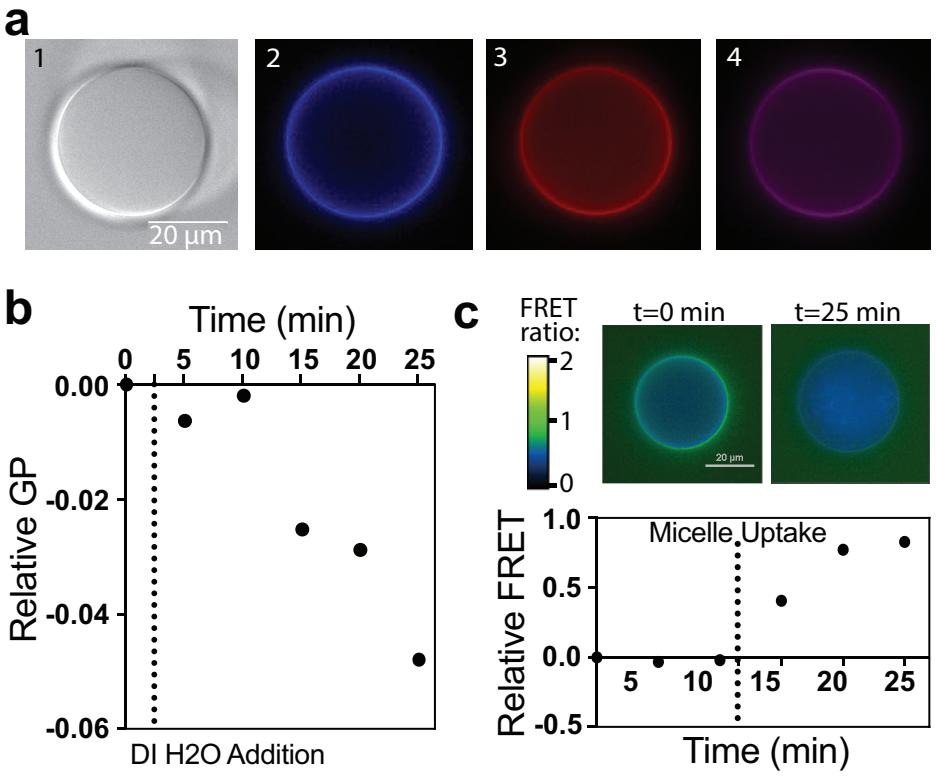

Figure 3.6 Optical probes enable detection of surface area and tension changes using fluorescence microscopy. A. DOPC vesicles containing membrane dyes are imaged via fluorescence microscopy and show (1) DIC, (2) Laurdan fluorescence, (3) Cy 5.5 fluorescence and (4) Cy 7 fluorescence. **B.** Representative curve showing that Laurdan GP values decrease as GUVs are exposed to osmotic pressure relative to vesicle exposed to an isotonic solution. **C.** FRET between Cy5.5 and C7 –labeled phospholipids is detected via microscopy. Pseudo-coloring indicates different FRET efficiencies detected across the image. Decreasing FRET values indicate increases in surface area after micelle addition (top). FRET efficiency was averaged across a representative vesicle over time (bottom). Both FRET and Laurdan fluorescence were analyzed in comparison to controls and relative values reflect the difference between GP or FRET values of hypotonically stressed vesicles vs isotonic controls for a representative GUV.

Similarly, FRET probes indicated large-scale surface area changes due to micelle addition, in agreement with data obtained for nanometer-scale vesicles (**Figure 3.6 C**). As shown

in the top panel of Figure 3.6 C, micelle addition led to observable increases in membrane surface area, as expected. An observable decrease in FRET efficiency was apparent; FRET efficiency is expected to increase in response to lipid uptake, but photobleaching effects lead to an overall decrease in efficiency in both control and experimental populations. We then calculated the difference in FRET signal between tensed and non-tensed vesicles to account for these contributions from photobleaching. This difference is reported as 'relative FRET' (**Figure 3.6 C, bottom panel**). We observed that the relative difference in FRET signal between tensed and non-tensed vesicles increased upon micelle uptake and membrane growth. Ultimately, these probes were capable of providing information about tension and surface area changes in GUVs via microscopy, which is critical for studies with individual model membranes. Photobleaching prohibited us from analyzing both responses in one vesicle, and all experimental populations were compared to control samples to account for spectral cross talk and photobleaching effects. The rapid photobleaching of the dyes in our study indicate that more robust dyes or higher concentrations of dyes would be useful for future studies. These results, however, demonstrate the ability to monitor dynamic membrane processes on a single vesicle level, allowing quantification of membrane tension and surface area in real-time.

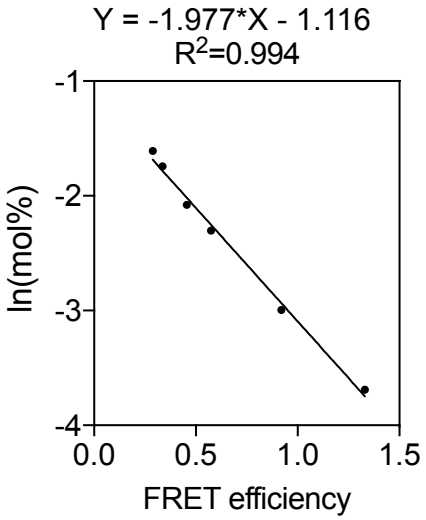

Figure 3.7 Sample GUV FRET standard curve. A standard curve can be generated by analyzing populations of vesicles with varying concentration of NBD/Rhodamine-Lissamine FRET pairs. FRET values increase as the average distance between FRET pairs increase. The f_{don}/f_{acc} value reflects the emission from a Green/Red filter cube in which Rhodamine emission is observed upon NBD excitation. Intensity ratios were averaged over $n > 60$ vesicles per concentration. Generation of a standard curve allows experimental fluorescence values to be translated into surface area changes via changing dye concentrations. For this curve, the corresponding relationship would be $mol\%\ dye = e^{-1.98*\mathrm{FRET}-1.12}$.

3.5 Conclusions

Using probes to monitor structurally distinct components of the membrane, we investigated whether we could optically detect and quantify changes in membrane tension and surface area. We found that membrane tension over a certain regime was optically reported through linear shifts in both Laurdan fluorescence, localized to the hydrophobic membrane core, and the FRET efficiency for two distinct FRET pairs, localized to the head groups of phospholipids.

We then used Laurdan and FRET probes in combination to monitor fluorescence changes during the process of fatty acid uptake in phospholipid vesicles. We found that membrane tension leads to faster and greater uptake of excess lipid, which occurs simultaneously with a partial recovery of Laurdan fluorescence – a possible indicator of tension relief. A current limitation of our approach is that it can be difficult to distinguish tension-induced hydration changes from chemical changes or changes in membrane fluidity in systems with complex membrane compositions. The approach of using probes isolated to distinct areas of the membrane could easily be extended to other sets of dyes with differing sensitivity to their chemical environment or to monitor different structural components of the membrane; this flexibility in probe selection may help isolate mechanical changes in the membrane from chemical ones. Importantly, all probes used in our study are compatible with both spectroscopy and microscopy-based experiments, allowing detection and real-time analysis of these processes on an individual and population level.

The translation of this approach into cellular applications is of significant interest, and we expect that this concept of using optically active molecules localized to distinct areas of the cell membrane can ultimately inform the design of molecularly encoded sensors to monitor membrane dynamics in cellular systems. To date, molecularly encoded and optically active molecules that have been used to measure forces in cellular systems have been predominantly limited to cytoskeletal components and focal adhesion complexes.[128-131] With the growing awareness of the important role of membrane tension in cellular regulation, molecularly encoded dyes that localize to various structural components of the membrane would undoubtedly help elucidate the role tension in a variety of cellular behaviors.

The ability to monitor tension and membrane deformation has implications in fields ranging from the analysis of basic cellular processes to the improvement of drug delivery systems, which rely on deformation of the plasma membrane or carrier interface, respectively. Optical probes are a powerful tool for such analyses, as they eliminate the need for physical interaction with the system and are easily incorporated into vesicle membranes. By coupling a polarity-sensitive probe with spatially sensitive counterparts, we were able to obtain a quantitative, multi-dimensional view of the dynamic processes that affect membrane tension and surface area regulation in simple model systems. Through this approach we can ultimately gain a better understanding of the series of events that accompany tension in model systems, and thereby uncover general physical principles that govern cellular behaviors.

Chapter 4: Vesicle-based platforms for biosensing

4.1 Foreword

The next step toward vesicle-based sensor development is the encapsulation of aqueous sensing systems. While the optical dyes discussed in Chapter 3 provide a handle by which to monitor the forces within the membrane, we now aim to expand these sensing capabilities to detect small molecule analytes in solution. A powerful property of membrane-based systems is the ability to encapsulate aqueous components, spatially segregating them from the surrounding environment with a semipermeable barrier. The membrane can provide an additional handle by which we can modulate sensing behaviors, whether through permeability-regulated change in composition or the incorporation of membrane transporters such as proteins and ionophores. Here, we review the current state of the field of encapsulated biosensors, with a particular focus on 1) membrane modification strategies to enhance sensing, and 2) the development of encapsulated cell-free protein expression-based biosensors. Finally, we offer perspectives toward future biosensor development. This chapter was adapted from the following publication:

Boyd, M. A. & Kamat, N. P. Designing Artificial Cells towards a New Generation of Biosensors. *Trends in Biotechnology* **39**, 927-939, doi:10.1016/J.TIBTECH.2020.12.002 (2021). ***Publication was featured as one of 15 articles in *Trends in Biotechnology's* "Best of 2021 Collection"**

4.2 Synthetic membranes advance artificial cells for biosensing capabilities

4.2.1 Biosensing as a critical tool to maintain human and environmental health

In environments ranging from natural ecosystems to living organisms, small molecule analytes and nanoscale forces serve as important markers of disease, pollution, and contamination. Unfortunately, these signals can be challenging to detect and monitor due to technological tradeoffs in analytical sensitivity, specificity, or deployment. With the expansion of modern agriculture and manufacturing techniques, as well as global health crises due to pollution and disease, the development of biosensors that allow for improved speed and accuracy of molecular detection in a variety of settings is critical for our ability to maintain human and ecological health. Accordingly, improved biosensing technologies are needed in fields including public health, food safety, agriculture, forensics, environmental protection, and homeland security.[132]

Many traditional biosensing techniques, including nucleic acid-based,[133] antibody-based,[134] and electrochemically based biosensing,[135] are exquisitely sensitive, but can be prohibitively expensive to develop and operate, require significant training, and use equipment that often makes point-of-detection sensing difficult.[136] Inspired by these limitations, biologically based sensors have emerged as an alternative that uses genetic circuits derived from living organisms to detect environmental signals. This approach has allowed the rapid development of new sensing platforms, which have shown great promise towards cost-effective, portable sensing.[137,138] Recently, progress has been made in the development of stimuli-responsive artificial cells - structures which recapitulate these genetically encoded sensing pathways within

a biologically inspired material chassis – which act as self-contained biological sensors. The design of artificial cells provides an opportunity to bridge functions brought forth by synthetic biology and biomaterials, an intersection which promises to bring about unprecedented advances in biosensing. Here, we discuss progress toward chassis functionalization for improved biosensing, particularly with regard to membrane engineering, and discuss recent advances toward the development of genetically encoded, stimuli-responsive artificial cells.

4.3 Biologically based sensing: cell-free, whole-cell and artificial cell approaches

Approaches to develop biologically based sensors use strategies from either top-down or bottom-up synthetic biology, which encompass the re-direction of sensing behaviors in living cells (whole-cell) or the extraction and isolation of biological machinery from cells (cell-free), respectively (**Figure 4.1**). Recent progress in whole-cell sensing has led to the development of cell-based sensors for insecticides,[139] antibiotics,[140] water contaminants,[141] disease markers,[142,143] heavy metals,[144,145] and bacterial colonization in vivo.[146] Cellular transcription and translation machinery has also been extracted and harnessed to create cell-free protein synthesis (CFPS)-based sensors for viral infection,[138,147,148] heavy metals and chemical contaminants,[149-151] herbicides,[152,153] date rape drugs,[149] and clinically-relevant biomarkers.[154,155] When it comes to deployment, however, these sensors have encountered a number of roadblocks. Whole-cell sensors have been limited by technological issues (e.g. plasmid loss and long response times[149,153]), concerns over biocontainment, and resource constraints associated with maintaining viability alongside complex genetic programs. CFPS-based sensors have exhibited

variable sensitivity for different samples, sensitivity to matrix effects,[156,157] and a loss of containment, protectivity, and certain sensing capabilities conferred by the cell membrane.[149,156]

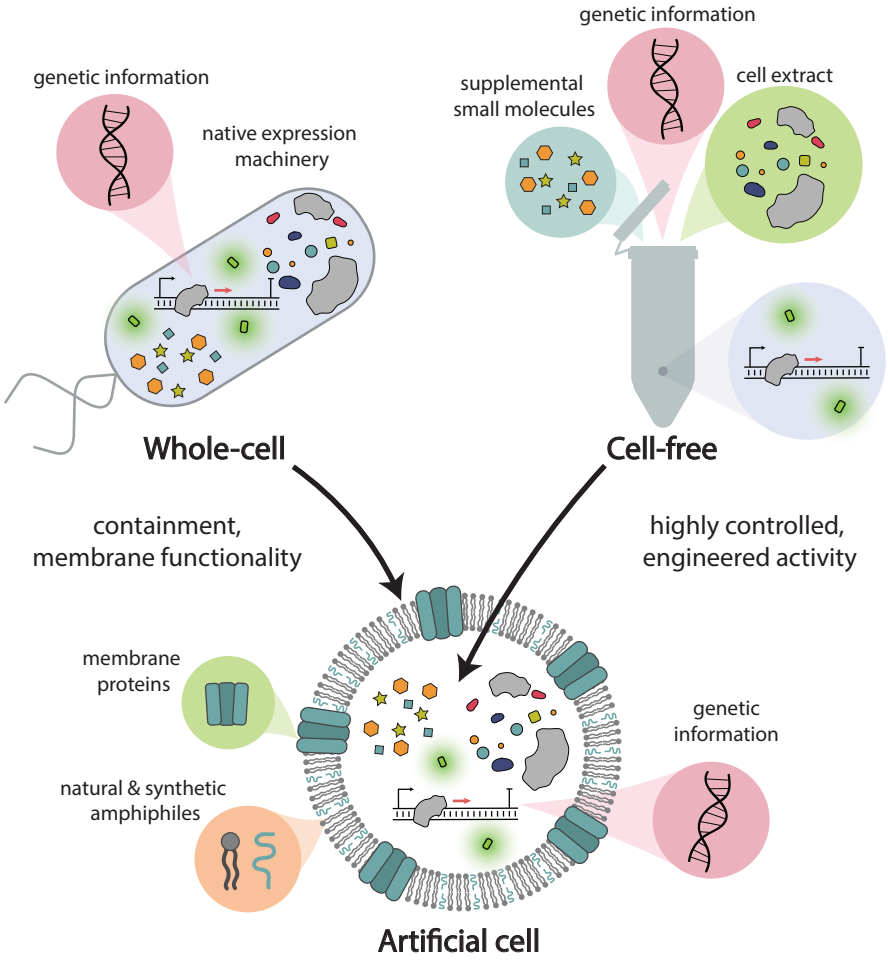

Figure 4.1 Artificial cells as biosensors. Artificial cells incorporate aspects of both whole-cell and cell-free biosensing strategies, including natural and synthetic membrane components and highly regulated, genetically encoded molecular sensors, in order to create a self-contained sensing environment. Through this combination, they recapitulate certain membrane functions of whole-cell sensors with the highly controlled genetic programs characteristic of cell-free biosensors. By including sensing-specific genes and limited reagents for protein synthesis, the risk of biocontainment may be significantly reduced and protective and gating features of the cell membrane can be re-introduced.

Leveraging attributes of both whole-cell and cell-free sensing, artificial cells may be well-poised to advance biologically based sensing. While artificial cells can encapsulate enzymatic and strand-displacement systems,[158-160] they are typically composed of a CFPS system and an encapsulating chassis, generally a bilayer membrane. By re-introducing certain stabilizing features of the cellular membrane, particularly the ability to contain molecular machinery in the face of dilution[38] and protect against environmental components,[24] artificial cells may reduce the impact of external conditions on the CFPS process while posing a lower biohazard threat than living cells. Although a number of CFPS sensors have been developed that may function within artificial cells, the use of an encapsulating membrane as an active participant in sensing activities has seen limited progress. In particular, the incorporation of materials into the membrane that selectively permit certain signals, such as small molecule analytes, to enter the artificial cell interior while retaining CFPS contents may significantly enhance sensing capabilities. As such, we expect membrane engineering to expand as a major factor in artificial cell design as it serves a critical role in recapitulating shielding and gating functions lost in the transition from whole-cell to CFPS sensing.

4.3.1 Artificial cell assembly

Artificial cell chassis can be assembled from a variety of encapsulating materials, including coacervates,[161] DNA-hydrogel compartments,[162,163] and protein-polymer shells,[159,164] however the majority of artificial cells to date have been assembled using bilayer membrane vesicles in the form of liposomes.[39,165] The use of a membrane-based chassis is often preferred due to its relative ease of assembly, compatibility with other biomolecules, and resemblance to

the cell membrane. Alternative chassis materials, particularly hydrogels and protein-based structures,[159,162-164] exhibit high mechanical stability and/or porosity suitable for protein diffusion, however the relatively enhanced control over features such as selective permeability and the incorporation of additional biological and synthetic components in liposomes has led to their widespread use in artificial cells. Paper-based systems have also been used to stabilize CFPS sensors, facilitating long-term storage and sensory assays in field settings, but like hydrogels and proteinosomes lack the ability to incorporate membrane functions.[137]

Assembly methods for liposomal artificial cells with encapsulated CFPS reactions typically derive from traditional methods to form Giant Unilamellar Vesicles (GUVs), including water-in-oil emulsions, thin film hydration, and microfluidics. Of these, emulsion phase transfer[78] and vesicle rehydration[166] are the most widely employed for artificial cell sensor development.[39,165] While these techniques can generate gene-expressing liposome populations, each suffers from certain drawbacks. In particular, emulsion and microfluidic methods lack the ability to control membrane composition due to residual solvents or stabilizing surfactants that may stay in the membrane after vesicle formation,[79,80] and thin film hydration methods exhibit poor encapsulation efficiency and generate heterogenous vesicle sizes and lamellarities.[167] Additionally, each demonstrated preparation method often results in heterogenous vesicle loading, with some vesicles exhibiting significantly higher protein expression than others.[38,168] Finally, while cellular membranes are composed of a large variety of lipids and biomolecules, artificial cells have, as of yet, not been recreated with this complexity.[169] Future work toward artificial cell development may require improvements in assembly methods that provide control over both vesicle physical properties and composition.

4.4 Functionalizing synthetic membranes through composition changes, protein insertion and surface conjugation

As the primary boundary of the artificial cell, the chassis membrane serves a critical role in regulating interactions between an encapsulated CFPS sensor and its surrounding environment. Through membrane functionalization, a major focus in artificial cell sensor design is creating a balance in which the membrane can contain desired reactants while allowing the receipt of specific signals, often small molecules.

4.4.1 Membrane composition controls stability, permeability, and membrane protein dynamics.

Amphiphile selection provides one strategy to modulate properties of the artificial cell membrane (**Figure 4.2 A**). These membranes have typically consisted of phosphatidylcholine (PC)-containing phospholipids, which are stable to modest changes in pH, temperature, and osmolarity, exhibit low phase transition temperatures, and are capable of self-assembly in the conditions suitable for CFPS.[39,165,170] Phospholipid membranes are semipermeable, allowing the passage of water and certain small molecules while excluding larger solutes.[170] The degree of permeability is dependent on membrane components and lipid packing density, which can be tailored to balance the permeability of a desired analyte versus the leakage of encapsulated materials.[171] For example, permeability can be tuned by changing the length and degree of unsaturation of the phospholipids' hydrocarbon chains,[170] by thermally inducing lipid packing defects,[172] or by incorporating components such as fatty acids[170,173] and cholesterol[174] into the

membrane. Alternatively, certain synthetic materials such as polymers can be blended with phospholipid membranes to impart higher stability, lower permeability, and to facilitate the expression and spatially localized insertion of membrane proteins.[22,24,54,175,176] Polyethylene glycol (PEG) polymers can similarly be conjugated to lipid headgroups to modulate interactions at the membrane interface.[177,178] This ability to incorporate natural and synthetic materials into bilayer membranes offers enhanced control of membrane properties over what can be achieved in engineered live cells, providing an important handle to assemble robust artificial cell sensors.

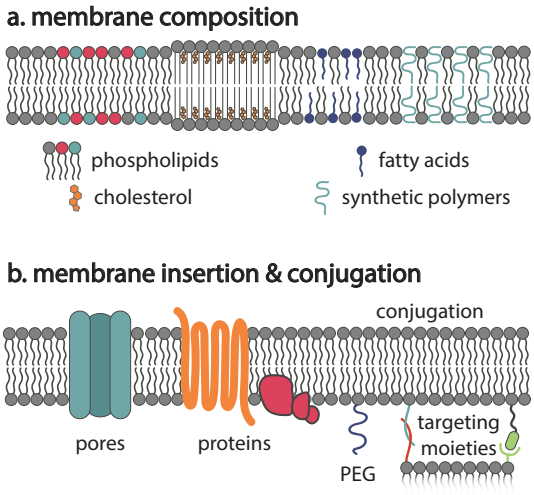

Figure 4.2 Membrane functionalization through changes in composition and biomolecular insertion. A. Membrane properties can be modulated by changing composition, for example, through the incorporation of phospholipids, cholesterol, fatty acids, and synthetic polymers. **B.** Membrane activity can be altered by inserting or conjugating proteins, polymers, and other biomolecules into the membrane or onto its surface. Abbreviation: PEG, polyethylene glycol.

4.4.2 Membrane proteins transmit environmental signals.

When compositional changes are insufficient to enable the detection of a specific signal, the incorporation of membrane proteins may be required (**Figure 4.2 B**). To date, most artificial

cell-based sensors for non-permeable analytes have employed simple pores to gate the entry or release of small molecules. In particular, the nonspecific, water-soluble pore alpha-hemolysin (αHL) has been widely explored in such systems.[38,84,164,171,179] αHL has been used to facilitate transport of small molecules up to 3kDa into and out of artificial cells,[179] enabling analyte entry,[38,171] genetically-regulated small molecule release,[38,84,164,180] and resupply of reactants from an external feeding solution.[179] While αHL incorporation provides a straightforward method to introduce small molecule transport functions, a major tradeoff in its functionality is the leakage of encapsulated reactants. In contrast, many other membrane proteins control analyte gating with a high degree of specificity, which may offer an alternative method to tune artificial cell sensitivity and introduce increasingly complex functions into encapsulated sensing pathways.

To date, the incorporation of transmembrane proteins into naturally derived or synthetic vesicle membranes has been demonstrated for a select number of model proteins. While detergent reconstitution has been a popular method for membrane protein incorporation, the past decade has seen the expansion of CFPS methods to co-translationally integrate membrane proteins into vesicle membranes.[22,181-183] Several proteins have been integrated into vesicles in this way; this includes large protein complexes like ATP synthase[184] as well as various membrane receptors, including G protein-coupled receptors.[185-187] There are many membrane proteins left to explore and much left to uncover regarding the effects of membrane composition on proper folding and activity of membrane proteins that are co-translationally inserted into membranes.[181] The level of success exploring these relationships so far is promising, however, and a better understanding of the design rules to incorporate a wider range of membrane proteins will expand the repertoire of behaviors that are possible in artificial cell systems.

4.4.3 Membrane functionalization can mediate encapsulated cell-free reactions.

Membrane properties not only impact signaling but can provide a route to further enhance or control encapsulated CFPS reactions. Pore incorporation and enzymatic reactions can be spatially localized to specific structures within a larger vesicle by creating nested vesicle-in-vesicle structures with distinct membrane compositions, much like cellular organelles.[188] Alternatively, the insertion of SNARE protein mimics and the conjugation of complementary DNA oligos to the vesicle membrane can control targeting and fusion between populations of vesicles (**Figure 4.2 B**).[38,189] This barcoding functionality provides a route to deliver genetic information, initiate and modulate genetically-encoded reactions, and control the sequence of fusion events between specific populations of vesicles to facilitate complex, multi-step reactions. Finally, membrane-localized PEG molecules can be harnessed to enhance encapsulated CFPS reactions and direct spatially localized protein assembly.[177,178] For sensing applications, in which the retention and activity of encapsulated CFPS components must be balanced with the receipt and processing of new environmental information, these types of membrane functionalization strategies to spatially and temporally control CFPS may expand the possibilities to tailor application-specific sensor platforms.

4.5 Artificial cells can sense small molecules, mechanical forces, and bacterial signals

Once assembled through the combination of an appropriate CFPS system and corresponding membrane components, the artificial cell can be harnessed for sensing. Artificial

cell sensing uses genetic circuits to translate a signal into a detectable output, which has primarily been accomplished through membrane gating (**Figure 4.3 A**), encapsulation of signal-responsive CFPS systems (**Figure 4.3 B**), and design of genetically encoded outputs, varying from reporter expression to membrane lysis (**Figure 4.3 C**). Recent studies have highlighted how these factors can be combined to develop stimuli-responsive artificial cells that serve as small molecule indicators, chemical translators, light sensors, and force sensors (**Table 4.1**).

4.5.1 Sensing molecular signals and engineering small molecule-based communication.

A major goal in biosensing is the ability to report the presence of specific small molecule signals. Toward this, artificial cell sensing for small molecules has focused on expanding the types of signals that can be detected, as well as incorporating genetically programmed outputs that can be initiated upon analyte detection. One focus of this work has been the development of artificial cells that sense membrane-permeable signals[38,82,84,171] to induce the expression of products including reporter proteins (**Figure 4.3 D**),[38,84] pore molecules (**Figure 4.3 E**),[38,82,84] and enzymes.[84] Membrane-permeable signals are straightforward for these applications in that no transporters are required for analyte entry, allowing the membrane barrier to remain largely intact. In contrast, αHL has been an effective mechanism to detect molecules that are large, polar, or otherwise unable to diffuse across the membrane,[38,171] but artificial cells generally need to be kept within a feeding solution to compensate for reactant loss.[179] While these strategies have each resulted in artificial cells capable of sensing various small molecule signals, it is the combinatorial use of these approaches that has been powerful in creating new sensing pathways.

The detection of permeable molecules can initiate the expression of αHL pores, allowing controlled release of impermeable cargo in response to a permeable signal. This can serve as a functional response itself but can also be used to send signals to other cells, living or artificial. For example, this process has been used to translate an otherwise unrecognizable molecule for Escherichia coli into a native signal,[82] and to send signals between different populations of αHL-functionalized artificial cells (**Figure 4.3 F**).[38] The development of artificial cells that respond to permeable and impermeable molecules has allowed for the creation of sensors that can detect small molecule signals and serve as sensing intermediates, and has facilitated the development of new stepwise signaling pathways, establishing population-specific responses[38] and circumventing the need to directly engineer live bacteria.[82]

While most artificial cell sensors for small molecules have used bilayer membranes in some capacity, non-membranous compartments have proven useful as vesicle-interfacing and stand-alone sensors as well. Proteinosomes, structures composed of protein-polymer conjugates, can exhibit enzymatic functionality that allows them to communicate chemically with αHL-expressing liposomes.[164] Alternatively, hydrogel compartments, which are more permeable and osmotically robust than their lipid counterparts, are well-suited for sensing pathways involving larger molecules, such as proteins (**Figure 4.3 G**).[162,163] While these hydrogel platforms exhibit improved mechanical stability compared to liposome-based artificial cells,[163] their increased porosity, which enables protein-based signaling, also significantly reduces the retention of CFPS reactants. The enhanced robustness of hydrogels or the enzymatic activity of proteinosomes may be advantageous over liposomes if selective permeability is non-critical and feeding solutions can be maintained. Liposomes, in contrast, offer improved abilities to selectively engineer

chassis permeability to retain CFPS reactants and to incorporate diverse membrane proteins and channels. While liposomes have been more widely used for artificial cell development to date, non-membranous artificial cells that have new material properties may be better suited to specific applications yet to be explored.

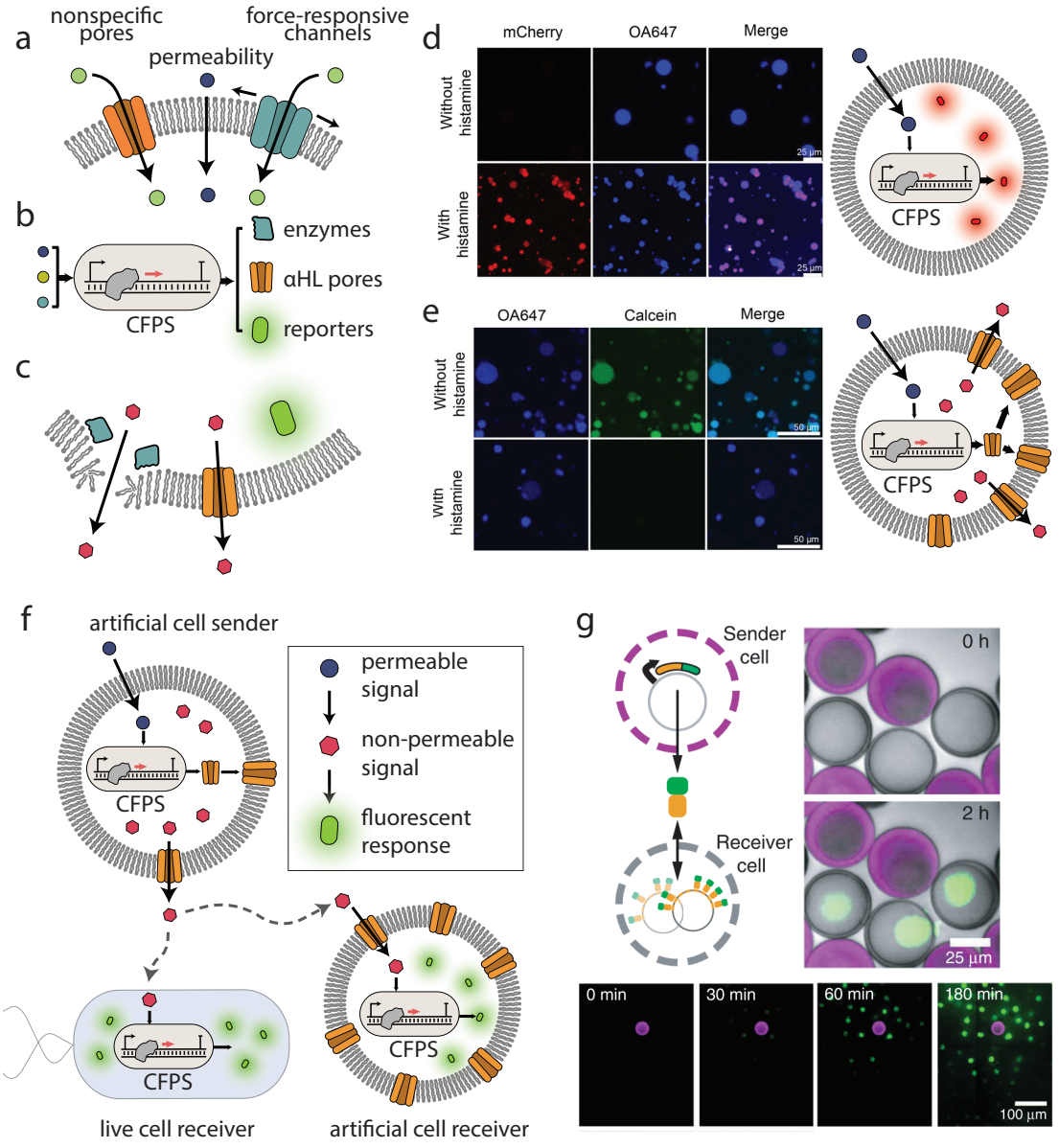

Figure 4.3 Cell-free sensor functionality. A. Signal detection is the first step in sensing, which has been achieved in artificial cells through permeability-regulated diffusion, nonspecific channels, and specific force and light-responsive membrane proteins. **B.** Once an analyte enters

the artificial cell, the initiation of a cell-free protein synthesis (CFPS) reaction leads to an observable output, often expression of an enzyme, pore, or reporter protein such as GFP. **C.** The cell-free production of these products generates an artificial cell response, often fluorescent signal retention, content release through pores, or membrane lysis. **D.** mCherry protein expression is observed in response to the diffusion of histamine into artificial cells, correlated with an encapsulated volume marker, OA647. Reprinted, with permission, from Dwidar *et al.*[84]. **E.** Content release through expressed, α hemolysin (αHL) pores is observed in response to histamine diffusion into artificial cells. Reprinted, with permission, from Dwidar *et al.*[84]. **F.** Artificial cells communicate through small molecule sensing and release. An artificial cell receiving a permeable signal expresses αHL pores, leading to the release of an impermeable cargo. This impermeable cargo is detected by either a live cell or another artificial cell nearby, which then generates an observable response. **G.** Protein-based signaling is observed in artificial cells with porous polymer membranes. A sender cell produces a tagged fluorescent protein, which binds to DNA in a receiver's hydrogel nucleus and generates a cell-type-specific response through accumulation. Protein diffusion can be observed spatially over time, leading to more dispersed signaling as time increases. Reprinted, with permission, from Niederholtmeyer *et al.*[163].

Table 4.1 Artificial cells with sensing behaviors.

Signal(s)	Mode of Entry	Artificial Cell Platform; Liposome Composition(s)	Interface	Output	Ref
Theophylline; IPTG[1]	Diffusion; αHL	Liposome; POPC[2], cholesterol	With *E. coli*	Translation of permeable to impermeable signal via αHL expression	Lentini *et al.*[82]

Arabinose, Theophylline; IPTG, Doxycycline	Diffusion; αHL	Liposome; POPC, cholesterol	Between artificial cell populations	Translation of permeable to impermeable signal via αHL expression; spatial segregation of transcription and translation processes	Adamala *et al.* [38]
Histamine	Diffusion	Liposome; EggPC[3], cholesterol	N/A	Expression of reporter protein, lytic enzyme, or αHL pore	Dwidar *et al.* [84]
3OC6HSL[4], DFHBI, IPTG, aTc[5]; Arabinose, Rhamnose, DAPG[6], Guanine	Diffusion; αHL	Lipid-based water-in-oil droplets; DOPC[7], DOPG[8], DPhPG[9], Cholesterol	Between spatially defined artificial cell populations	Diffusion range sensor, feed-forward circuit, positive-feedback circuit	Dupin & Simmel [171]
3OC6HSL; Glucose	Diffusion	Proteinosome & Liposome; POPC, cholesterol	Between liposomes and proteinosomes	Translation of permeable to impermeable signal via αHL expression; glucose release leading to fluorescent output in proteinosomes	Tang *et al.* [164]

TetR-sfGFP[10], TetR-mCherry[11], T3 RNA Polymerase	Diffusion	Polymersome & clay-DNA hydrogel	Between artificial cell populations	Reporter protein expression	Niederholtmeyer *et al.* [163]
IPTG	Diffusion	Aptamer-grafted hydrogel	N/A	Reporter protein expression	Lai *et al.* [162]
Osmotic pressure, Ca^{2+}	MscL	Liposome; EggPC, DOPC, cholesterol	N/A	Reporter protein expression	Majumder *et al.* [190]
Osmotic pressure, IPTG	MscL	Liposome; DOPC, DOPE[12], cholesterol	N/A	Cytoskeletal protein (MreB) expression	Garamella *et al.* [191]
Ca^{2+}, lipid catalysis	αHL, MscL	Liposome; DOPC, DOPG, POPC	N/A	Dye release	Hindley *et al.* [188]
Light	Photo-labile DNA cage	Liposome; DMPC[13]	N/A	Reporter protein and enzyme expression	Schroeder *et al.* [192]
Light	ATP synthase, Bacterio-rhodopsin	Liposome; POPC, cholesterol	N/A	Bacteriorhodopsin expression in response to light-stimulated ATP generation	Berhanu *et al.* [193]
3OC6HSL, IPTG	Diffusion	Surfactant-based water-in-oil droplets	With *E. coli*	AHL detection, production and release; IPTG AND gate	Schwarz-Schilling *et al.* [194]

Various bacterial AHLs	Diffusion	Liposome; POPC, cholesterol	With *V. fischeri*, *V. harveyi,* and *E. coli*	Reporter protein expression; AHL detection, production and release	Lentini *et al.* [195]
3OC6HSL	Diffusion	Liposome; DOPC, POPC, EggPC, cholesterol	With *E. coli*	Reporter protein expression; AHL detection, production and release; Environmental conditions	Ding *et al.* [196]
3OC6HSL	Perfringolysin O pores (PFO)	Liposome; POPC, cholesterol	Between artificial cells and neural stem cells	PFO expression in response to 3OC6HSL, subsequent release of BDNF leading to neural differentiation; Physiological conditions	Toparlak *et al.* [197]

4.5.2 Artificial cells expand the capabilities of cell-free sensing for mechanical forces and light.

Within a dynamic environment, small molecule signals are not the only stimuli present. For example, signals such as physical force or light intensity may be important contextual clues for environmental monitoring. With this in mind, the development of mechanosensitive and

light-sensitive artificial cells are powerful examples of how membrane engineering can expand the sensing capabilities of CFPS systems.

In order to develop force-sensitive artificial cells, one approach has been the incorporation of mechanically sensitive membrane proteins, such as the E. coli mechanosensitive channel of large conductance (MscL). Originally an osmotically activated release valve in bacteria, MscL can be expressed into artificial cell membranes using CFPS, creating a mechanosensitive gate which opens in response to membrane stretching.[22,188,190,191] MscL in artificial cells has been shown to open to form a 3 nm pore, allowing an influx of small molecule inducers into the artificial cell interior to initiate encapsulated CFPS reactions in an AND gate fashion.[188,190,191] This has been demonstrated to occur in response to both osmotic stress[190,191] as well as enzymatically-induced changes in lateral membrane pressure.[188] MscL function in these platforms has been coupled to protein expression, including fluorescent reporter expression[190] and cytoskeletal protein expression and assembly,[191] as well as controlled content release.[188] The role of membrane composition remains important here, as recent work by Hindley and colleagues demonstrated that, through the creation of a vesicle-in-vesicle superstructure with distinct compositions and protein incorporation, MscL could respond to membrane morphological changes to allow the release of a fluorescent dye from the innermost vesicles.[188] By harnessing the natural function of MscL for use in artificial cell settings, these studies illustrate how the incorporation of a specific membrane protein can expand force sensing capabilities in dynamic environments.

In addition to mechanical force, artificial cells have been developed that express protein products in response to light stimuli. This has been accomplished through both CFPS and

membrane-based methods, including the incorporation of light-cleavable protecting groups on CFPS DNA,[192] and the functional incorporation of ATP synthase and bacteriorhodopsin membrane proteins.[193] Importantly, the latter approach capitalized on naturally-existing photosynthetic pathways to drive protein synthesis in a positive feedback loop, harnessing energy generation to drive further membrane protein expression. This use of specialized light-sensitive membrane proteins in particular highlights an exciting step toward artificial cells that are capable of recapitulating certain sensing features that have, until now, been unique to living cells.

4.5.3 Artificial cells to infiltrate, monitor and modulate bacterial communities.

With the demonstrated ability to sense, report, and respond to biological signals, artificial cells present an opportunity to infiltrate and interact with communities of live cells in order to direct cellular behavior (**Figure 4.3 F**). A particular focus in this regard has been the use of artificial cells to interact with communities of live bacteria through quorum sensing molecules, which serve as indicators of cell density and play important roles in cooperative processes such as biofilm formation.[198] These quorum sensing molecules - especially acylated homoserine lactones (AHLs), which readily diffuse through lipid membranes – have proven to be a useful handle to allow artificial cells to communicate with live bacteria.[82,194,195] Artificial cells have been designed not only to respond to AHLs received from bacteria but to serve as actuators of live cell behavior by synthesizing and releasing bacteria-specific AHLs. This has been demonstrated both within populations of a single type of bacteria, specifically *E coli.*,[194] as well as between different bacterial species.[82,195] Highlighting the modularity of these strain-specific AHL circuits, Lentini and colleagues recently explored the use of various AHLs in artificial cells

to communicate with four different species of bacteria: *Vibrio fischeri*, *Vibrio harveyi*, *E. coli*, and *Pseudomonas aeruginosa*.[195] By combining genetic instructions to detect an AHL from one bacterial species and release an AHL for another, they created a new communication pathway between incompatible bacterial species with artificial cells as a sensing intermediate. They also demonstrated the ability to inhibit signaling by designing artificial cells that released an enzyme to break down *P. aeruginosa* AHLs when *V. fischeri* was present, disrupting quorum sensing altogether. This ability to combine genetically encoded instructions for different quorum sensing molecules with separate AHL outputs shows how artificial cells can serve as a checkpoint for cell-cell interactions, leading to new pathways that enable artificial cells to hijack or sever bacterial communication.

4.6 Moving from the lab to the field

To date, artificial cells show exciting promise in the development of self-contained biological sensors. However, many of these proof-of-concept studies have been conducted in highly controlled conditions to maintain stability, function, and cell viability. Real-world applications may present new constraints associated with naturally occurring conditions, which could differ considerably from lab conditions. Ding and colleagues recently investigated the consequences of variable environmental conditions on the function of artificial cell sensors,[196] finding significant improvement in the performance of encapsulated quorum sensing networks upon optimizing artificial cells to overcome osmotic imbalances, increase molecular crowding, and improve membrane stability. Similar considerations arise when creating interfaces with eukaryotic cells in physiological conditions, particularly with maintaining the viability of living

cells. To address this challenge, Toparlak and colleagues engineered artificial cells which could express a nonspecific pore, perfringolysin O (PFO), to release brain-derived neurotropic factor (BDNF) in response to an AHL signal.[197] By optimizing a CFPS system for low toxicity and physiological osmolarity, artificial cells could produce and release protein signals in the presence of live neural stem cells, ultimately stimulating cellular differentiation. While artificial cell sensors have yet to be widely deployed in many sensing contexts, these studies demonstrate factors that are likely to become increasingly important in artificial cell design and give insight into future modifications that will be necessary to achieve this goal.

4.7 Conclusions and future perspectives

As the technologies of cell-free sensing and membrane engineering converge, the development of stimuli-responsive artificial cells is rapidly expanding. While significant progress has been made toward artificial cells that can sense environmental signals, critical limitations include a small number of analytes that can currently be detected, a lack of physical stability, and poor balance between membrane permeability and reaction retention. In order to address these issues, it is likely that techniques to assemble multi-component artificial membranes, which confer stability and molecular gating, and CFPS sensing systems that detect diverse analytes will need to expand in parallel, with new strategies to create more dynamic interfaces between the two. An increasing number of analytes may be detectable through the incorporation of additional protein or nucleic acid-based sensing strategies that do not rely on gene expression. These modules offer temporal improvement over the hours-long response times characteristic of genetically encoded systems.[159,160] Analyte transport may be further modulated

through membrane compositional changes or through fusion-based reagent delivery in order to introduce small molecules to the artificial cell interior without suffering reactant loss. Finally, structural components such as artificial cytoskeletons may help push artificial cells closer to whole-cell robustness.[191] With the various components that can be incorporated into these sensor platforms, it is possible that artificial cells may ultimately be applicable in many different biosensing fields. In particular, applications that require monitoring of aqueous systems, such as environmental remediation, agriculture, and in vivo sensing,[197,199] may be the first to see field-applicable artificial cell sensors (**Figure 4.4**). This is primarily a result of the biological nature of cell-free systems, which inherently require an aqueous environment to function, as well as the stability of self-assembling chassis materials in aqueous conditions. Moving forward, sensing in non-aqueous environments may be facilitated by employing new materials that interface aqueous and organic environments.[200]

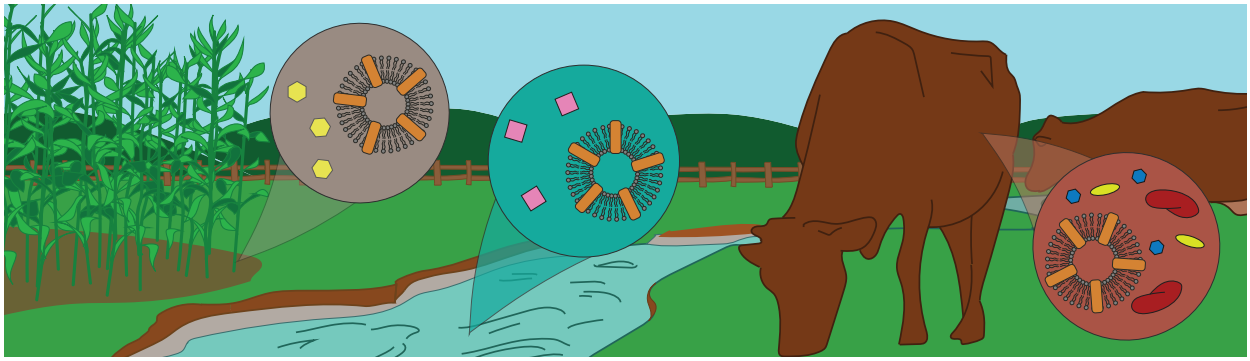

Figure 4.4 Outlook of artificial cell sensing. Artificial cells may be useful platforms for biosensing in a number of contexts, particularly in aqueous environments. For example, they may be useful for monitoring soil in agricultural applications, for monitoring water quality, or even for use as in vivo biosensors in live organisms such as livestock. While membrane transport remains a hurdle to be addressed, artificial cells may eventually be able to detect pesticides, contaminants, bacteria, disease markers, and other important signals in a number of environments.

The examples highlighted here represent exciting steps toward the use of artificial cells for a number of complex, analyte-responsive behaviors, which range from simple sensors to actuators of live cell behavior. With the limited applications to date, however, artificial cells have yet to realize the breadth of possibilities for both encapsulated CFPS sensors as well as membrane functionalization strategies. In part, this is because the assembly of artificial cells involves complex interactions between a large number of molecules, a system that can be particularly hard to troubleshoot and optimize. Additionally, our toolbox of available natural and synthetic components – although expanding – is still extremely limited compared to that found in nature. As a result, significant work remains to fully characterize both the artificial systems and the natural cell inspiration. In particular, artificial cell technologies could be expanded through a better understanding of CFPS/chassis interactions, methods to improve loading efficiency, and membrane protein design and incorporation rules. Importantly, these investigations will be informed by ongoing characterization of cellular membrane functions and identification of additional intracellular sensing pathways in living cells. Together, these strategies could ultimately identify and isolate additional cell-inspired sensing modalities while better characterizing the biophysical and biochemical properties of artificial cell assemblies, furthering the transition to diverse, robust, and technologically viable biosensing platforms. While we are yet unable to recapitulate the complexities of a living cell, we are consistently working toward a better understanding of the pathways that allow them to monitor and respond to their environment. Eventually artificial cells may be able to receive and process a number of inputs into complex outputs, much like live cells, in order to build user-defined, biologically based systems to monitor the world around us.

Chapter 5: Membrane functionalization to improve specificity of an encapsulated indicator

5.1 Foreword

Membrane gating is a powerful strategy by which encapsulation within bilayer membranes can modulate the sensitivity and specificity of encapsulated aqueous sensors. As a first step toward the development of encapsulated sensors, we first developed a vesicle-based sensor which leverages ionophore-based membrane gating to improve the specificity of an encapsulated ion indicator for potassium. By encapsulating a small molecule indicator rather than a gene expression-based sensor we can explore the effect of encapsulation on sensing more generally on a far simpler sensor system. These materials are more accessible to the scientific community, facilitating their adaptation to other types of sensors or to other applications. Finally, a number of other small molecule indicators and membrane transporters are commercially available, meaning this platform could be easily generalized to detect alternative analytes. Here, we show how membrane modifications facilitate improvements in sensing of a commercially available fluorescent indicator, highlighting the power of membrane gating to modulate biosensor characteristics. In collaboration with Peter Tran and Arthur Prindle in the Prindle lab at Northwestern, we then demonstrate that these sensors can detect changing potassium conditions in cultures of live bacteria. This chapter was adapted from the following publication:

Boyd, M. A., Davis, A. M., Chambers, N. R., Tran, P., Prindle, A., Kamat, N. P. Vesicle-Based Sensors for Extracellular Potassium Detection. *Cell Mol Bioeng* **5**, 459-469 doi:

10.1007/s12195-021-00688-7 (2021). ***Publication featured in "2021 Young Innovators" issue of CMBE**

5.2 Introduction

Potassium ions (K^+) are one of the most abundant cations present in intracellular fluid, playing a critical role in maintaining cell potential and excitability, cell volume, and acid-base balance.[201,202] As such, the concentration of this ion both in and outside of the cell affects a wide variety of cellular processes in living organisms, from driving neuronal activity to coordinating communication between bacteria in biofilms.[203,204] In humans, irregularities in extracellular K^+ levels contribute to a range of pathologies, including cardiovascular disease, immunological diseases, and some cancers.[205-209] In addition, disruption of K^+ channels in bacteria can abolish the coordinated growth of bacterial communities.[203] Despite the critical role of K^+ ions in a wide range of cellular behaviors, the detection, quantification and monitoring of K^+ remains difficult in a number of contexts. In particular, ion-sensitive electrodes, the state-of-the-art method to quantify K^+ in biological samples, are invasive and unable to report the spatiotemporal dynamics of K^+ variations in living systems.[210-212] While we continue to learn about the role of K^+ in driving cellular function, this limitation in our abilities to measure the concentrations of K^+ both intra- and extracellularly subsequently limits our understanding of how these fluctuations may accompany healthy and irregular cellular and organelle function. For this reason, the design of fluorescent potassium sensors that can optically report variations in extracellular K^+ concentrations *in situ* would be greatly valuable.

Several optical probes that respond to K^+ ions have been developed to date.[213-217] Unfortunately, these small-molecule probes can be unable to selectively measure K^+ ions when in the presence of other ions— particularly ions with similar charge states, such as Na^+ [218,219]— and can be difficult to deploy in biological studies due to technological limitations in cell loading or toxicity.[211,220,221] One commonly used, commercially-available K^+ probe is potassium-binding benzofuran isophthalate (PBFI),[214,218] which has been used for the intracellular quantification of K^+.[222-224] Cells establish a significant K^+/Na^+ gradient in order to maintain proper membrane potential, with ~150 mM KCl and 10 mM NaCl concentrations maintained intracellularly.[216,223] Extracellularly, however, these concentrations are inverted, with high Na^+ and K^+ concentrations as low as 3-5 mM.[205] PBFI exhibits poor selectivity against Na^+, with only 1.5x higher selectivity for K^+ than Na^+, which limits its use to intracellular applications where K^+ concentrations far outweigh the concentration of Na^+.[223] Similar limitations are encountered with other optical probes, including Asante Potassium Green and its variants.[219] Without the ability to control for the effects of other cations, this lack of specificity in ion detection ultimately limits the accuracy of K^+ sensing by certain optical sensors in many biological environments.

One strategy to improve the specificity of small-molecule ion indicators is to selectively gate which ions are able to access the indicator. Previous approaches have incorporated optical ion indicators within silica-based nanoparticles, however the assembly and characterization of these sensor platforms rely on multiple coating and characterization steps and may not be easily transferrable to other ion types.[221,225] An alternative approach is to encapsulate these optical indicators within bilayer membranes, which are easily assembled and can incorporate a wide variety of naturally-derived or synthetic components.[12] Lipid vesicles formed through the self-

assembly of phospholipids can encapsulate water soluble cargo within a semipermeable barrier.[12,170] Mimicking the structure of cellular membranes, these particles can be co-assembled with peptides and proteins that selectively interact with ions to enable their passage across a membrane in order to interact with an encapsulated ion indicator.[226,227] Valinomycin, an ionophore, is one such molecule that selectively transports alkali metals through both biological and synthetic membranes.[228] This cyclic peptide can form an ion-peptide complex with select metallic cations, including K^+, Rb^+, and Cs^+, but the cavity of the valinomycin ring is too large for Na^+.[229] As a result, valinomycin selectively transports K^+ over Na^+ ions across bilayer membranes.

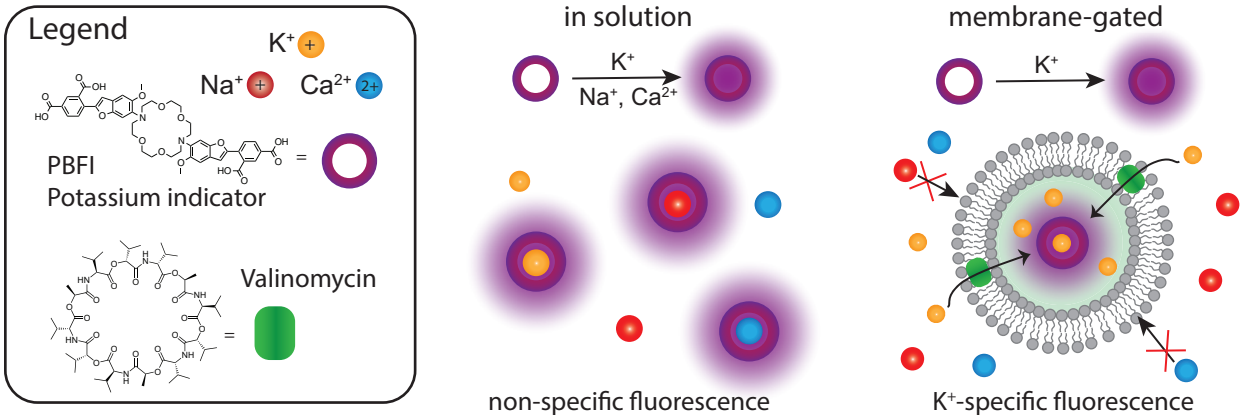

Figure 5.1 Design of a vesicle-based K+ nanosensor. PBFI, a commonly used indicator of K^+ ions, fluoresces in the presence of K^+ as well as other ions, such as Na^+ and Ca^{2+}. In solution, PBFI fluorescence due to K^+ binding is indistinguishable from PBFI fluorescence due to Na^+ and Ca^{2+} binding. Membrane gating provides a route to selectively exclude ions from binding to PBFI. By encapsulating PBFI in lipid vesicles that contain valinomycin, a cyclic peptide that selectively transports K^+ ions across bilayer membranes, K^+ can selectively diffuse in and out of the vesicle. Once inside the vesicle nanosensor, K^+ can bind PBFI to generate an optically detectable fluorescence shift. By contrast, Na^+ and Ca^{2+} ions are excluded from the vesicle interior and their presence will not be reported.

Here, we present a new approach to selectively detect K^+ in the presence of Na^+ by developing a vesicle-based nanosensor. To achieve this goal, we assemble lipid vesicle membranes encapsulating the K^+ indicator PBFI in the vesicle lumen, and incorporate valinomycin into the vesicle membranes (**Figure 5.1**). We show that this nanosensor can selectively detect K^+ in the presence of other important biological cations, and demonstrate the nanosensor can detect changes in extracellular K^+ concentration in bacterial cultures. The approach presented here should be extendable to a range of ions, which can be customized by altering the ion transporter and ion indicator. As a result, we expect our methods will enable a new generation of ion sensors that will reveal new information about extracellular ion variations during normal and pathological functions.

5.3 Materials & Methods

Materials

DOPC (18:1 (Δ9) 1,2-dioleyoyl-sn-glycero-3-phosphocholine, 25 mg/mL in chloroform) was obtained from Avanti Polar Lipids, Inc. PBFI Tetraamonium Salt (4,4'-[1,4,10,13-Tetraoxa-7,16-diazacyclooctadecane-7,16-diylbis(5-methoxy-6,2-benzofurandiyl)]bis-1,3-benzenedicarboxylic acid), Tris buffer (pH 7), KCl, $MgCl_2$, $CaCl_2$, and NaCl were obtained from Thermo Fisher. Valinomycin Ionophore and Sepharose 4B were obtained from Sigma-Aldrich. MSgg media was prepared as described below, all buffer components were obtained from Sigma Aldrich. Size exclusion chromatography columns were obtained from BioRad. BL21 bacteria was obtained from New England Biolabs.

MSgg buffer: 100 mM MOPS (pH 7.0 with NaOH), 5 mM Potassium phosphate (pH 7.0), 0.5% Glycerol, 0.5% Glutamate monosodium salt, 700 μM $CaCl_2$, 2 mM $MgCl_2$, 1 μM $ZnCl_2$, 100 μM $FeCl_3$ $6H_2O$, 50 μM $MnCl_2$, 2 μM Thiamine HCl. Supplemented with ddIH_2O to reach final concentrations above.

Vesicle Preparation

Small unilamellar vesicles were prepared through thin film hydration as described by Boyd *et al*.[230] Briefly, DOPC in chloroform was dried down in glass vials under nitrogen gas and placed under vacuum pressure overnight. Lipid films were hydrated immediately or were frozen at -20°C and used within one week. Films were rehydrated overnight at 4°C with Tris buffer (100 mM for specificity studies, 200 mM for bacterial studies) containing 0.5 mM PBFI dye to a final concentration of 20 mM or 40 mM lipid. Films were vortexed briefly to form vesicles, then extruded through 100 nm polycarbonate filters (Avanti Polar Lipids, Inc.) to 7 passes. Unencapsulated PBFI dye was removed by purifying vesicles using size exclusion chromatography, and vesicle fractions were collected using an FC 204 Fraction Collector (Gilson). Size characterization was performed through dynamic light scattering on a Keck-II Zetasizer. Vesicles were diluted in buffer to a final concentration of 100 μM; vesicle samples were run in triplicate and the intensity mean was taken as the average diameter size.

A 100 μM valinomycin stock solution was prepared in 100 mM Tris + 1% DMSO and added to purified vesicles at various mol %s (0, 0.1, 0.2); vesicles were then incubated for >30 minutes at room temperature to allow for ionophore insertion. Control vesicles were prepared by adding the same volume of 100 mM Tris + 1% DMSO without valinomycin. Vesicles were prepared with valinomycin in triplicate.

For reversibility studies, DOPC vesicles were prepared at a concentration of 40 mM and, before purification, were incubated with either 0.2 mol% valinomycin or the corresponding volume of DMSO buffer for 30 minutes. Vesicles were then incubated in either 0 mM K^+ or 100 mM K^+ for 1 hour. Following salt incubation, samples were purified through size exclusion columns containing either 100 mM Tris running buffer or 100 mM Tris + 100 mM K^+ running buffer. Following purification, samples were incubated at room temperature for 1 hour before reading PBFI fluorescence.

For calcein release assays, vesicles were prepared by hydrating lipid films as described above with 100 mM TRIS buffer containing 20 mM calcein dye. Vesicles were incubated at 37°C for 24 hrs, vortexed briefly, then extruded through 100 nm polycarbonate filters (Avanti Polar Lipids, Inc.) to 7 passes. Unencapsulated calcein dye was removed by purifying vesicles using size exclusion chromatography, and vesicle fractions were collected using an FC 204 Fraction Collector (Gilson). Valinomycin was incorporated into vesicle membranes as described above.

Sensor Characterization

Vesicles were incubated in 384 well plates or 0.5 mL cuvettes with varying salt buffers and monitored for changes in PBFI fluorescence ratio. Final vesicle concentration was 1 mM during incubation, and salt conditions were varied between 0-100 mM in 100 mM Tris buffer pH 7. PBFI fluorescence in vesicles was measured either over time for kinetic scans or following 1 hour buffer incubation. For free dye characterization, PBFI was added to buffers with varying salt content at a concentration of 0.0125 mM to obtain a similar overall dye concentration to that

of the vesicle samples following purification and dilution. For kinetic studies, 1 μL 10% TritonX-100 was added per 30 μL volume and fluorescence was monitored to determine maximum PBFI ratio.

For vesicle stability assays, calcein fluorescence was monitored at an excitation of 495 nm and emission at 515 nm. Following vesicle incubation in buffers with increasing KCl concentration, 1 μL 10% TritonX-100 was added per 40 μL volume and incubated for 30 minutes to lyse vesicles and determine the fluorescence associated with 100% dye release. The stability of the vesicles was assessed by evaluating the calcein leakage with each valinomycin concentration relative to the control.

Statistical analysis and model fitting were conducted with GraphPad Prism. Results were analyzed via Two-Way ANOVA using Tukey's Multiple Comparisons Test to assess significance between conditions. P-values are reported as: ****$p \leq 0.0001$, ***$p \leq 0.001$, **$p \leq 0.01$, *$p \leq 0.05$, nonsignificant (ns) $p > 0.05$.

Fluorescence Spectroscopy

PBFI fluorescence was measured by taking spectral scans monitoring emission intensity at 505 nm with excitation wavelengths ranging from 320 to 400 nm. PBFI ratios were calculated by taking the fluorescence emission at 505 nm when excited at 340 nm divided by the fluorescence emission at 505 nm when excited at 380 nm:

$$Ratio\ 340/380 = 505\ Em.Intensity_{340\ ex}/505\ Em.Intensity_{380\ ex} \quad \textbf{(5.1)}$$

Spectroscopic measurements were collected on a SpectraMax i3x plate reader (Molecular Devices) and a Cary Eclipse Fluorescence Spectrophotometer (Agilent Technologies).

Bacterial studies

Wild type BL21 *E. coli* were grown overnight in MSgg media (see SI) at 37°C with shaking. Bacteria were centrifuged at 12,000 rcf for 2 minutes to form a pellet, MSgg supernatant was removed, and bacteria were re-suspended in equiosmolar Tris (326 mmol/kg, measured using a Wescor Vapro 5520 vapor pressure osmometer). Vesicles were prepared with 0.2 mol% Valinomycin (or an equal volume of DMSO) and 0.5 mM PBFI as described above. Vesicles were mixed in a cuvette with buffer to a final concentration of 1 mM, and bacteria were added in three separate concentrations, keeping final volume constant. Final OD was measured on a Cary UV Vis Spectrophotometer, zeroed to vesicles in buffer. PBFI excitation spectra from 330 nm to 390 nm were monitored for 30 minutes in the absence of any salt on a Cary Eclipse Fluorescence Spectrophotometer with high PMT sensitivity at an emission of 505 nm. After a 30-minute incubation of vesicles and bacteria, 50 mM KCl and 150 mM NaCl was added to each cuvette and mixed via pipetting. Fluorescence was monitored for 60 minutes following salt addition. To account for differences in optical densities, final PBFI ratios were assessed by dividing the final fluorescence ratio after salt addition by the initial fluorescence ratio with vesicles and bacteria only.

Samples were imaged on a Nikon Ti2 microscope in the presence of WT BL21 to assess stability and localization. Vesicles were prepared as described but with the addition of 0.1 mol% of Cy5.5-PE, a membrane dye. Vesicles and bacteria were mixed together in buffer and allowed

to incubate for 1 hour. Images were taken with filters for DIC, Cy5.5-PE (650 nm excitation, 720 nm emission) and the 340 nm excitation of PBFI (350 nm excitation, 525 nm emission).

5.4 Results and Discussion

5.4.1 Spectral characterization of PBFI in solution

We first characterized the fluorescence of free PBFI in solution as a function of KCl concentration to verify this relationship in our selected buffer. PBFI was mixed with a Tris buffer (pH 7) containing increasing concentrations of KCl and the emission of PBFI at 505 nm was monitored upon excitation with light ranging from 320 to 400 nm, as previously described.[218] As expected, emission maxima were detected at an excitation wavelength of 340 nm, and emission intensity increased in response to both increasing KCl and NaCl concentrations (**Figure 5.2 A & B**). Spectral shifts in PBFI fluorescence were subsequently reported ratiometrically, where the fluorescence intensity ratio was determined at the emission maximum of 505 nm when excited at 340nm/380 nm.[218] Using this metric, we then measured the PBFI fluorescence intensity ratio as a function of monovalent ion identity and concentration, as well as the response to a combination of ions (**Figure 5.2 D**). We observed that PBFI responds to both ions and appears to saturate in signal at approximately 50 mM (**Figure 5.2 B & D**). In the presence of a combination of Na^+ and K^+ with a constant total salt concentration, however, no change in PBFI ratio is observed even as K^+ concentration increases; this result demonstrates the lack of indicator specificity and an inability to distinguish K^+ from Na^+ ions when free in solution (**Figure 5.2 D**).

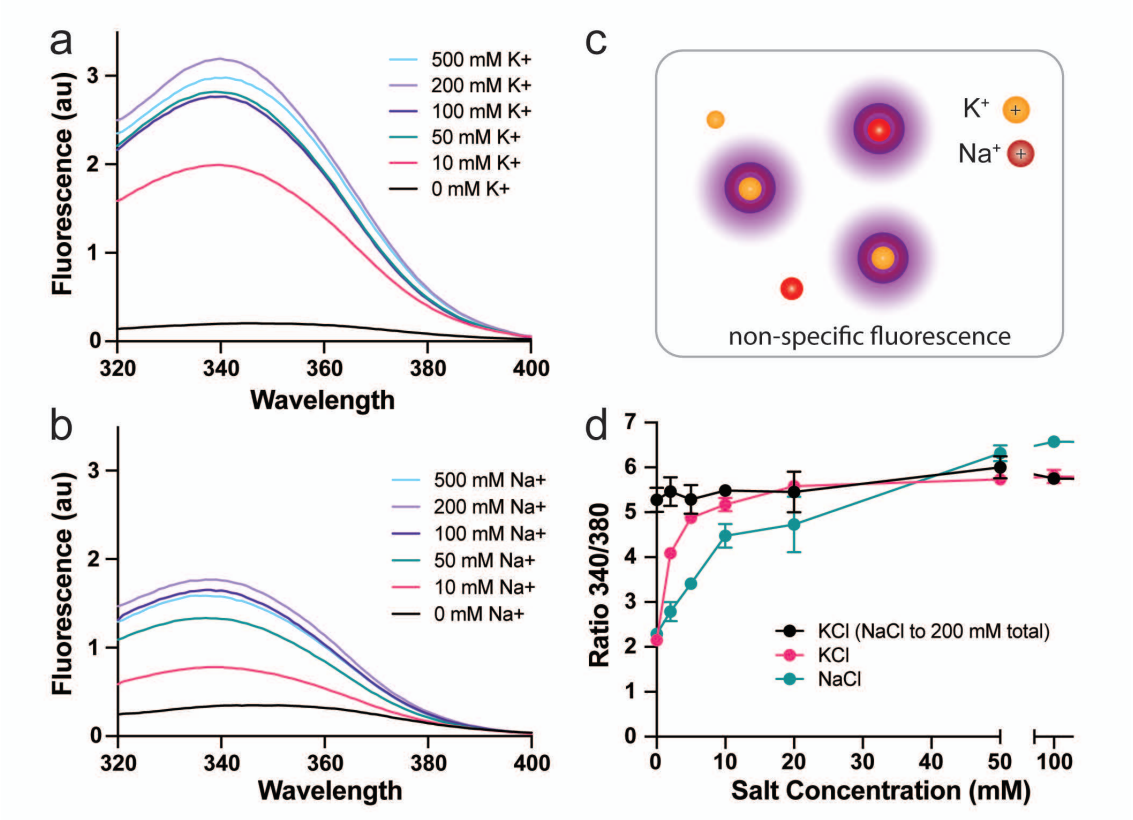

Figure 5.2 Spectral characterization of the PBFI indicator. A. Emission spectra of PBFI in solution as a function of K^+ concentration and **B.** Na+ concentration. **C.** A schematic of these studies shows that, in solution, a variety of ions are expected to interact with PBFI and shift the fluorescence of the indicator. **D.** The fluorescence intensity ratio of PBFI emission at 505 nm when excited at 340 and 380 nm is reported as a function of salt concentration for KCl and/or NaCl. This reported 340/380 intensity ratio is standard to assess K^+ concentrations when using PBFI. N=3, error bars represent standard deviation.

5.4.2 Encapsulation in lipid vesicles increases the specificity of PBFI

We hypothesized that one strategy to address the nonspecific response of PBFI to various cations could be to introduce a secondary molecular gating method through the incorporation of bilayer membranes. Ionic balances must be constantly maintained in living organisms, and as such, a number of naturally-occurring membrane transporters exist for various ions.[227] One such

transporter, a bacterially-derived ionophore called valinomycin, specifically transports K^+ ions across membranes.[229] We hypothesized that encapsulating PBFI within valinomycin-containing bilayer vesicles would allow for a specific response to K^+ over other ions. To assess this, lipid vesicles encapsulating PBFI were assembled from thin film hydration techniques using 1,2-dioleoyl-sn-glycero-3-phosphocholine (DOPC) lipids, extruded to a size of 100 nm, and purified to remove unencapsulated dye. The average vesicle diameter was measured using dynamic light scattering and was found to be 99.32 nm, with a polydispersity index of 0.151. To incorporate valinomycin into vesicle membranes, we solubilized the ionophore in DMSO and added it to preformed, purified vesicles. Vehicle controls were prepared by adding the same final volume of DMSO to vesicles in the absence of valinomycin. We expected our resulting vesicle-based nanosensor with incorporated valinomycin would allow us to spatially segregate PBFI from environmental ions and gate transport of K^+ ions to the vesicle interior (**Figure 5.1**).

Once assembled, we first focused on determining the specificity of these nanosensors to K^+ over Na^+ ions (**Figure 5.3 A**). The PBFI fluorescence ratio was measured as a function of valinomycin concentration across varying salt conditions (**Figures 5.3 B-D**). We examined three K^+/Na^+ conditions in which we increased K^+ concentrations in the presence of Na^+ or increased only K^+ or Na^+ in the absence of the other ion. When vesicles were incubated in the presence of both K^+ and Na^+ with a constant total salt concentration of 100 mM (i.e. increasing $[K^+]$ paired with decreasing $[Na^+]$) (**Figure 5.3 A**), the valinomycin-containing vesicles demonstrated a fluorescent response specific to increasing $[K^+]$, while vesicles without ionophore did not exhibit any changes in fluorescence. These results indicate that valinomycin is necessary for the

transport of K^+ across the membrane, and that these nanosensors respond specifically to [K^+] rather than the total salt concentration.

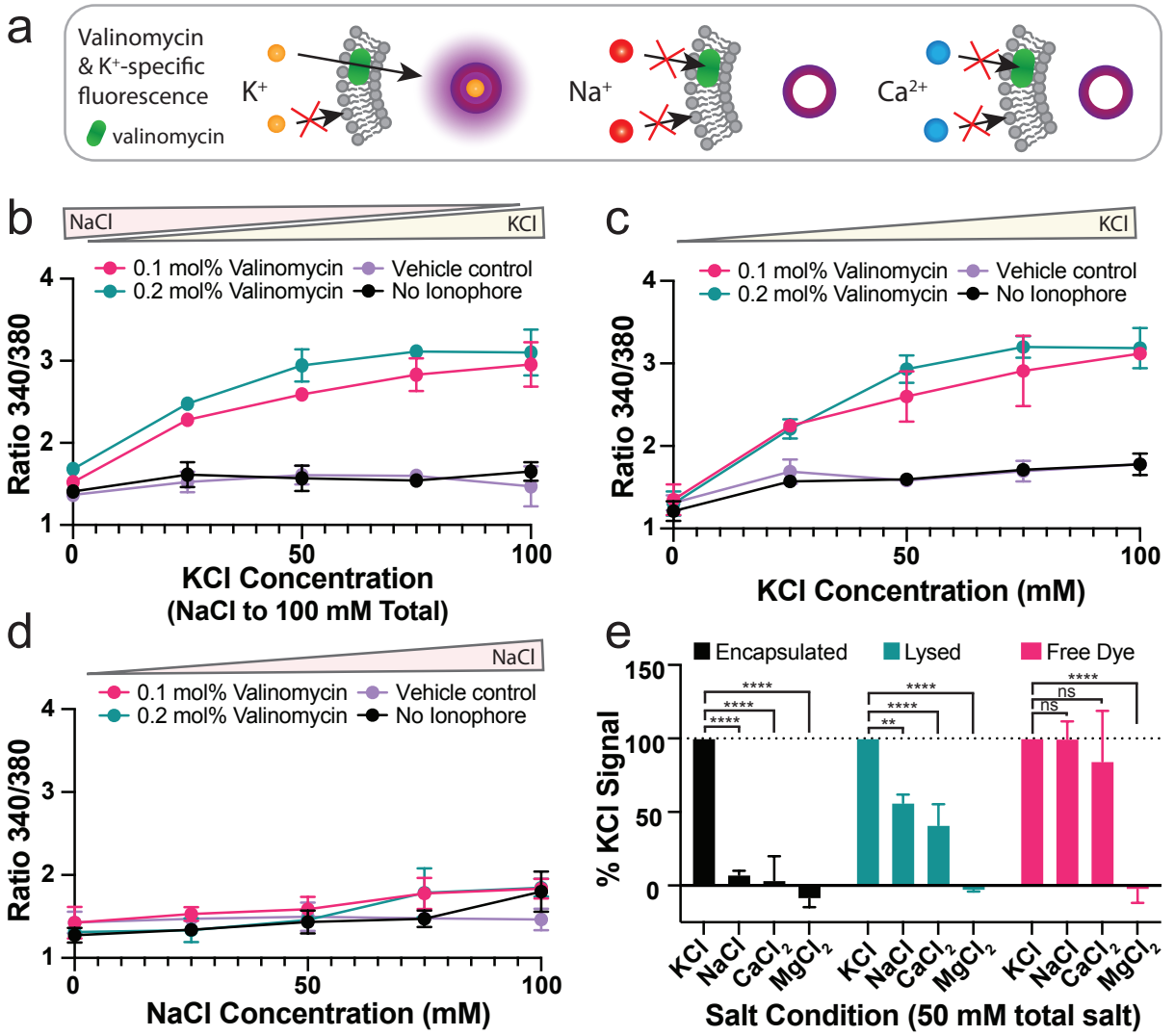

Figure 5.3 Encapsulation of PBFI with valinomycin as a membrane gate improves specificity to K+. A. Schematic illustrating how membrane gating with valinomycin results in K^+-specific access to encapsulated PBFI dye. **B.** Vesicles with either 0.1 mol% or 0.2 mol% valinomycin exhibit a significant increase in PBFI ratio as K^+ concentration increases compared to respective control vesicles, even when Na^+ is present at a total salt concentration of 100 mM ($p \leq 0.0001$, [K^+] > 0 mM). Vesicles without ionophore or with DMSO only (vehicle controls) do not exhibit a response, indicating that increases in PBFI ratio are due to cross-membrane

transport of K^+ by valinomycin. **C.** Vesicles with valinomycin exhibit significant increases in PBFI ratio as K^+ concentration increases compared to respective control vesicles ($p \leq 0.0001$, $[K^+] > 0$ mM), which do not exhibit a significant response. **D.** Vesicles with and without valinomycin do not exhibit significant changes in fluorescence as Na^+ concentrations increase up to 50 mM (samples are not significantly different when $[Na^+] < 75$ mM), with slight nonspecific leakage leading to increased PBFI fluorescence at high Na^+ concentrations compared to respective controls but samples are significantly different ($p \leq 0.05$,) when $[Na^+] = 100$ mM. **E.** Fluorescence ratios reported as a percentage of the maximum KCl signal observed for either PBFI encapsulated in vesicles, PBFI released into solution through vesicle lysis, or free PBFI in solution. In the absence of intact membranes, PBFI reports a higher fluorescence ratio in the presence of NaCl and $CaCl_2$ in addition to KCl. *N=3*, error bars represent standard deviation. ****$p \leq 0.0001$, **$p \leq 0.01$, *$p \leq 0.05$, nonsignificant (ns) $p > 0.05$; p-values generated using a Two-Way ANOVA and Tukey's Multiple Comparisons Test.

Next, nanosensors were incubated with K^+ or Na^+ separately. In the presence of increasing $[K^+]$ alone, PBFI fluorescence in vesicles with valinomycin increased to a similar degree compared to vesicles in the presence of both K^+ and Na^+ (**Figure 5.3 C**). In comparison, vesicles incubated with only Na^+ exhibited minimal fluorescent response, indicating that Na^+ is not able to pass through valinomycin or the vesicle membrane to interact with encapsulated PBFI dye (**Figure 5.3 D**). A small amount of nonspecific leakage of Na^+ into vesicles was observed at high salt concentrations ($[Na^+] \geq 75$ mM), as expected in highly hypertonic conditions. Importantly, the magnitude of the fluorescent output of the sensor when K^+ is the only ion present (**Figure 5.3 D**) is nearly identical to the fluorescent output when both K^+ and Na^+ are present (**Figure 5.3 B**), further indicating that nanosensors are sensitive to and specific for K^+ even when Na^+ is present.

We then assessed the specificity of these nanosensors in the presence of an expanded range of biologically relevant divalent cations, specifically Ca^{2+} and Mg^{2+} (**Figure 5.3 E**). To compare PBFI responses between conditions where PBFI was encapsulated or free in solution, we kept the total PBFI concentration in samples constant. To do this, we prepared vesicles containing PBFI and measured the fluorescence ratio in the presence of 50 mM total salt when vesicles were intact or lysed with a detergent, TritonX-100. As an additional control, we compared these results to PBFI in solution at the estimated final concentration of PBFI following vesicle purification. The fluorescent responses of lysed vesicles and free dye in the presence of various cations show off-target responses to both Na^+ and Ca^{2+} when vesicle membranes are disrupted or are not present. In contrast, intact vesicles containing valinomycin exhibit fluorescent responses to K^+ specifically. While the overall magnitude of fluorescence was reduced in vesicles compared to lysed vesicles or free dye (**Figure 5.4 A-C**), when compared to the maximum K^+ signal for a given encapsulation condition, the specificity to K^+ over Na^+ and Ca^{2+} is significantly improved (**Figure 5.3 E**). Taken together, these results demonstrate the ability of these nanosensors to modulate interactions between encapsulated PBFI and the surrounding environment, allowing specific detection of K^+ concentrations—even in the presence of other cations.

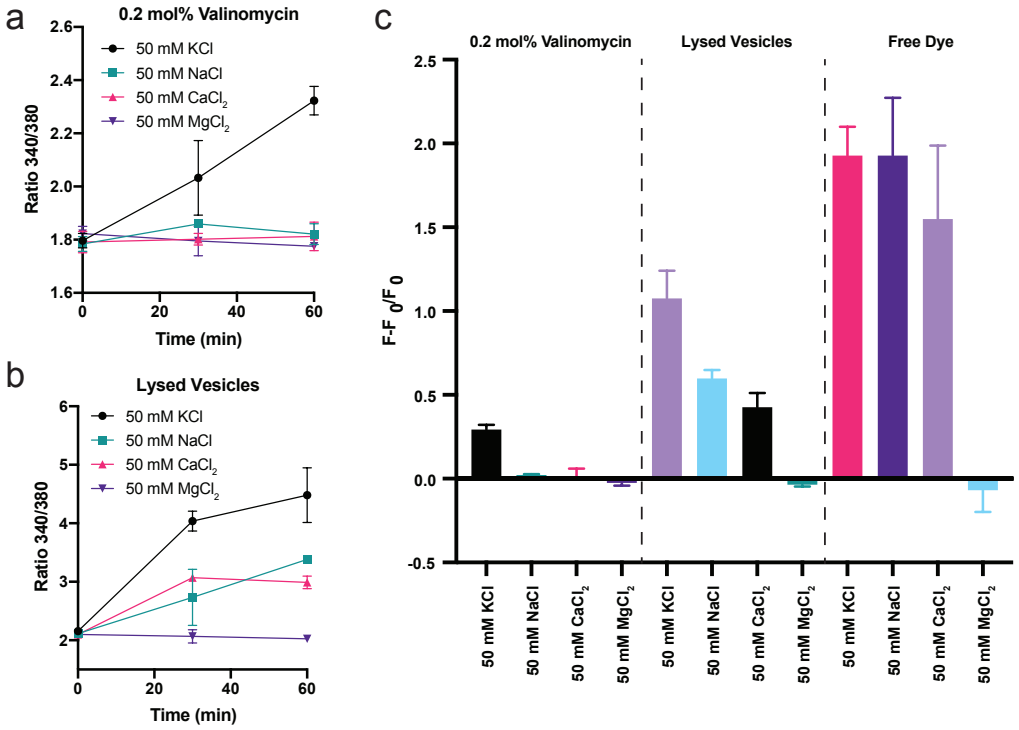

Figure 5.4 PBFI specificity in the presence of various cationic salts. A. Vesicles with 0.2 mol% valinomycin exhibit an increasing PBFI ratio over time only in the presence of KCl. **B.** Lysed vesicles exhibit an increasing PBFI ratio over time in the presence of KCl, NaCl, and $MgCl_2$. **C.** Changes in fluorescence observed in intact vesicles with 0.2 mol% Valinomycin, lysed vesicles, or free dye. Overall PBFI fluorescence is much lower when encapsulated, however the response to off-target ions is significantly reduced. Free dye in solution exhibits the highest overall increase in fluorescence, but responses to off target cations Na^+ and Ca^{2+} are at or near the magnitude of response to K^+, making K^+-specific sensing impossible in this condition.

The responses of our K^+ nanosensor in all salt conditions were observed to be limited to vesicles with intact membranes and incorporated valinomycin ionophores. Vesicles remained stable across the range of salt concentrations assessed (**Figure 5.5 A & B**), further indicating that improved specificity to K^+ occurs through gated entry into the vesicle lumen. Additionally, in this set of stability studies we observed that valinomycin concentrations up to 0.2 mol%

maintained K^+-specificity, and therefore chose to proceed with our studies using 0.2 mol% valinomycin in vesicles. Further, we verified that the quantity of DMSO used to solubilize valinomycin does not lead to significant nonspecific leakage of PBFI or transport of ions into vesicle membranes, as indicated by vehicle controls.

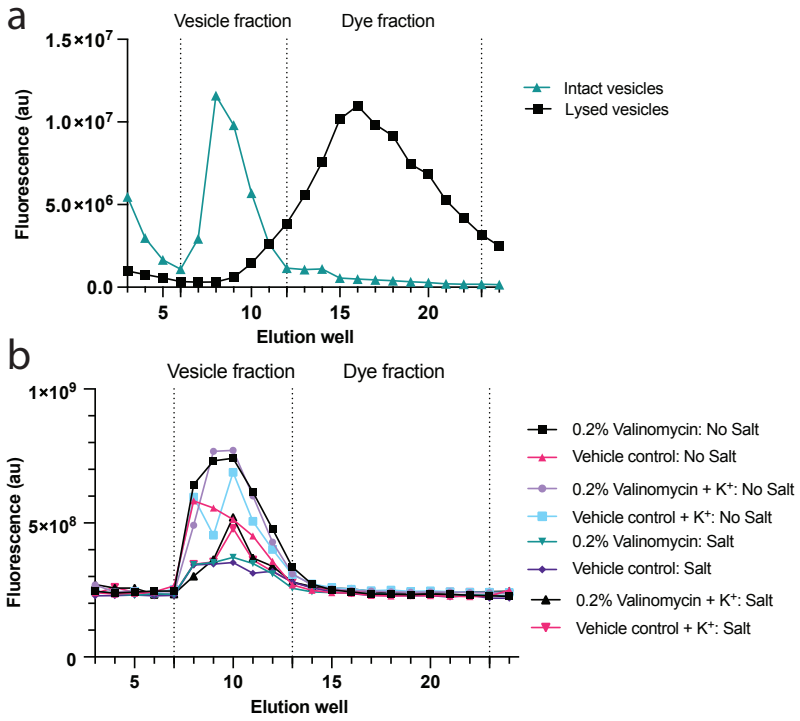

Figure 5.5 Vesicle stability in varying salt conditions. Dye release assays were conducted under various salt conditions to assess vesicle stability. **A.** Vesicles encapsulating a fluorescent dye were purified either before lysis or after lysis with TritonX. The resulting SEC curve shows the elution profile of calcein dye when encapsulated in intact vesicles vs when vesicles are lysed (free dye fractions). Due to its smaller size, the unencapsulated dye elutes later than vesicles. **B.** Vesicles with encapsulated calcein were incubated in buffer either with or without the addition of 100 mM KCl, following which they were purified through SEC columns with or without 100 mM KCl (sample + incubation condition: purification condition). Unlike in A., no free dye peak is observed, demonstrating that the dye remained encapsulated and vesicles remained intact following incubation and/or purification with KCl.

5.4.3 Kinetics and reversibility of K^+ nanosensors.

Having demonstrated that the encapsulation of PBFI with valinomycin-based membrane gating improves the specificity of vesicle nanosensors to K^+, we next wanted to explore the response of these nanosensors to changing KCl concentrations over time. While membrane gating reduces the ability of off-target cations to access encapsulated PBFI, it also creates a barrier between the dye and free K^+ ions. To determine the effect of this spatial segregation on sensing kinetics, we monitored the PBFI response in nanosensors over time following the external addition of 50 mM KCl. Intact nanosensors with 0.2 mol% valinomycin exhibited increasing PBFI fluorescence ratios over time, with a significant difference in signal observable within 10 minutes (**Figure 5.6 A**). PBFI signals were observed to plateau after 1 hour (**Figure 5.6 B**); these results were fit to a one-phase association model, with PBFI fluorescence described as: $Ratio\ 340/380 = 1.86 + 0.42(1 - e^{0.04t})$ (R^2=0.84), yielding a rate constant of 0.04 min^{-1}. No fluorescence changes were observed in vehicle controls, and vesicles lysed with TritonX-100 exhibited significantly higher PBFI ratios than either intact vesicle condition, indicating dye release (**Figure 5.6 A**). Additionally, high PBFI ratios following vesicle lysis indicate that valinomycin-gated vesicles remained intact during salt incubation (**Figure 5.6 B**). While these results indicate that membrane gating does introduce a physical barrier to sensing, thereby increasing the time it takes for nanosensors to reach maximum signal, increases in PBFI ratios were clearly observable on shorter timescales. It is important to note that the maximum increase in PBFI fluorescence is only about 2-fold, which may make the determination of a specific K^+ concentration difficult without sample-specific calibration. Despite this, these nanosensors allow improved comparison between samples, and could also be used as a binary sensor to indicate the

presence or absence of K^+ above a given threshold. These effects could possibly be improved in the future by incorporating faster transport mechanisms, such as counter ion pores, or by increasing the amount of valinomycin in the membrane.

We also wondered whether the response of these nanosensors was reversible, and if the removal of salt from the surrounding environment would cause PBFI fluorescence to decrease. To assess this, we altered the running buffers used for size exclusion chromatography to add or remove salt from vesicle buffers. We first incubated unpurified nanosensors with or without 100 mM KCl for one hour, allowing them to saturate with K^+. We then purified them using running buffer both with and without 100 mM KCl, with some nanosensors experiencing addition of KCl during purification and others experiencing KCl removal, and allowed them to incubate in these new conditions for another hour. As expected, nanosensors incubated without KCl exhibited low PBFI ratios when purified without salt, whereas PBFI responses increased significantly when 100 mM KCl was introduced in the running buffer. In contrast, nanosensors incubated with saturating levels of KCl prior to purification exhibited a further increase in PBFI signal following purification with excess KCl, while the PBFI signal when purified without salt was decreased. Dye leakage assays indicated that nanosensors remain stable throughout the incubation and purification processes (**Figure 5.5**). Importantly, the reduced signal observed in the preincubated-with-salt/purified-without-salt condition compared to the preincubated-without-salt/purified-with-salt condition indicates some degree of reversibility in the nanosensor signal in response to changing K^+ (**Figure 5.6 C**). We therefore expect these nanosensors could ultimately respond to dynamic salt conditions, increasing and decreasing fluorescence with changes in $[K^+]$ over time.

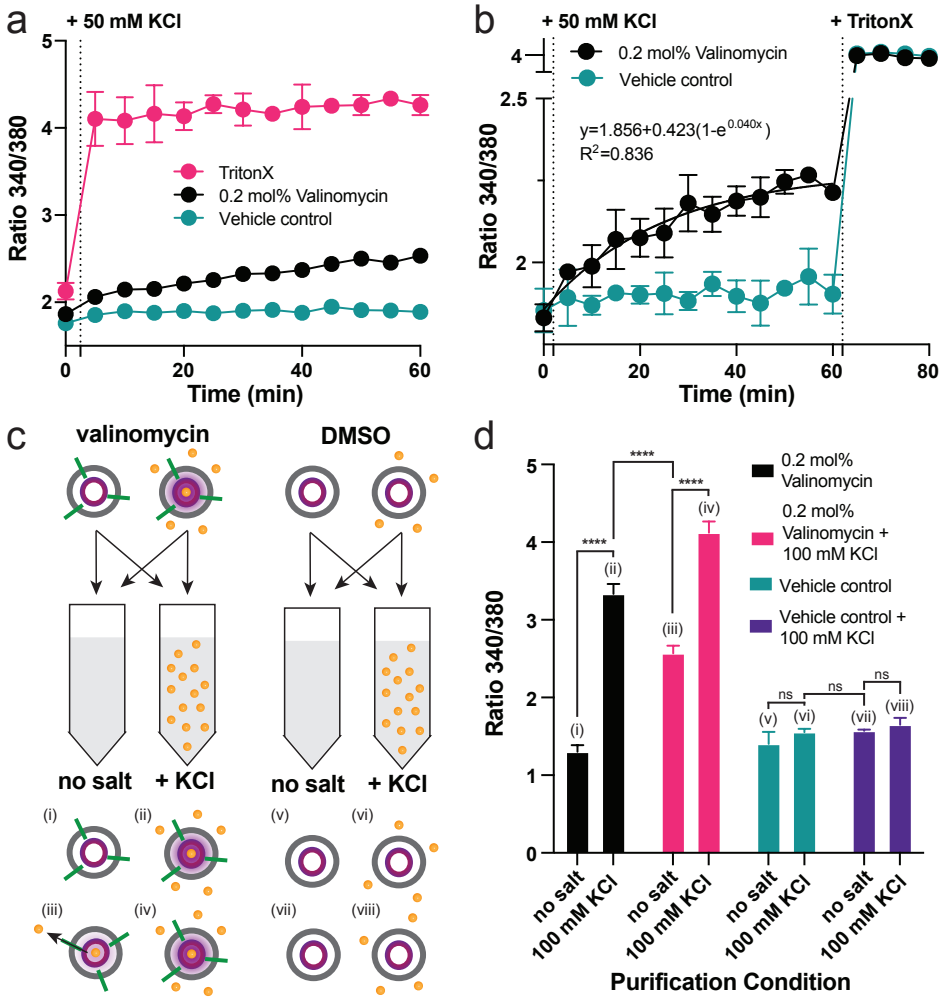

Figure 5.6 Response of vesicle sensors to changing salt conditions over time. A. PBFI fluorescence in vesicles with valinomycin in the membrane increases over time following 50 mM KCl addition to surrounding buffer. Fluorescence does not change in corresponding vehicle controls, indicating that increasing PBFI ratios in vesicles are due to valinomycin-specific transport of K+, and high PBFI ratios in TritonX-lysed controls indicate that valinomycin-containing vesicles remained intact. 0.2% valinomycin vesicles exhibit a significantly higher PBFI ratio than vehicle controls within 10 minutes ($p \leq 0.05$). **B.** PBFI ratios in valinomycin-containing vesicles fitted to a one-phase association model (equation shown on graph). After lysis with TritonX, an increase in PBFI ratio indicates that vesicles remained intact following KCl addition. **C.** Schematic of reversibility assays. Four populations of vesicles were generated:

with and without valinomycin and with and without 100 mM KCl. Each population was purified through two columns, resulting in eight final salt conditions. Numerals correspond to results in D. and yellow circles represent potassium. **D.** Vesicles incubated without KCl (black) show a significant increase in PBFI ratio when purified through SEC columns with 100 mM KCl in the running buffer, while vesicles incubated with 100 mM KCl (pink) show a significant reduction in PBFI ratio when purified through SEC columns without salt in the running buffer. Vesicles with and without pre-incubation in KCl show significantly higher PBFI ratios when purified with KCl in the running buffer compared to salt-free buffer. Vehicle control vesicles both with (purple) and without pre-incubation (green) show no significant difference in fluorescence following purification. N=3, error bars represent standard deviation. ****$p \leq 0.0001$, ***$p \leq 0.001$, **$p \leq 0.01$, *$p \leq 0.05$, nonsignificant (ns) $p > 0.05$; p-values generated using a Two-Way ANOVA and Tukey's Multiple Comparisons Test.

5.4.4 Assessing K^+ nanosensors in bacterial cultures

Finally, we wanted to determine if these nanosensors could monitor K^+ concentrations in a biological context. Specifically, we wanted to assess whether nanosensors could detect changes in salt concentrations due to bacterial release or uptake. To accomplish this, we resuspended pelleted BL21 *Escherichia coli* grown in MSgg media into Tris buffer, and mixed bacteria with nanosensors (0.2 mol% valinomycin and vehicle control, 1 mM final concentration in Tris buffer) in fluorimeter cuvettes to three different optical densities. We monitored nanosensor fluorescence in the presence of increasing concentrations of bacteria without any salt for 30 minutes in order to assess any changes in fluorescence due to bacterial addition alone. We observed slightly decreased levels of baseline fluorescence as the concentration of bacteria increased, but variations were small and did not change over time (**Figure 5.7 A & B**).

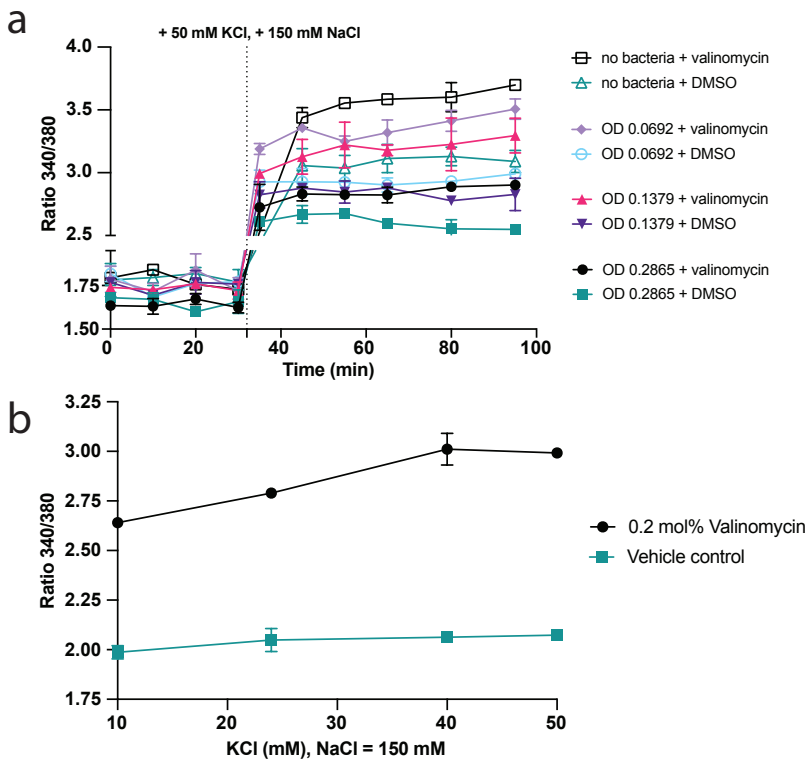

Figure 5.7 Changes in vesicle fluorescence decrease as bacterial OD increases. A. Following the addition of KCl and NaCl, sensors exhibit increases in PBFI fluorescence that vary depending on the concentration of bacteria present. Slight variations with OD and higher overall PBFI ratios were observed, indicating that some vesicle instability may occur during bacterial incubation and buffer transfers, however valinomycin conditions remain higher than vehicle controls as assessed in Figure 5. N=2. **B.** Sensor calibration in the salt conditions used for bacterial assays. With high NaCl some nonspecific leakage is observed, as expected for vesicles under osmotic stress. A slight decrease in PBFI fluorescence ratio in sensors can be observed as KCl concentration decreases. N=2.

We then added 150 mM NaCl and 50 mM KCl to each cuvette to generate a salt shock and monitored PBFI spectra for 1 hour (**Figure 5.8 A**). To control for variations in baseline fluorescence due to increased optical density, final PBFI fluorescence in nanosensors was normalized to initial pre-salt values (**Figure 5.8 C**). In the presence of NaCl and KCl, we

observed a significant decrease in the change in PBFI ratio as bacterial concentration increased (**Figure 5.8 C**), indicating a lower K^+ concentration detected by the nanosensors. We expect that this is due to NaCl creating a hyperosmotic shock, inducing the bacteria to take up K^+ from the surrounding buffer.[231-235] With a higher number of bacteria present, we expect that this uptake would have an overall greater effect on the bulk K^+ concentration.[236] A nonsignificant decrease in fluorescence was observed in vehicle controls, however this is consistent with nonspecific leakage observed in high salt conditions (**Figure 5.7**).

We then imaged vesicles co-incubated with bacteria for 1 hour to assess stability and localization. We were unable to assess the 380 nm excitation of PBFI and therefore the ratiometric response to K^+, however we observed the fluorescence of a vesicle membrane dye, Cy5.5-PE, co-localized with faint PBFI fluorescence at the 340 excitation, indicating vesicles remain intact in the presence of bacteria (**Figure 5.8 B**). Overall, these results indicate that these nanosensors are able to detect changes in K^+ concentrations in biological samples, even in the presence of high Na^+ concentrations. Moving forward, however, buffers may need to be optimized or matched for a given biological environment and sensor calibration may be required for diverse sample types. In addition, other ionophores whose excitation/emission wavelengths are more compatible with microscopy should be explored. With these factors taken into account we expect these results could be expanded to other biological contexts, including samples from eukaryotic systems.

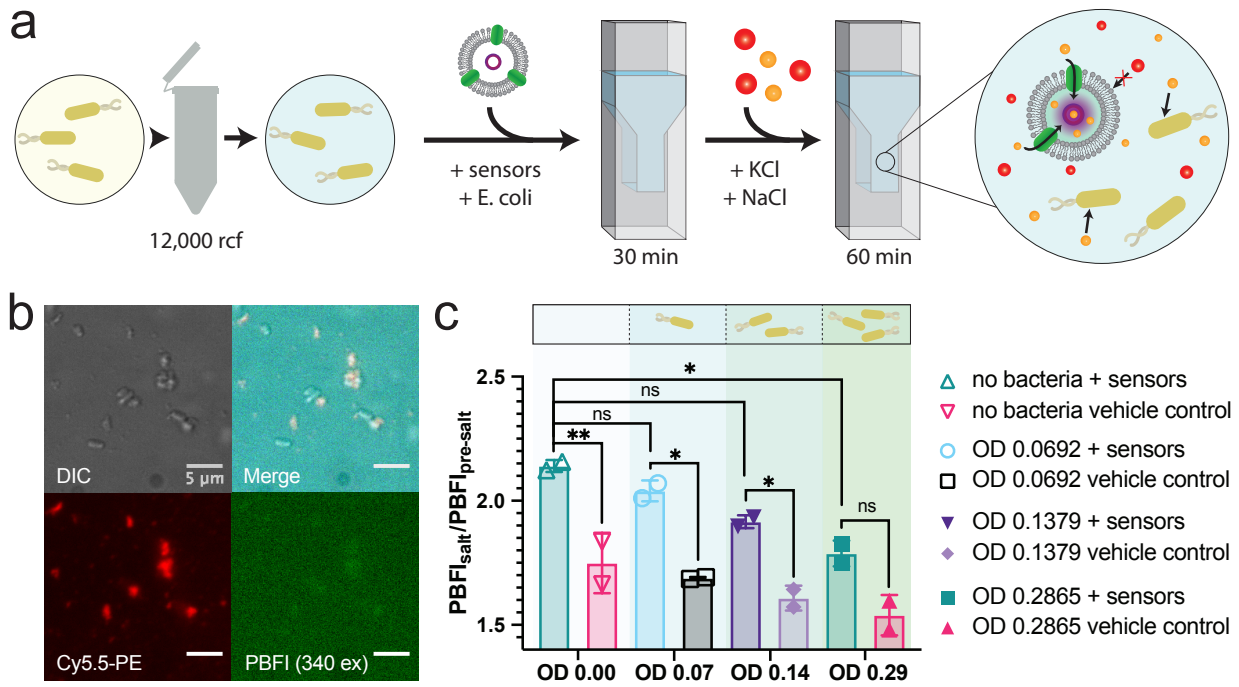

Figure 5.8 Vesicles detect variations in [K+] in the presence of increasing concentrations of bacteria. A. Schematic of bacterial studies with nanosensors. First, bacteria grown in MSgg media are spun down and resuspended in equiosmolar Tris. Bacteria diluted to varying final optical densities are added to a fluorimeter cuvette with 1 mM nanosensors. Following a 30-minute incubation in the absence of salt, 50 mM KCl and 150 mM NaCl are added to cuvettes. Nanosensor fluorescence was assessed via fluorimeter after 1 hour incubation following salt addition. **B.** Nanosensors imaged after 1 hour of co-incubation with bacteria show distinct fluorescence of Cy5.5-PE, a membrane dye, and faint localization of PBFI measured at the 340 nm excitation wavelength. Nanosensors can be observed to be intact and in solution surrounding bacterial cells. **C.** Change in nanosensor fluorescence following salt addition decreases as the concentration of bacteria increases, indicating potassium uptake by bacteria. Nanosensors in the absence of bacteria exhibit a significantly higher change in fluorescence compared to nanosensors incubated with bacteria at an optical density of 0.2865. Similarly, a significant difference was observed between sensor and vehicle control conditions in the absence of bacteria, while significance between these conditions decreases as bacterial optical density increases. No significant differences were observed between any vehicle control conditions (pink, black, light purple and pink bars; ns $p > 0.05$), not shown. N=2, error bars represent

standard deviation. **$p \leq 0.01$, *$p \leq 0.05$, nonsignificant (ns) $p > 0.05$; p-values generated using a Two-Way ANOVA and Tukey's Multiple Comparisons Test.

5.5 Conclusions

Here, we have demonstrated that the specificity of an optical K^+ indicator can be improved by spatially segregating the indicator from its surrounding environment and introducing molecularly specific transporters to modulate its access to various ions. We observed that the encapsulation of PBFI dye in lipid vesicles prevented the indicator from interacting with off-target cations, particularly Na^+ and Ca^{2+}, which cannot readily pass through bilayer membranes.[170] We then showed that the incorporation of the K^+-specific transporter valinomycin subsequently restored the access of K^+ to the vesicle interior, allowing sensors to respond to increasing K^+ concentrations in the surrounding buffer. While this physical barrier does impact the speed of detection for these nanosensors compared to free dye, it also greatly improves the specificity of K^+ detection for this indicator. Finally, we were able to detect changes in K^+ concentrations in bacterial cultures in response to hyperosmotic shock, showing that changes in extracellular K^+ concentrations and bacterial uptake of K^+ can be detected. While buffer components and incubations times are important factors to consider in deployment of these nanosensors, the improved specificity, ease of use, and straightforward assembly of this platform may expand the applications of small-molecule, ion-specific sensing.

In many biological contexts in which various cations are present simultaneously, the ability to distinguish between ions of varying identities is key to understanding the role of electrolyte balance in biological functions. Nanosensors such as the one described here may help

improve the functionality of existing technologies, namely fluorescent, small-molecule indicators, toward these applications. Vesicles in particular provide an exciting platform to expand the environments in which ion indicators can be used, as they can incorporate a wide variety of natural and synthetic components, can be engineered to be highly biocompatible, and can retain stability in a range of extravesicular environments.[12] They might also serve as a "handle" to concentrate and retain these signals in a localized environment, something difficult to achieve with free dye alone. Understanding how vesicle encapsulation balances the kinetics and signal of ion indicators will be an important next step for investigation. Drawing from a diverse toolbox of naturally-derived membrane transporters, synthetic and naturally-derived lipids, and water-soluble small molecule indicators, a diverse set of sensors could be developed which allow for the specific detection of small molecule target molecules—even in the presence of similar analytes.

Chapter 6: Aptamer-based sensing inside lipid vesicles using transcription

6.1 Foreword

Indicator-based nanosensors can be incredibly useful when a specific small molecule indicator exists for a given analyte of interest. The required properties of the indicator depend on the desired application, for example sufficient specificity, brightness and photostability, cytotoxicity, etc. While there are a number of chemical indicators that are commercially available (and many more that have been developed in research labs globally), these systems generally hinge on a single intermolecular interaction for detection, which must be properly designed in a synthetic context to allow detection, and often suffer from limited selection of fluorescence wavelengths and problems with toxicity and loading.[237,238] A powerful alternative is to engineer and encapsulate genetically encoded biosensors to detect a wider array of analytes. These systems allow the redirection of a wide variety of naturally derived and naturally inspired molecular detection mechanisms to sense a broad range of biologically and technologically important molecular targets.[238-240]

As a first step towards the encapsulation of complex, genetically encoded biosensors which use both transcription and translation to detect a molecule of interest, we first sought to encapsulate a transcription-only system with an RNA aptamer readout. We also demonstrate that the addition of nonspecific membrane pores can allow Magnesium (Mg^{2+}) ions – a required cofactor of T7 polymerase – to enter the vesicle interior and initiate encapsulated transcription reactions. This chapter serves as preliminary work towards the encapsulation of a riboswitch-based sensor for fluoride ions in Chapter 7.

6.2 Introduction

Cells are adept at sensing their environment and initiating a respective response - in fact, this is regarded as one of the key capabilities that serves as a defining feature of living organisms.[241,242] Certain sensing mechanisms exist within cells to allow this behavior; these mechanisms are encoded within the cell's DNA and are generally enacted through their resulting proteins, directing appropriate responses to promote cell survival within a changing environment.[241] Many of the molecular targets for these sensing circuits are small molecules that we are also interested in detecting in our environment, for example nucleic acids, antibiotics, and heavy metals.[239,243-245] While we can design chemical indicators for these molecules from scratch, an alternative approach is to leverage the pre-existing sensing mechanisms found in cells to our advantage by incorporating these sensors into technologically useful constructs in cell-free expression systems.[239] In this way, genetically encoded sensors can extract the strong, specific, naturally existing molecular interactions used by cells and can harness them for directed sensing behaviors in an *in vitro* context.

As our ability to engineer nucleic acid constructs has advanced, these genetically encoded systems can also be engineered to interact with synthetic components to improve sensing or readout characteristics.[238] One example of this type of hybrid platform is RNA aptamer-based sensors, in which RNA binds to and structurally alters a chemical indicator to generate an optical response.[238,246-248] While the chemical indicator remains an integral part of the system, it is not participating in the sensing behavior and instead is incorporated into the system as a bright readout of RNA production. These types of sensors are advantageous in particular due to their bright and photostable output compared to fluorescent proteins, which can exhibit poor stability

and low fluorescence.[247] Importantly, RNA transcription-based sensors are significantly faster than expression-based outputs because they eliminate all downstream steps of protein expression and folding.[150] As RNA aptamer transcription can be dictated through DNA encoding, these readouts can then be coupled to genetic or protein-mediated sensing mechanisms to design genetically encoded systems with a bright indicator-based readout.[247,249]

While RNA-based sensing can offer improved kinetics and output compared to protein-based sensing, a critical limitation is the instability of RNA in many environments due to the widespread prevalence of its degradative pathways.[250] For this reason, it would be of interest to encapsulate these sensors in bilayer vesicles, which would allow protection from RNA degradation by external nucleases and could create mobile, nanoscale sensors. While the incorporation of a membrane barrier between the RNA sensor and the surrounding environment can serve to protect the encapsulated nucleic acids, a barrier is also introduced between the sensor and its given analyte. For this reason, strategies to allow analytes to enter the vesicle interior are necessary to allow the encapsulated system to detect a given small molecule. This cross-membrane transport can be achieved multiple ways; first, specific molecules like ionophores or membrane proteins can be incorporated into the membrane to transport a specific target to the vesicle interior.[12,242] Alternatively, sensor targets can be chosen such that they are membrane permeable, which doesn't require any additional transporter incorporation, and which can be modulated by changing membrane composition.[12] Finally, nonspecific pores can be used to allow any molecule below a given size to enter the vesicle. This strategy offers the most diversity in terms of analyte selection and can easily be achieved through the external addition of water-soluble membrane pores.[38,84,164,171,179]

Here, we encapsulate a transcription-based sensor inside of bilayer vesicles. We explore the compatibility of encapsulated aptamer dyes with membranes and establish the effect of membrane composition on membrane pore insertion. We then initiate an encapsulated reaction through the pore-mediated transport of magnesium (Mg^{2+}) ions into the vesicle interior through nonspecific alpha hemolysin (αHL) pores. We chose Mg^{2+} as a model analyte as it is not membrane permeable but is a required cofactor for T7 polymerase,[251] allowing us to modulate T7 activity and subsequently initiate transcription through external addition of Mg^{2+}. By compartmentalizing this transcription reaction inside lipid bilayers, we show that we can detect Mg^{2+} in the surrounding buffer - even with degradative enzymes present - with a response that is proportional to the concentration of pores that are added to the membrane.

6.3 Materials & Methods

Chemicals

DOPC and cholesterol were purchased from Avanti Polar Lipids, Inc. TO1-3PEG-Biotin was purchased from Applied Biological Materials. DFHBI was purchased from Sigma Aldrich. αHL, NTPs (as a Tris buffered set) and DTT (Dithiothreitol) were purchased from Thermo Fisher. Tris, KCl and $MgCl_2$ buffers were purchased as a buffer kit from Life Sciences. Proteinase K, DNAse I and Exonuclease III were purchased from New England Biolabs. T7 polymerase and nucleic acid constructs were prepared by the Lucks Lab.

Vesicle formation in TxDx buffer

Vesicle formation was validated in transcription buffer, denoted here as “TxDx”. 10x TxDx buffer: 20 mM spermidine, 400 mM Tris-HCl pH 8, 100 mM DTT, 8 mM $MgCl_2$ and 200 mM KCl, diluted in MilliQ water. DOPC vesicles were prepared via thin film hydration in PBS and TxDx buffers with 20 mM calcein dye and extruded to 100 nm in diameter. Vesicles were purified using Size Exclusion Chromatography to remove unencapsulated dye using a Gilson Fraction Collector. Vesicles were incubated for 24 hours at room temperature and purified a second time to assess how much dye had leaked out of the vesicles over time. Elution fraction was assessed via plate reader (ex: 495 nm, em: 515 nm). GUVs were also formed via thin film hydration in TxDx buffer and imaged via DIC microscopy to visually confirm the presence of vesicles.

Encapsulation and membrane interactions of DFHBI and TO1-3PEG-Biotin

To assess interactions between DFHBI dye and lipid membranes, GUVs were formed via thin film hydration encapsulating the dye and all transcription reaction components except for NTPs (to inhibit the reaction). Vesicles were imaged via epifluorescent microscopy using DIC and GFP filters. DFHBI was observed to fluoresce nonspecificially in the presence of lipid membranes, therefore the Mango apatamer/TO1-3PEG-Biotin system was explored as an alternative. Membrane-dye association with the Mango aptamer was first assessed by both encapsulating the TO1-3PEG-Biotin dye in lipid vesicles and incubating it with pre-formed vesicles and assessing nonspecific activation via plate reader (ex: 510 nm, em: 535 nm) and via microscopy using a GFP filter. Then, RNA/TO1-3PEG-Biotin dye/Membrane interactions were assessed by encapsulating a purified RNA aptamer at 4 uM with a tenfold excess of dye in electroformed DOPC and 1:1 DOPC:Cholesterol GUVs prepared in sucrose buffer (Nanion

Vesicle Prep Pro, standard protocol). GUVs were imaged using epifluorescent microscopy via DIC and GFP filters (ex: 495 nm, em: 520 nm).

Encapsulation of a strand-displacement reporter system

Vesicles were formed via electroformation (Nanion Vesicle Prep Pro, standard protocol) containing sucrose buffer and various ratios of reporter and quencher DNA strands. DNA sequences were as follows:

InvadeR-Quencher (KKA.C36): CCTTGTCA TAGAGCTC /3IABkFQ/

InvadeR-Reporter (KKA.C37): /56-FAM/ GAGCTCTA TGACAAGG GCTAGGTT

Vesicles were assembled encapsulating DNA strands at a 1:0, 2:1 and 1:2 ratio of reporter:quencher (1 μM reporter concentration) and imaged via epifluorescent microscopy using DIC and GFP filters.

Mango aptamer reaction preparation

DNA sequences were as follows:

KKA.E06 Mango3(trunc)top:

taatacgactcactatagGGCGTACGAAGGAAGGATTGGTATGTGGTATATTCGTACGCC

KKA.E97 Mango3(trunc)bottom:

GGCGTACGAATATACCACATACCAATCCTTCCTTCGTACGCCctatagtgagtcgtatta

DNA strands were annealed together at a 1:1 ratio at 95°C for 1 minute to a final concentration of 5 μM. 10x TxDx buffer was prepared in MilliQ water with 20 mM spermidine, 400 mM Tris-HCl pH 8, 100 mM DTT (prepared fresh for each experiment), and 200 mM KCl. Reactions were assembled on ice to a final volume of 200 μL in MilliQ water with 0.25 μM annealed

DNA, 50 μM TO1-3PEG-Biotin dye, 8 μM NTPs, 4 μL T7 polymerase stock (provided by Lucks Lab), and 20 μL 10x TxDx buffer. Magnesium was omitted from the buffer preparation.

Encapsulation of functional Mango aptamer construct

Transcription reactions were encapsulated in 1:1 DOPC:Cholesterol vesicles using thin film hydration. Briefly, lipid films were prepared to 20 mM final concentration in chloroform and dried under vacuum pressure overnight. Films were hydrated with 200 μL of transcription reaction mixture, prepared as described above, for 3 hours at 4°C with shaking. Following hydration, vesicles were extruded to 400 nm (7 passes through a polycarbonate membrane, Avanti Polar Lipids, Inc.) and kept on ice until use.

Vesicle purification, aHL addition and aptamer transcription

Vesicles were purified via enzymatic degradation (SEC and dialysis were tried as well but resulted in high background fluorescence due to an inability to purify T7 away from membranes using these methods). For a 200 μL sample, 1.25 μL DNAse I, 1 μL Exonuclease III + 1 μL 100 mM $CaCl_2$, and 10 μL Proteinase K were added to the vesicle solution on ice and mixed thoroughly by pipetting up and down.[172] Vesicles were diluted in 1x TxDx buffer in a plate and then fluorescence was read for 30 minutes at 37°C via plate reader (ex: 510 nm, em: 535 nm) to allow digestion to proceed before αHL and Mg^{2+} addition. After 30-minute digestion was complete, the plate was removed and αHL in 1x buffer and Mg^{2+} stock were added. Mg^{2+} was added to a final concentration of 8 mM. αHL was added to final concentrations of 0 μg/mL, 10 μg/mL, 20 μg/mL and 30 μg/mL. Fluorescence was then monitored via plate reader (ex: 510 nm, em: 535 nm) for 10 hours at 37°C.

6.4 Results and Discussion

6.4.1 Stable lipid membranes can be formed in transcription buffers and can encapsulate nucleic acids

The first consideration in transitioning from an indicator-based sensor to a gene expression-based sensor is that the incorporation of biological sensing circuits requires the presence of specific small molecules and certain buffer conditions. As a first step towards encapsulating these systems, we set out to confirm that vesicles could be formed in a transcription-specific buffer, here referred to as TxDx Buffer. To assess vesicle formation and stability, we encapsulated a self-quenching dye, calcein, which exhibits an increase in fluorescence upon release from the more concentrated environment of the vesicle interior. Following a 24-hour incubation in TxDx buffer, vesicles remained stable and dye remained encapsulated in similar amounts compared to a PBS control (**Figure 6.1 A & B**). Vesicles could also be visualized on the microscope (**Figure 6.1 C**).

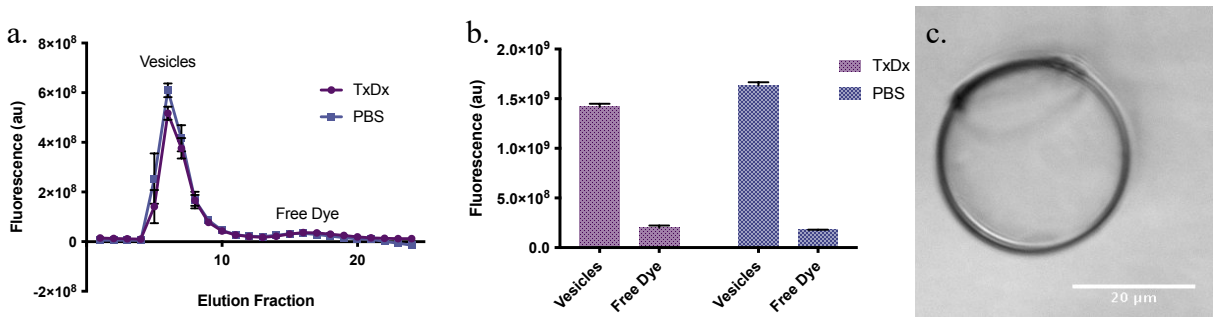

Figure 6.1 Vesicle formation and stability in TxDx buffer. A. Size exclusion chromatography elution fraction of vesicles encapsulating a self-quenching dye, calcein, after 24 hours incubation at room temperature. Both free dye peaks are small compared to vesicle peaks, indicating vesicles remain stable and dye remains encapsulated. **B**. Fluorescence under each peak in (A).

Vesicle fractions are significantly larger than free dye fractions. **C.** Micrograph of thin film GUV in TxDx buffer. Scale = 20 μm.

Having established that vesicles can be formed in a transcription-specific buffer, we next sought to encapsulate nucleic acid constructs inside vesicles. One way to quantify nucleic acid encapsulation is to incorporate fluorescently tagged DNA strands into the hydration buffer and to assess localization to the vesicle interior. Fluorescence can then be reduced by introducing invading DNA strands with quencher molecules conjugated to them; these strands invade the self-interacting fluorescently tagged strands and bind to them, bringing dye and quencher molecules into close proximity and resulting in a quenched fluorescent signal.[252] These quencher/reporter pairs can serve as a readout of genetically encoded sensors, in which the analyte triggers expression of an invading nucleic acid strand. More simply, however, they can serve as a straightforward indicator to show that DNA segments are encapsulated within vesicles and localized to the vesicle interior.

Following the addition of fluorescently tagged DNA strands into the TxDx buffer used for hydration, GUVs were observed via microscopy to assess DNA localization to the vesicle interior. DNA reporter and quencher strands were encapsulated at a ratio of 1:0 reporter:quencher, 2:1 reporter:quencher and 1:2 reporter:quencher, resulting in an unquenched, a partially quenched and a fully quenched state. Fluorescence inside vesicles was observed to decrease as the ratio of quencher strands was increased, consistent with increased interactions between reporter and quencher molecules caused by DNA binding (**Figure 6.2 A-C**). These results indicate that nucleic acids can be encapsulated within lipid vesicles in order to localize them to vesicle interiors.

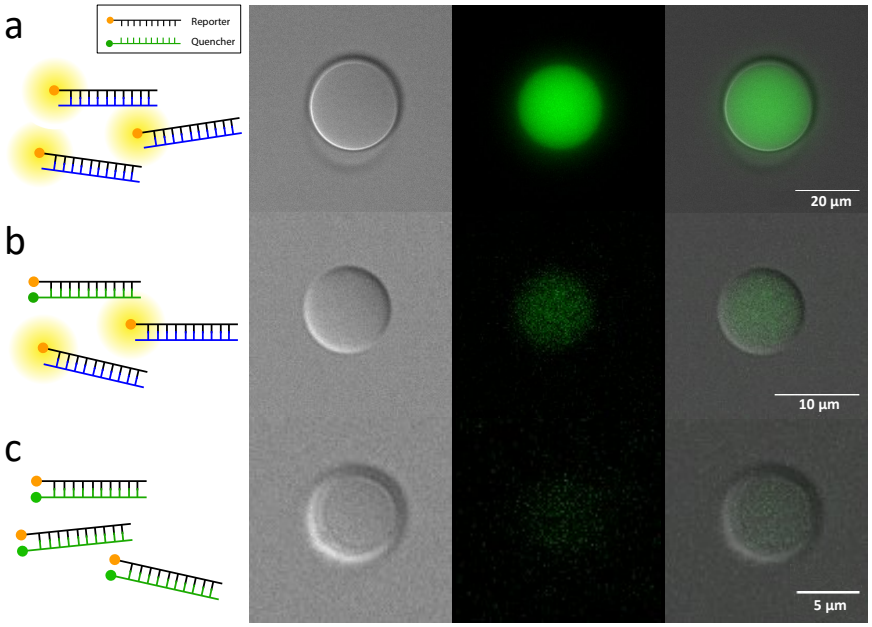

Figure 6.2 Encapsulation of DNA strands with reporter-quencher pairs. A. Strands of DNA conjugated to a fluorescent reporter molecule are encapsulated inside lipid vesicles (Micrographs left to right: DIC, GFP, Merge). Scale = 20 µm **B.** Upon the introduction of complementary DNA strands conjugated to a quencher molecule the fluorescence inside vesicles is observed to decrease, consistent with binding of quencher and reporter DNA strands. Scale = 10 µm **C.** With an excess of quencher molecules the fluorescence inside vesicles is effectively eliminated. Scale = 5 µm.

6.4.2 Aptamer dyes interact nonspecifically with lipid bilayer membranes

Although encapsulated strand displacement systems can serve as a reporter of gene expression, we aimed to incorporate genetically encoded sensors that could instead bind to a small molecule dye rather than requiring a strand-displacement-regulated output to function. We expected this approach to yield greater flexibility in aptamer selection and reduce the number of large molecules which need to be encapsulated. In order to accomplish this, we first set out to assess the compatibility of aptamer dyes with membrane encapsulation. Many aptamer-based

readouts function by generating a fluorescence-activating structural change in a small molecule dye upon binding to an RNA molecule.[247] A commonly used aptamer is the Broccoli aptamer, which interacts with a small molecule dye called DFHBI.[247,253] Upon encapsulation of DFHBI in lipid vesicles, however, we observed significant nonspecific fluorescence in the absence of the RNA aptamer (**Figure 6.3 A**). We hypothesize that this is due to insertion of the hydrophobic portions of the dye into the membrane during the vesicle formation process (**Figure 6.3 B**), which could force the dye into its activated planar form.[247] We therefore sought to find an alternative that may interact less with bilayer membranes.

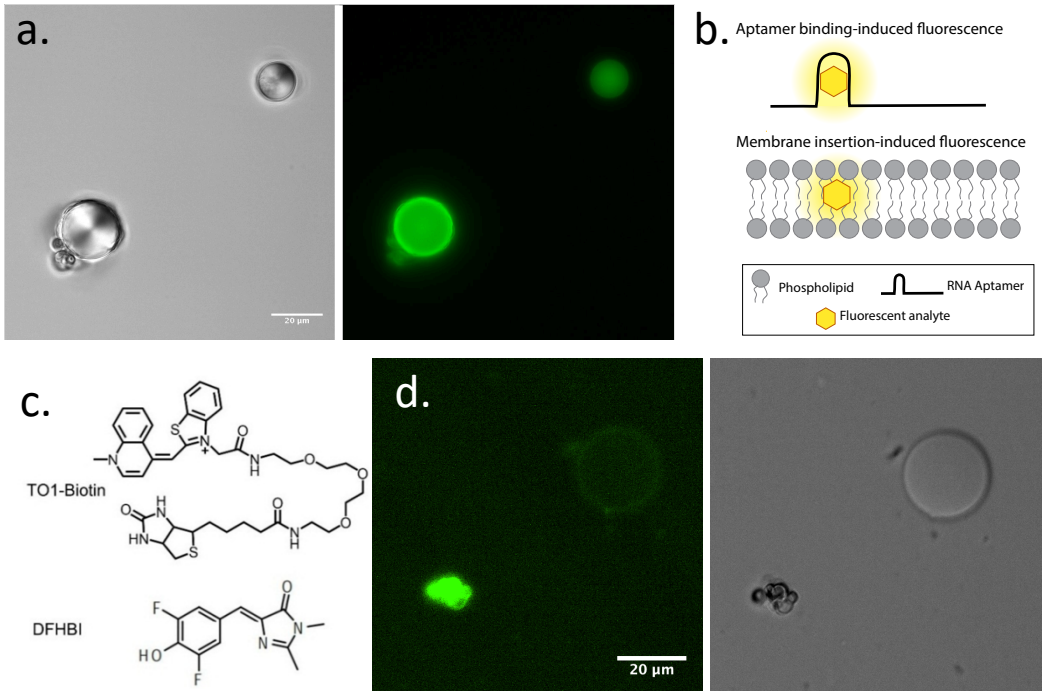

Figure 6.3 Aptamer dye encapsulation in GUVs. A. Encapsulation of DFHBI dye in thin film GUVs results in high nonspecific fluorescence in the absence of RNA aptamer product. Scale = 20 µm. **B.** Hypothesized model of nonspecific fluorescence. **C.** Dye structure of TO1-3PEG-Biotin and DFHBI, dyes for the Broccoli and Mango aptamers, respectively. Reprinted, with permission, from reference [238]. **D.** Encapsulation of TO1-3PEG-Biotin dye results in some

nonspecific fluorescence in lipid aggregates, but very low nonspecific fluorescence in unilamellar GUVs. Scale = 20 μm.

As an alternative to the nonspecific DFHBI dye, we next assessed the encapsulation of the TO1-3PEG-Biotin dye, which interacts with the Mango RNA aptamer.[253] TO1-3PEG-Biotin is a larger molecule with less relative hydrophobicity compared to DFHBI (**Figure 6.3 C**). We hypothesized that these chemical and structural differences would prevent some of the nonspecific signal observed with DFHBI. As anticipated, upon encapsulating the dye in lipid vesicles we observed lower levels of nonspecific fluorescence in vesicle membranes (**Figure 6.3 D**). While nonspecific fluorescence was significantly lower than that observed with DFHBI, it was not completely eliminated; there were still low levels of fluorescence observed in unilamellar GUVs, and relatively bright nonspecific fluorescence was observed in lipid aggregates. These aggregates are often a byproduct of thin film GUV formation, and we expect improved unilamellarity in extruded SUVs;[167] therefore, the signal was sufficiently low in unilamellar vesicles that we expected it would not overpower RNA-specific fluorescence in our extruded vesicles. We therefore chose to move forward with the Mango/TO1-3PEG-Biotin system for future transcription studies.

Finally, as a first step toward reaction encapsulation, we sought to establish the expected signal output of RNA-dye interactions inside vesicles. The fluorescent output of the Mango aptamer is produced through the transcription of an RNA molecule that interacts with TO1-3PEG-Biotin dye. While we observed that the reaction components and DNA were compatible with encapsulation, we wanted to confirm that the presence of the RNA product would also be compatible with the vesicle membrane – particularly as RNA is known to interact

electrostatically with bilayer membranes.[254,255] To assess this, we co-encapsulated the aptamer dye in electroformed GUVs with and without purified RNA product present. We added cholesterol to the membrane, which improves vesicle stability and allows future pore incorporation. We observed intact vesicles (**Figure 6.4 A & D**) that exhibited high fluorescence in the presence of the RNA product (**Figure 6.4 B & C**) and low fluorescence in the absence of the RNA product (**Figure 6.4 E & F**), consistent with the results observed in the presence and absence of RNA in bulk conditions (**Figure 6.4 G**). We did not observe any strong fluorescence localization to the membrane, indicating that the presence of RNA and dye does not cause significant membrane interactions. These results indicate that the RNA product is also compatible with encapsulation, and that we can detect a higher concentration of RNA based on the intensity of fluorescence inside vesicle lumen.

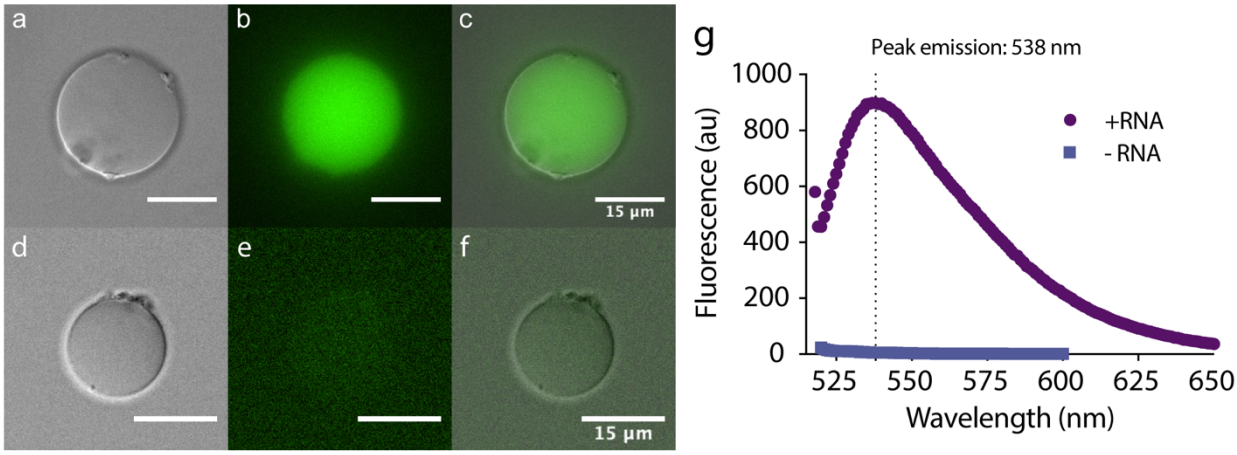

Figure 6.4 Encapsulation of RNA-dye aptamer product. Micrographs of 1:1 DOPC:Cholesterol vesicles with encapsulated RNA (4 uM) with 40 uM TO1-3PEG-Biotin dye. **A.** DIC, **B.** GFP, **C.** Merge, scale = 15 um. Micrographs of 1:1 DOPC:Cholesterol vesicles with 40 uM encapsulated TO1-3PEG-Biotin dye in the absence of aptamer RNA. **D.** DIC, **E.** GFP, **F.** Merge, scale = 15 um. **G.** Fluorescent spectra of TO1-3PEG-Biotin dye in bulk conditions in the presence of 4 uM purified RNA or in the absence of RNA. Peak emission is observed at 538 nm (excitation: 510 nm).

6.4.3 An aptamer-based, transcription-only reaction can be initiated inside lipid vesicles through insertion of nonspecific membrane pores

As we observed that the components, buffers, and product of our Mango aptamer-based transcription reaction can be encapsulated and are compatible with lipid membranes, we next sought to explore the functionality of the transcription reaction to develop nanoscale sensors. Our goal was to encapsulate a functional transcription reaction inside lipid vesicles and initiate transcription through the addition of an ion to the surrounding solution. Here, we chose to detect magnesium ions added to the external buffer surrounding the vesicles. Because Mg^{2+} is a required cofactor for T7 polymerase,[251] the omission of Mg^{2+} from the transcription buffer and subsequent reintroduction to the external solution provides an easy handle by which we can control the initiation of transcription. Importantly, this strategy did not require us to engineer any further sensing mechanisms or incorporate an analyte-specific sensing mechanism, which served to simplify our sensor and establish the general effect of encapsulation and pore-mediated ion entry in the absence of confounding effects of complex sensing reactions.

We first validated our reaction in bulk conditions. We used thin film hydration to form vesicles with encapsulated transcription reactions and used an enzymatic purification method to eliminate non-encapsulated reactions. To achieve this, we incubated vesicles for 30 minutes with Proteinase K, DNAse I and Exonuclease III in the surrounding solution to digest proteins and nucleic acids that are not protected within the interior of vesicles. More traditional methods of purification – SEC and dialysis – did not sufficiently prohibit unencapsulated reactions from occurring. This method required that we added Mg^{2+} to initiate the reaction following the 30-

minute digestion to remove unencapsulated reactants. We first validated that 1) enzymatic digestion eliminated the reaction in bulk conditions, and 2) that addition of 8 mM Mg^{2+} at t = 30 minutes allowed reaction initiation (**Figure 6.5 A**), observing that these strategies allowed sufficient control over transcription. We then assessed pore incorporation into our vesicle membrane compositions of choice using a calcein dye release assay. We observed little pore insertion into pure lipid membranes, as expected,[180] but observed increasing dye release as the concentration of pores increased in 1:1 DOPC lipid:Cholesterol membranes (**Figure 6.5 B**). The concentration of added pore can therefore serve as a handle to control the degree of molecular transport into and out of the vesicle interior. Taken together, these results indicate that we can spatially and temporally control transcription reactions, and that we can add αHL pores in increasing amounts to promote increasing molecular exchange between vesicles and the surrounding solution.

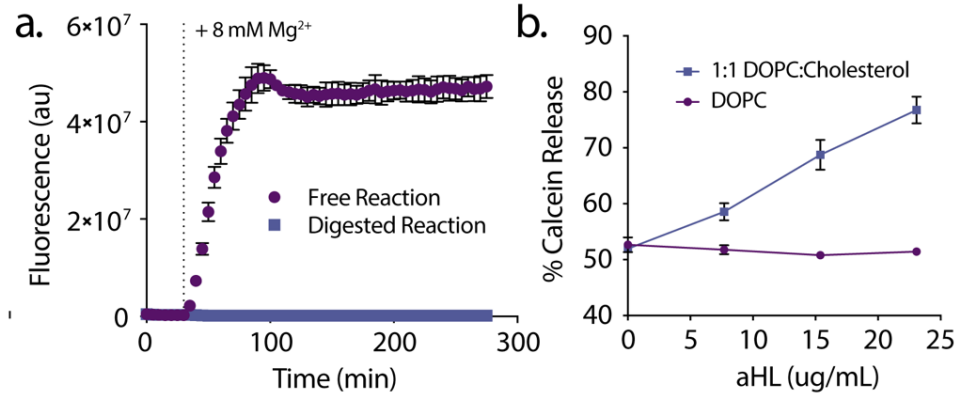

Figure 6.5 Control over transcription and membrane permeability. A. Transcription reactions in bulk in the presence or absence of digestive enzymes. Mg^{2+} added at t = 30 minutes initiates non-digested reactions. **B.** Pore insertion in lipid vs. lipid:cholesterol membranes. In the presence of cholesterol-containing membranes, increasing concentrations of nonspecific pore added to the vesicle sample results in increasing content release from the vesicle lumen.

We next sought to encapsulate functional transcription reactions inside lipid vesicles and initiate RNA transcription through the external addition and cross-membrane transport of Mg^{2+}. We encapsulated transcription reactions using thin film hydration on ice and extruded vesicles to 400 nm in diameter. We added digestion enzymes to the vesicle exterior, incubated for 30 minutes, then added αHL pores and Mg^{2+} to the surrounding solution, monitoring fluorescence of the TO1-3PEG-Biotin/RNA complex for 10 hours at 37°C. We similarly prepared samples of vesicles without DNA (no reaction control) and of reactions without digestive enzymes (full reaction control). Upon the addition of increasing amounts of αHL pores we observed increasing overall fluorescence inside of vesicles, as indicated by the Mango aptamer output (**Figure 6.6 A**). Fluorescence values inside vesicles were observed to increase over ~3 hours, after which fluorescence plateaued. These results are consistent with the steric effect of a physical barrier being introduced between the sensor and the sample, causing Mg^{2+} to diffuse through small pores into the vesicle interior. Overall fluorescence was significantly lower than the maximum fluorescence observed without enzymatic degradation (**Figure 6.6 B**), consistent with the loss of unencapsulated reactants through degradation. Fluorescence does not increase significantly inside vesicles in the absence of DNA or without αHL, which is consistent with a lack of transcription template and an inability of the Mg^{2+} to reach the polymerase, respectively (**Figure 6.6 B**). Of note, fluorescence reads below ~ t = 35 minutes were affected by sample heating and plate reader opening, causing an artificial spike at t = 30 minutes. Together, these results demonstrate that transcription reactions can functionally be encapsulated within lipid vesicles, and the addition of increasing amounts of nonspecific membrane pores and a small molecule initiator can provide a handle by which the initiation of encapsulated transcription can be temporally controlled.

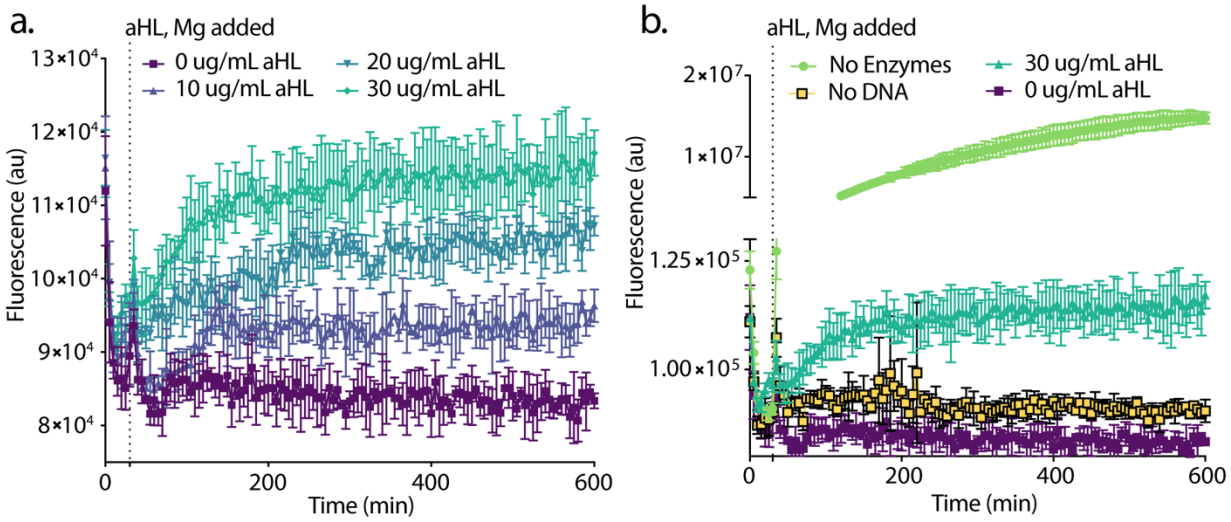

Figure 6.6 Pore-mediated initiation of encapsulated transcription reactions. A. Encapsulated transcription reactions can be initiated to varying degrees through the external addition of Mg^{2+} ions and increasing concentrations of nonspecific αHL pores. **B.** Fluorescence in the absence of digestive enzymes is significantly higher than inside vesicles, however no fluorescence increases are observed in the "no reaction" conditions compared to in the presence of high pore concentrations.

6.5 Conclusions

Here, we have demonstrated that simple transcription reactions can be encapsulated inside lipid vesicles in order to generate nanoscale sensors for a small molecule signal. By incorporating RNA-based aptamer readouts, we can encapsulate sensor systems that rely purely on transcription to generate an optical output; these systems require fewer components to be encapsulated and can operate on faster timescales than expression-based readouts, which may provide an important technological advantage for the use of such sensors.[150] Dye incorporation is a critical consideration in these systems, however, as we observed nonspecific dye interactions that can occur between membranes and some aptamer indicators. Finally, we established that

nonspecific, water-soluble pores like αHL can be added to the solution surrounding vesicles in increasing amounts to allow small, charged molecules to enter the vesicle. In this way, ions like Mg^{2+} can be used to temporally control the initiation of transcription inside vesicles.

The system described here can serve as a useful proof-of-concept for the incorporation of more sophisticated cell-free sensing systems. While reaction initiation was possible, thin film hydration results in relatively low encapsulation efficiency and can cause overall optical outputs to be very low in fluorescence compared to their counterparts in bulk conditions.[167] Additionally, while Mg^{2+} served as a useful initiator molecule due to its nature as a cofactor for T7 polymerase, it is of relatively limited technological importance. The use of nonspecific pores in this application would easily translate to alternative analytes, however, and numerous strategies exist to design sensors for important small molecules with aptamer-based readouts.[246-249] We therefore expect that these results could be generalizable to alternative sensing mechanisms, which may diversify the types of molecules that can be detected. Overall, the encapsulation of transcription reactions established here can provide a simplified platform to develop genetically encoded sensors for small molecule analytes with enhanced temporal and spatial control.

Chapter 7: Encapsulation of a transcriptionally regulated fluoride riboswitch

7.1 Foreword

Our final goal towards the development of vesicle-based sensors was to engineer a sensor which incorporated a more complex cell-free protein expression-based output to detect a small molecule of technological and biological importance. There are a wide variety of cell-free sensors that have been developed, and cell-free technology has become an increasingly important platform with which to develop genetically encoded sensors. Few of these sensors have been encapsulated, however, and the detection of molecules beyond common "proof-of-concept" targets has been even more limited. In collaboration with Walter Thavarajah and Julius Lucks in the Lucks Lab at Northwestern, we set out to achieve this goal by encapsulating a cell-free riboswitch that responds to fluoride ions inside lipid vesicles. Surprisingly, we found that fluoride was membrane permeable, so we focused on membrane engineering strategies to modulate the sensitivity of the encapsulated sensor. This work represents an additional increase in complexity compared to our previously developed indicator-based and transcription-based sensors, and highlights the power of encapsulated cell-free sensing for complex microsensor development.

This work has recently been submitted for publication, and it is publicly available online at BioRxiv as follows:

Boyd, M. A., Thavarajah, W., Lucks, J. B., Kamat, N. P. Robust and tunable performance of a cell-free biosensor encapsulated in lipid vesicles. *BioRxiv* 2022. DOI: 10.1101/2022.03.02.482665

7.2 Introduction

Cell-free systems have emerged as a powerful technology to detect a wide variety of molecular signals, including chemical contaminants relevant to the environment and human health[149-153,157,256-258] and markers of disease and infection.[138,147,148,154,155,259-261] By reconstituting purified cellular machinery *in vitro*, these systems enable use of natural microbial sensing mechanisms in a low-cost, distributable, and easily tunable platform. Despite these key advantages, removal from the cell also eliminates certain features of the cell's native membrane barrier - such as reaction containment, protection from reaction inhibitors, and selective gating - all of which can add important functionality to cell-free biosensors.[12]

Efforts to deploy sensors highlight these limitations caused by the absence of cellular membranes. For example, without a barrier between the sensor and the sample, detecting targets in complex matrices like polluted water or biological samples requires additional modifications to the reaction or preparation protocols.[156,157,262] Cell-free sensors are also sensitive to dilution, and therefore require a controlled reaction environment.[38] One strategy to mitigate these limitations is to recapitulate some of the lost features of the cell membrane by encapsulating cell-free sensors inside of synthetic membranes. Encapsulation enables tuning of the reaction environment on a molecular scale, enabling control of molecular interactions and addition of active membrane features to advance sensing capabilities, all the while maintaining many of the tunable, advantageous features of cell-free systems.[12]

There are two major considerations in designing encapsulated cell-free sensors: determining the impacts of a confined reaction environment on sensor function and choosing an

appropriate target molecule and application. In terms of reaction confinement, the small scale of the encapsulated environment can impact reactant loading, reaction time, and limit of detection.[263-265] These effects have been shown to impact the basic processes of gene expression,[168] which in turn affects cell-free biosensors that regulate reporter gene expression at the level of transcription or translation.[34] Of the wide range of biosensing mechanisms, RNA-based biosensors that regulate transcription require the fewest components and operate on a faster timescale,[150] which may reduce the impacts of confinement on sensor function. Riboswitches - noncoding RNA elements upstream of protein coding genes that change their fold in response to specific ligands to regulate gene expression - could offer an opportunity to address these constraints due to reaction confinement.

Previous proof-of-concept studies have focused on encapsulation of two synthetic, translationally regulated riboswitches that respond to membrane-permeable signals: theophylline[38,82,83] and histamine.[84] Both riboswitches have been successfully encapsulated in bilayer vesicles, generating either a fluorescent protein readout or a protein-mediated response upon analyte entry into the vesicle interior.[38,82-84] Encapsulation of transcriptionally regulated riboswitches has proven difficult to date, however; efforts to encapsulate a transcriptionally regulated adenine riboswitch showed very poor switching activity and were subsequently abandoned.[83] This could be due to specific features of the adenine riboswitch or due to a general property of transcriptional riboswitches, which require dynamic conformational changes during transcription to enact their mechanism – a process which could be impacted by general features of confinement or electrostatic interactions with the lipid bilayers.[254,255] Despite these potential challenges, the mechanisms underlying transcriptionally regulated riboswitches are being further

uncovered.[266] These sensors have demonstrated the feasibility of detecting environmentally important analytes in cell-free systems and can function with RNA-level outputs[150] - a key feature which may mitigate resource constraints - motivating further efforts for their encapsulation and deployment.

A second major consideration in encapsulated sensor development is the selection of an appropriate target and application. Of the many potential uses of encapsulated biosensors, water quality monitoring is one of the most compelling from a global perspective. One in three people globally lack access to safe drinking water,[267] and the ability to identify contaminated water sources is essential for their quarantine or remediation.[268] Fluoride is among the most concerning of these contaminants; chronic exposure to fluoride binds it to the calcium in teeth and bones, weakening them and causing lifelong health consequences.[269] From both environmental and anthropogenic sources, fluoride exposure is especially problematic in parts of China, Africa, South America, and India,[269,270] with high fluoride concentrations also found in groundwater across the United States.[270] This diversity of sample sources comes with a corresponding increase in potential reaction inhibitors, presenting the need for a robust sensor that retains function in complex matrices. Encapsulated fluoride biosensing reactions would address this need, delivering far-reaching global health benefits and establishing a framework to address future water quality challenges.

In this study, we sought to develop vesicle-based sensors for fluoride by encapsulating a transcriptionally regulated, fluoride-responsive riboswitch within bilayer membranes (**Figure 7.1**). We first encapsulate the riboswitch, then demonstrate its ability to detect externally added fluoride and show that membrane composition can be modified to tune sensitivity to exogenous

ions. We also demonstrate that encapsulation protects cell-free reactions from sample degradation, particularly from extravesicular degradative enzymes. Finally, we couple riboswitch output to both fluorescent and colorimetric reporters and show that vesicle-based sensors can detect fluoride in real-world water samples. This work demonstrates the potential of encapsulated, riboswitch-based sensors for biosensing applications, complimenting existing cell-free sensor engineering strategies and enabling sensing in otherwise inhospitable environments.

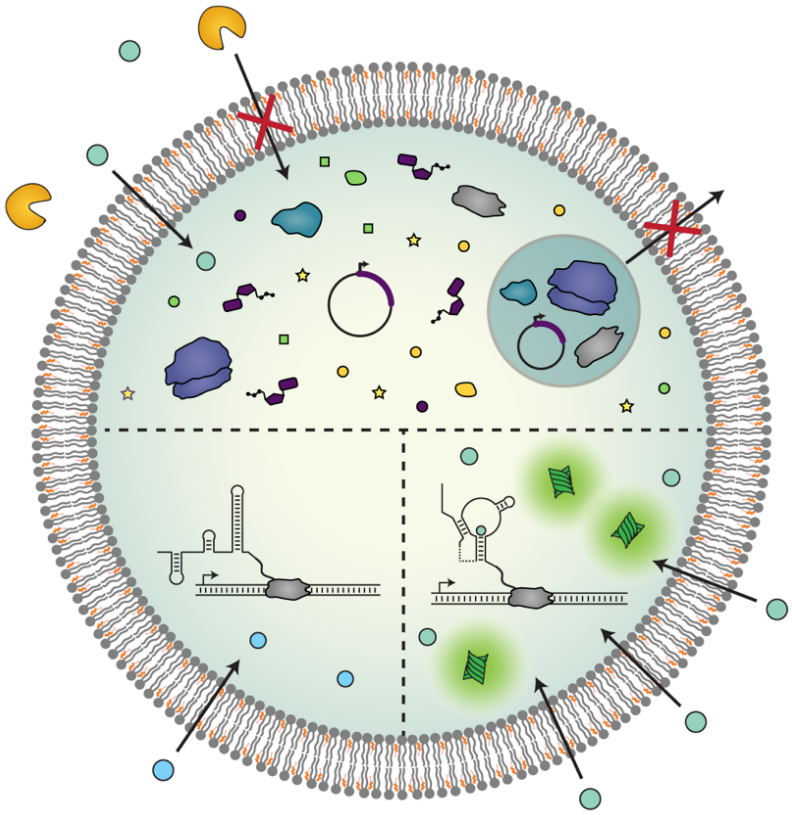

Figure 7.1 Encapsulated cell-free sensors. Encapsulation of cell-free systems creates a semipermeable barrier between sensor components and the environment, which modulates their molecular interactions. Reactants are contained within the vesicle interior, while proteins and other large molecules in the external sample are excluded from vesicle entry (top). Small, membrane-permeable molecules can diffuse into the vesicle interior, initiating a riboswitch-

mediated response that is specific to an analyte of interest (bottom right). The riboswitch folds into a terminating state in the absence of the target analyte, even in the presence of off-target molecules (bottom left).

7.3 Materials & Methods

Materials

POPC (1-palmitoyl-2-oleoyl-glycero-3-phosphocholine) and cholesterol were purchased from Avanti Polar Lipids Inc. Oleic acid (OA), glycerol, sucrose, glucose, HPTS (8-Hydroxypyrene-1,3,6-trisulfonic acid trisodium salt), BioUltra Mineral Oil, phosphate-buffered saline (PBS), bovine serum albumin (BSA), and NaF were purchased from Millipore Sigma. 1.8k Peo-b-Pbd polymer was purchased from Polymer Source. Ovalbumin-conjugated AlexaFluor 647 (OA647), calcein dye and HEPES buffer were purchased from Thermo Fisher. RNAse A was purchased from New England Biolabs.

Plasmid sequences available on Addgene with accession numbers 128809 (pJBL3752) and 128810 (pJBL7025).

Cell-free reaction assembly

Cell-free extract and reactions were prepared according to established protocols.[150,271] Briefly, cell-free reactions were assembled by mixing cell extract, a reaction buffer containing the small molecules required for transcription and translation (NTPs, amino acids, buffering salts, crowding agents, and an energy source), and DNA templates and inducers at a ratio of approximately 30/30/40. Sucrose was added to a final concentration of 200 mM to facilitate encapsulation. Each reaction was prepared on ice to 16.5 μL final volume in batches of 7. Reactions were prepared with 10 nM pJBL3752 (riboswitch-GFP plasmid) or pJBL7025

(riboswitch-enzyme plasmid) + 1 mM catechol. Reaction master mix was assembled, then added to DNA, inducers, sucrose, and water to a final volume of 16.5 µL per reaction aliquot. For reactions containing volume marker, reaction mix was supplemented with 1.4 µL OA647. Preparation conditions were kept consistent between reactions, only varying NaF concentration or omitting DNA for extract-only controls.

Encapsulation of cell-free reactions

Encapsulated sensors were prepared via water-in-oil double emulsion methods. Lipid films were prepared by mixing amphiphiles (lipid, cholesterol, fatty acid or polymers) in chloroform to a final amphiphile concentration of 25 mM at a volume of 200 µL. Films were dried onto the side of a glass vial under nitrogen gas, then placed in a vacuum oven overnight. 200 µL of BioUltra mineral oil was added to lipid films and heated at 80°C for 30 minutes, followed by 30 seconds of vortexing to incorporate amphiphiles into the oil. Lipid/oil mixtures were cooled on to room temperature, then placed on ice during cell-free reaction assembly. Cell-free reactions were prepared on ice as described above. Reactions were layered on top of lipid/oil mixture, then vortexed for 30 seconds to form an emulsion. Emulsions were incubated at 4°C for 5 minutes, then layered onto outer solution containing all small molecules required for transcription and translation, 100 mM HEPES buffer (pH 8), and 200 mM glucose. Samples were again incubated at 4°C for 5 minutes, then centrifuged for 15 minutes at 18,000 rcf at 4°C. Vesicle pellets were collected by pipette and placed into fresh Eppendorf tubes. Prepared vesicles were then added in 10 µL aliquots to 20 µL fresh outer solution supplemented with NaF, certain water samples and/or RNAse A (5 ug/mL final concentration). Osmolarity of NaF stock

solution was adjusted to match that of the outer solution by adding glucose to minimize osmotic effects on vesicles.

Cell-free protein expression

For bulk assays, unencapsulated reactions were prepared as described above and added to 384-well plates. Protein expression was monitored at 37°C in a SpectraMax i3x plate reader (Molecular Devices). GFP was monitored at ex: 485 nm, em: 510 nm. Catechol absorbance was monitored at 385 nm.

Encapsulated sensors with a colorimetric readout were monitored at an absorbance of 385 nm using a SpectraMax i3x plate reader at 37°C until expression reached a plateau, about 2.5 hours, after which samples were removed from plates and placed into Eppendorf tubes or microscopy chambers for imaging. Images of tubes and through the microscope eyepiece were taken using an iPhone 8. Absorbance measurements in the plate reader are reported relative to initial absorbance to control for slight differences in vesicle concentration between vesicle preparations.

Encapsulated sensors expressing GFP were incubated in outer solution for 6 hours at 37°C, then imaged on a Nikon Ti2 inverted microscope. Imaging chambers were blocked with BSA for 20 minutes, then triple rinsed with 766 mOsm PBS. Vesicles were added to equiosmolar PBS and allowed to settle for 5 minutes before imaging. Images were taken using DIC, GFP (ex: 470, em: 525) and Cy 5.5 (ex: 650, em: 720) filters under 10x magnification, 20% laser intensity, and 1 second exposure. Images were analyzed using Nikon NIS-elements AR software

Advanced Analysis tool.[272] Statistical analysis and graphing were conducted in Graphpad Prism.[273]

Vesicle analysis using NIS Elements AR

Vesicles were selected using the OA647 channel. General analysis protocol was set with the following settings. Preprocessing: Local contrast, size 105, power 50%. Threshold minimum: 393. Smooth 1x, clean 1x. Size minimum: 2 μm. Return Mean GFP, Mean OA647, Max GFP.

HPTS pH assay

Vesicles were prepared via thin film hydration with 33% Cholesterol and 66% POPC. Lipid and cholesterol in chloroform were dried onto the side of a glass vial under nitrogen gas to form a lipid film. Vesicle films were hydrated with HEPES + 0.5 mM HPTS dye overnight at 60°C. Vesicles were extruded to 400 nm, purified via Size Exclusion Chromatography (SEC), and added to a 384-well plate with equiosmolar HEPES buffer + varying concentrations of NaCl and NaF. HPTS fluorescence was monitored with excitation at 405 and 450 nm and emission at 510 nm, as characterized by Hilburger *et al*.[180] HPTS fluorescence is reported as the ratio of emission intensities when excited at 450 nm/405 nm.

Calcein content leakage assay

Vesicles were prepared via thin film hydration with 33% Cholesterol and 66% POPC. Lipid and cholesterol in chloroform were dried onto the side of a glass vial under nitrogen gas to form a lipid film. Vesicle films were hydrated with HEPES + 20 mM calcein dye overnight at 60°C. Vesicles were extruded to 400 nm, purified via SEC, and added to a 384-well plate with equiosmolar HEPES buffer and increasing volumes of 0.02% glycerol solution or RNAse

prepared in buffer to the same final glycerol concentration. Vesicles were incubated for 4 hours at 37°C and calcein fluorescence was measured (ex: 495 nm, em: 515 nm). Vesicles were lysed with 1 μL 10% TritonX and total calcein fluorescence was measured to determine fraction release.

7.4 Results and Discussion

7.4.1 A transcriptionally regulated fluoride riboswitch can function inside lipid vesicles

We first sought to confirm that a transcriptional riboswitch can function when encapsulated inside lipid vesicles. For the riboswitch, we chose the fluoride responsive riboswitch from *Bacillus cereus*, which we showed in a previous study can be used to control the expression of several different reporter proteins and fluorescent RNA aptamers in bulk *E. coli* extract-based cell-free systems.[150] In this system, the fluoride riboswitch is encoded within a single DNA template, downstream of a consensus *E. coli* promoter sequence, and upstream of a reporter coding sequence. In the absence of fluoride, *E. coli* polymerase transcribes the riboswitch sequence, causing it to fold into a conformation that exposes a transcriptional terminator hairpin, which causes RNA polymerase to stop transcription.[274] In the presence of fluoride, fluoride binding to the riboswitch aptamer domain prevents the terminator from folding, allowing transcriptional elongation of the reporter coding sequence.

In this study, we first chose to use a super folder green fluorescent protein (GFP) reporter, as it allows convenient measurement of riboswitch activity. For the cell-free system, we chose to use an *E. coli* S30 lysate prepared with runoff and dialysis, which has been shown to

allow the function of biosensors that require bacterial polymerases.[271] Embedding the riboswitch DNA template into the extract system alongside varying concentrations of sodium fluoride (NaF) showed, as expected,[150] an increase in GFP fluorescence as fluoride concentrations increased up to 3 mM, followed by a decrease in fluorescence (**Figure 7.2 A**). This decrease is likely caused by fluoride inhibition of the gene expression machinery.[275] This result was consistent with previous studies[150] and informed the use of 3 mM NaF for the rest of this study to obtain the expected maximum fluorescent output of the system.

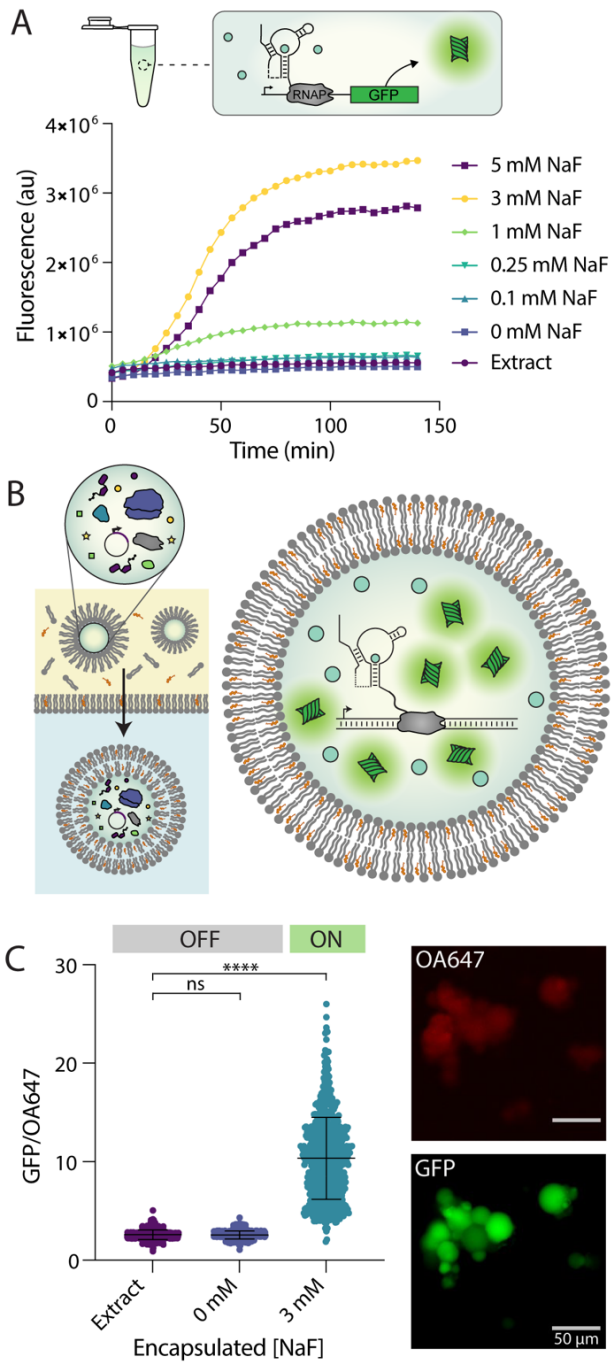

Figure 7.2 A fluoride riboswitch can function within bilayer vesicles. A. Riboswitch-regulated GFP expression in bulk conditions in response to increasing fluoride concentrations. In the presence of NaF, the riboswitch folds into an "ON" state, which allows expression of a GFP reporter molecule. B. Double emulsion allows the encapsulation of functional cell-free reactions. Assembled reactions are vortexed into a lipid/oil mixture, then centrifuged into an aqueous

solution (left). The resulting vesicles contain cell-free reactions which can respond to co-encapsualted fluoride by expressing GFP (right). C. GFP/OA647 fluorescence, which indicates relative GFP concentration inside each liposome, inside of vesicles when 3 mM NaF is co-encapsulated compared to no DNA (Extract) or no fluoride (0 mM NaF) controls. Micrographs show variations in GFP fluorescence between vesicles from the same population, which results in a distribution of fluorescence values. Scale = 50 mm. Black lines indicate mean fluorescence and standard deviation. **** $p \leq 0.0001$, nonsignificant (ns) $p > 0.1234$; p-values generated using a One-Way ANOVA and Tukey's Multiple Comparisons Test.

We then set out to assess whether the fluoride riboswitch could be functionally encapsulated within lipid vesicles. Vesicles were synthesized using a water-in-oil emulsion transfer method (**Figure 7.2 B**).[78] In this method, various membrane amphiphiles (e.g. lipids, cholesterol, fatty acids, diblock copolymers) are dissolved into an oil phase and an emulsion is formed by vortexing the aqueous cell-free reaction into this mixture. The emulsion is then layered onto a second aqueous layer, and emulsified droplets are centrifuged through to generate unilamellar vesicles. Vesicle synthesis using this approach yields a distribution of different vesicle sizes, which could impact our quantification of fluorescence.[276] To control for this, we also incorporated a protein-conjugated dye, ovalbumin-conjugated Alexafluor 647 (OA647), which served as a volume marker and allowed us to detect the vesicle interior regardless of GFP expression level.[84,85] After synthesis, vesicles were incubated under varying conditions at 37°C, and protein expression was assessed using epifluorescent microscopy. Vesicles were imaged using GFP and Cy5.5 channels, and images were analyzed using the NIS-elements AR software program,[272] which allowed us to automatically select vesicle interiors using the OA647 marker and report GFP fluorescence in those regions. This protocol allowed us to analyze hundreds of vesicles per sample, maintain the same selection parameters between samples, and minimize the

impact of user selection bias in the analysis. Additionally, the encapsulated volume marker allowed us to report GFP expression relative to OA647 fluorescence to control for possible variability in vesicle size or loading. Using this method, we were able to ensure that our measurements were isolated to intact (non-lysed) vesicles which retained their protein cargo (**Figure 7.3**).

Using the above approach, we encapsulated cell-free reactions with and without fluoride present in the bulk reaction mixture. We chose to use a 2:1 ratio of cholesterol and POPC phospholipid as membrane amphiphiles due to their previous use in similar encapsulated expression studies.[38,82-85] Upon co-encapsulation of the riboswitch with 3 mM NaF we observed increased GFP expression inside vesicles, indicating the riboswitch was in the "ON" state (**Figure 7.2 C**). In contrast, in the absence of DNA (extract only) or in the absence of fluoride (0 mM NaF) we observed minimal GFP expression, indicating an "OFF" state (**Figure 7.2 C**). This high level of GFP induction inside vesicles by fluoride indicates that membrane encapsulation does not eliminate the ability of the riboswitch to fold properly and does not cause significant nonspecific expression.

We observed that populations of vesicles exhibited variations in GFP fluorescence between individual liposomes after 6 hours of incubation (**Figure 7.2 C**), a phenomenon which has been observed in similar studies across multiple encapsulation protocols.[38,84,265,276-279] It has been hypothesized that these variations in gene expression may be caused by variability in vesicle loading and/or varied levels of molecular exchange with the surrounding buffer for vesicles of different sizes.[177,265,277,278] To report this variability across vesicle populations we have included metrics of skew for each population result. Even after taking this variability into

account, however, induction of GFP expression is clearly observable across the vesicle population, indicating proper riboswitch sensor activity and a robust response to fluoride in encapsulated sensors.

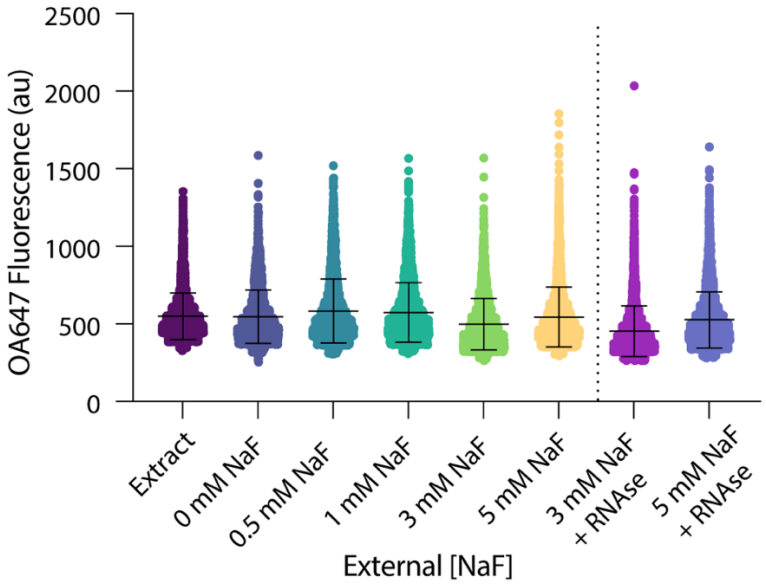

Figure 7.3 OA647 retention in 2:1 cholesterol:POPC vesicles following encapsulation and protein expression. Vesicle populations exposed to increasing fluoride in the external solution exhibit the retention of a volume marker, OA647, even when RNAse A is present externally. While average fluorescence varies slightly between populations, corresponding to differences in the size of analyzed vesicles between conditions, all samples exhibit similar fluorescence profiles consistent with the retention of protein-sized molecules within the vesicle interior.

7.4.2 External fluoride can be detected by an encapsulated riboswitch

We next sought to determine whether the encapsulated riboswitch could detect fluoride added to the external solution of pre-assembled sensor vesicles. To assess this, we prepared vesicles containing cell-free reactions without NaF present in the reaction mixture. We then titrated in NaF into the solution surrounding vesicles (**Figure 7.4 A**) and imaged vesicles

following incubation for 6 hours at 37°C. We observed increasing GFP expression as NaF concentrations increased up to 3 mM with a slight decrease in average fluorescence at 5 mM, consistent with bulk studies (**Figure 7.4 B-D**). All fluoride-containing conditions exhibited a significant increase in fluorescence compared to no-DNA and no-fluoride controls (**Figure 7.4 B & C, Table 7.1**).

Table 7.1 Permeability to NaF and riboswitch-regulated gene expression.

External NaF concentration	Mean Fluorescence GFP/OA647	SEM	Significantly different than 0 mM?	Skewness	Kurtosis
Extract	1.596	0.0054	ns	0.5225	0.8674
0 mM	1.625	0.0062		0.4007	0.4155
0.5 mM	2.250	0.0126	****	2.205	13.12
1 mM	2.388	0.0143	****	1.824	9.110
3 mM	2.500	0.0167	****	2.083	8.960
5 mM	2.372	0.0166	****	4.587	46.19

**** $p \leq 0.0001$, nonsignificant (ns) $p > 0.1234$; p-values generated using a One-Way ANOVA and Tukey's Multiple Comparisons Test.

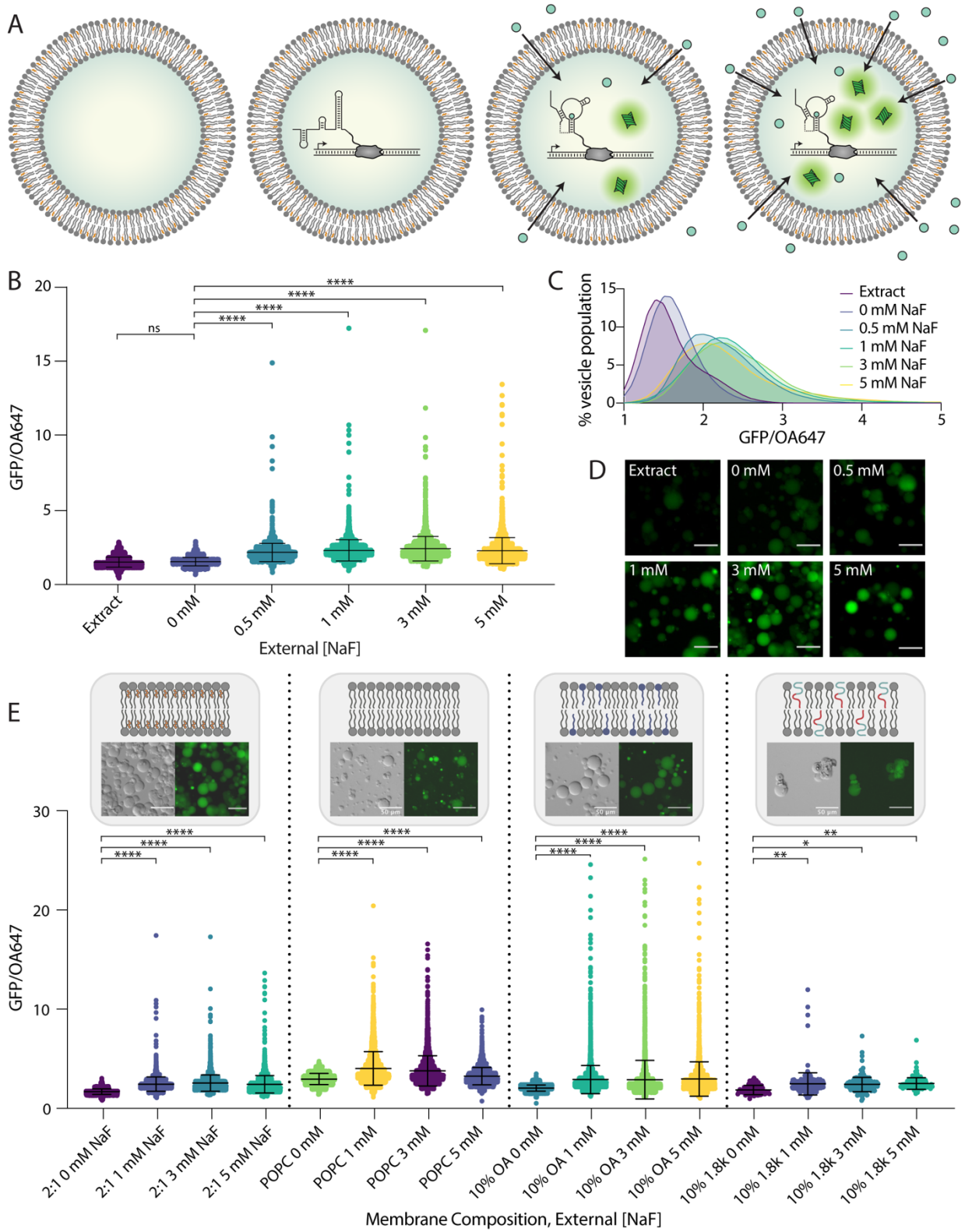

Figure 7.4 Detection of external fluoride by encapsulated sensors. A. Schematic of conditions. Vesicles were prepared encapsulating extract only (left), or fully assembled reactions

without NaF. Upon addition of increasing fluoride to the vesicle exterior, expression of GFP inside vesicles increases (right). **B**. GFP/OA647 fluorescence as a result of riboswitch activity in 2:1 cholesterol:POPC vesicles in response to increasing NaF added externally. Black lines indicate mean fluorescence ratio and standard deviation. **C**. Histogram of vesicle populations shown in (B). Data plotted with lowless curve fitting. **D**. GFP fluorescence in micrographs of vesicles with increasing external concentrations of NaF. Scale = 50 μm. **E.** GFP/OA647 fluorescence in response to increasing fluoride shown from left to right: 2:1 cholesterol:POPC membranes (data from B); pure POPC lipid membranes; POPC + 10% oleic acid membranes; POPC + 10% 1.8k Peo-b-Pbd membranes. Composition and morphology of each membrane composition indicated by schematics and micrographs, respectively. **** $p \leq 0.0001$, ** $p \leq 0.0021$, * $p \leq 0.0332$, nonsignificant (ns) $p > 0.1234$; p-values generated using a One-Way ANOVA and Tukey's Multiple Comparisons Test.

When incubated with chloride, a similarly monovalent anion, a slight response to increasing ion concentration was observed, however these responses were significantly lower than any response to fluoride and did not exhibit any highly active vesicles as were observed in all fluoride-containing conditions (**Figure 7.5**). These responses were easily distinguishable between fluoride and chloride, indicating sufficient specificity to fluoride, as has been observed previously.[150] These results are consistent with those observed in bulk studies in which the riboswitch signal reaches a maximum around 3 mM NaF, indicating fluoride anions permeate the membrane and access the vesicle interior.

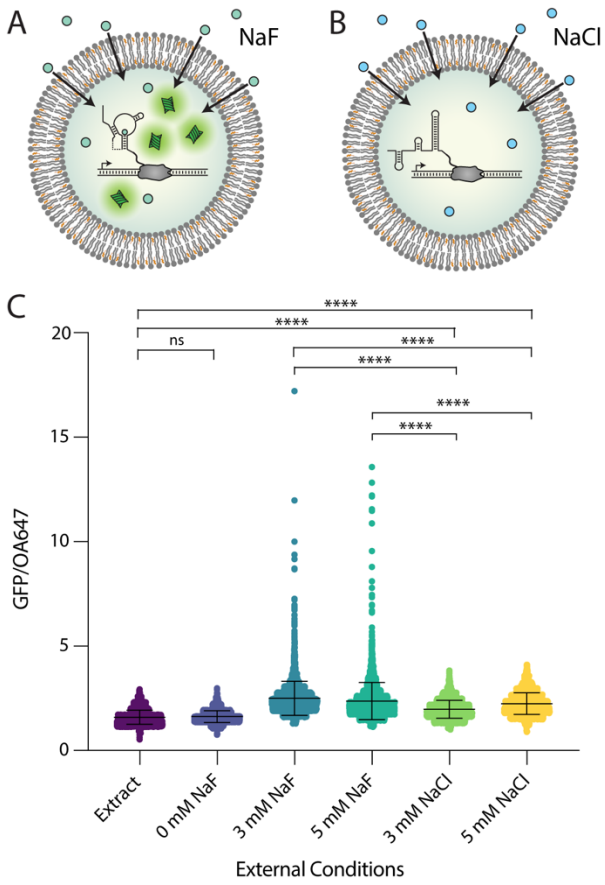

Figure 7.5 An encapsulated riboswitch responds specifically to fluoride. A. Fluoride permeates the vesicle membrane to initiate the expression of a GFP reporter inside vesicles. **B.** The external addition of NaCl does not result in robust GFP expression inside vesicles. **C.** GPF/OA647 fluorescence in vesicles with either NaF or NaCl added to the external buffer. While a response is observed to increasing chloride, the magnitude is significantly less than the response to fluoride and there is no observed population shift towards highly active vesicles. Differences in expression between fluoride and chloride containing conditions were clearly distinguishable, indicating sufficient specificity to fluoride over chloride. **** $p \leq 0.0001$, nonsignificant (ns) $p > 0.1234$; p-values generated using a One-Way ANOVA and Tukey's Multiple Comparisons Test.

This result was somewhat unexpected, as we anticipated that the membrane would be relatively impermeable to charged fluoride ions. The observed magnitude of fluoride

permeability may be explained in part by the transient formation of hydrofluoric acid (HF). HF has been shown to exhibit a permeability coefficient that is seven orders of magnitude greater than fluoride anions through lipid/cholesterol bilayers, indicating that HF travels through the membrane much more readily than its anionic F^- counterpart.[275,280] We confirmed this effect by encapsulating a pH sensitive dye, HPTS, which reported a slight decrease in pH in the vesicle lumen upon the addition of fluoride to the external buffer, indicating an increase in proton concentration inside the vesicle as fluoride concentration increased (**Figure 7.6**). Permeability to exogenous fluoride in this system may therefore be increased by the formation of HF. Taken together, these results indicate that increasing concentrations of fluoride added to the extravesicular environment can be detected by the encapsulated riboswitch.

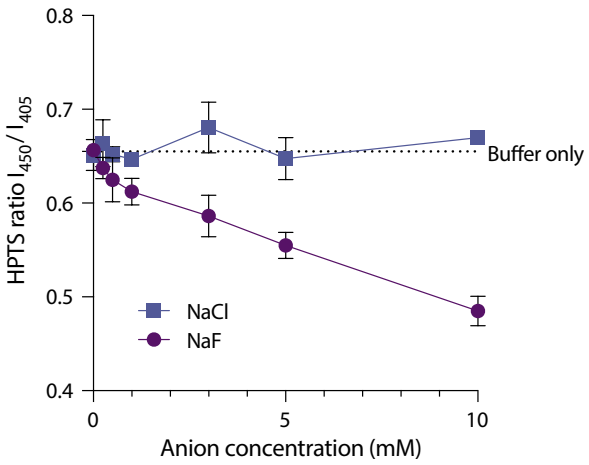

Figure 7.6 pH decreases as increasing NaF is added externally to vesicles. Lipid/cholesterol vesicles containing HPTS dye without cell-free expression systems show changes in fluorescence after addition of anions to the external solution, indicating a cross-membrane effect on pH caused by externally added NaF. Compared to NaCl and buffer only controls, the pH of the vesicle interior decreases in the presence of externally added NaF, as indicated by a decreasing fluorescence ratio of HPTS, a pH-sensitive dye. These results indicate that fluoride

ions may permeate the membrane as HF, bringing H^+ ions with them as they pass through the membrane.

As fluoride was observed to pass through the membrane to interact with the encapsulated riboswitch, we wondered if we could alter the composition of vesicle membranes to modulate the sensitivity of these sensors to external fluoride. Membrane permeability to small molecules depends significantly on membrane composition, as various lipid chain chemistries and contributions from other amphiphilic components can impart an effect on membrane physical properties. Cholesterol, a major component of our original 2:1 cholesterol:POPC lipid composition, is known to decrease membrane permeability by increasing lipid packing and altering membrane fluidity and rigidity.[281] Peo-b-Pbd diblock copolymers are similarly known to reduce membrane permeability by increasing membrane elasticity and introducing steric barriers of increased thickness within the hydrophobic portions of the membrane.[22,25] In contrast, fatty acids such as oleic acid have been shown to increase membrane permeability to ionic solutes by incorporating single hydrocarbon chains of different length and unsaturation into the bilayer.[66,170] Using this series of amphiphilic molecules, we set out to assess the capacity of membrane amphiphiles and the resulting membrane permeability to modulate the performance of an encapsulated cell-free sensor.

To explore the effect of these amphiphiles on membrane permeability to fluoride, we prepared vesicles with either 1) pure POPC lipid, 2) POPC lipid + 10% oleic acid (OA), or 3) POPC lipid + 10% 1.8k Peo-b-Pbd polymer (1.8k) components in the lipid/oil mixture, encapsulating cell-free reactions as normal (**Figure 7.4 E**). We observed an increase in overall GFP expression in both pure POPC lipid and POPC + 10% OA conditions compared to our

original 2:1 cholesterol:POPC lipid composition, consistent with the removal of cholesterol and the addition of oleic acid, respectively (**Figure 7.4 D**). In addition, sensitivity to variations in fluoride concentration appeared to be reduced in vesicles containing oleic acid, indicating high permeability to any amount of external fluoride. In contrast, vesicles containing 10% 1.8k diblock copolymer exhibited very little GFP expression, indicating reduced membrane permeability. Mean POPC vesicle fluorescence peaked at 1 mM NaF, while 10% OA and 10% 1.8k diblock copolymer responses were maximum at 5 mM NaF (**Table 7.2**). Taken together, these results indicate that exchanging membrane components to control membrane permeability provides a handle to tune the sensitivity of an encapsulated riboswitch to an analyte of interest. Further, the selection of highly permeable amphiphiles does not necessarily improve sensor performance and may instead increase overall signal but limit sensor resolution. A balance between analyte access and desired sensing behavior is likely an important consideration for engineering encapsulated biosensing systems depending on the desired application.

Table 7.2 NaF permeability and riboswitch-mediated GFP expression vs membrane composition.

External NaF concentration	Mean GFP/OA647	SEM	Different than 0 mM?	Skewness	Kurtosis
POPC, 0 mM	2.904	0.01074		0.1471	-0.3680
POPC, 1 mM	3.968	0.02997	****	2.063	7.183
POPC, 3 mM	3.724	0.02570	****	2.433	9.854
POPC, 5 mM	3.190	0.01478	****	1.528	5.072
10% OA, 0 mM	1.997	0.004865		0.3135	0.1434
10% OA, 1 mM	2.850	0.02232	****	6.120	59.59
10% OA, 3 mM	2.839	0.03147	****	4.848	32.92

10% OA, 5 mM	2.909	0.03352	****	5.038	38.90
10% 1.8k, 0 mM	1.807	0.05333		0.6967	-0.2151
10% 1.8k, 1 mM	2.414	0.07304	**	5.698	39.98
10% 1.8k, 3 mM	2.353	0.04787	*	2.199	11.16
10% 1.8k, 5 mM	2.458	0.04654	**	3.247	19.66

**** $p \leq 0.0001$, ** $p \leq 0.0021$, * $p \leq 0.0332$, nonsignificant (ns) $p > 0.1234$; p-values generated using a One-Way ANOVA and Tukey's Multiple Comparisons Test.

7.4.3 Encapsulation protects sensor components from degradation

Having established that these vesicle sensors can detect external fluoride, we next wanted to explore how they might function in complex samples. One of the major benefits of membrane encapsulation is the ability to leverage the semipermeable barrier formed by the membrane to contain and protect encapsulated components. Cell-free reactions, particularly those using riboswitches, are highly sensitive to the presence of nucleases and proteases which can degrade sensor components before a target analyte is encountered.[262] Due to their large size, however, enzymes are unable to pass through the vesicle membrane to access encapsulated reactants.

To determine whether the vesicle membrane can sufficiently protect encapsulated reactions from external degradation, we tested various vesicle assemblies in the presence of RNAse A (**Figure 7.7 A**). We observed that RNAse completely eliminated the riboswitch response to NaF both in bulk conditions and when RNAse was co-encapsulated with the cell-free reaction in vesicles (**Figure 7.7 B & C**). In contrast, encapsulated sensors maintained the ability to respond to externally added NaF when RNAse was present in the external sample (**Figure 7.7 D, Table 7.3**).

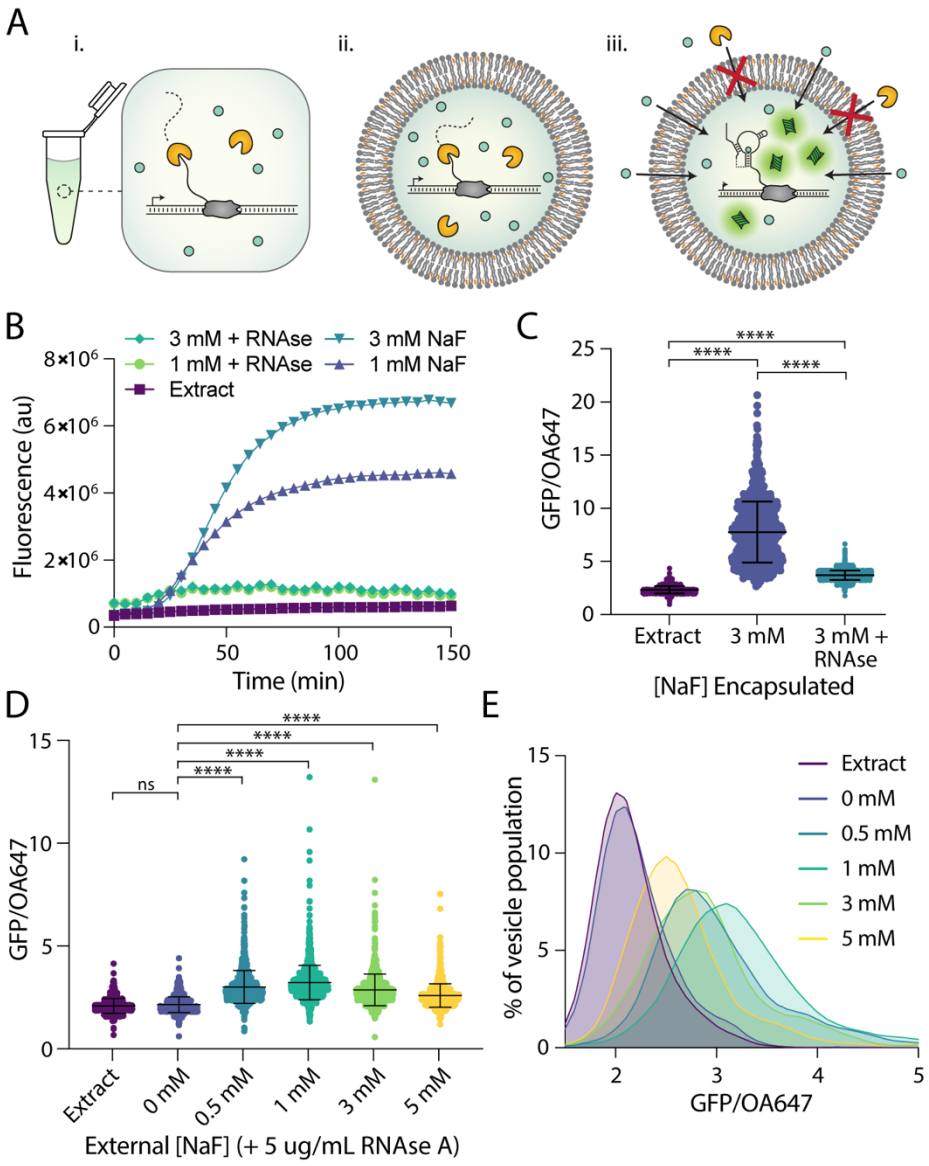

Figure 7.7 Encapsulation protects from degradation by RNAse A. A. Schematic of RNAse-containing conditions. RNAse A degrades the riboswitch (i) in bulk conditions and (ii) when co-encapsulated with reactants but is unable to reach reactants contained within vesicles (iii). **B.** Riboswitch response to NaF in bulk conditions with RNAse A added to reaction. **C.** Riboswitch activity as indicated by GFP/OA647 fluorescence when encapsulated with 3 mM NaF compared to the co-encapsulation of both 3 mM NaF and RNAse A. **D.** Response of encapsulated riboswitch to externally added NaF with RNAse A present in external solution. Black lines indicate mean and standard deviation. **E.** Histogram of data in (D). Data plotted with lowless

curve fitting. **** $p \leq 0.0001$, nonsignificant (ns) $p > 0.1234$; p-values generated using a One-Way ANOVA and Tukey's Multiple Comparisons Test.

Table 7.3 NaF permeability and riboswitch-mediated GFP expression with external RNAse.

External NaF concentration	Mean Fluorescence GFP/OA647	SEM	Significantly different than 0 mM?	Skewness	Kurtosis
Extract only	2.152	0.013	ns	0.9806	2.661
0 mM	2.213	0.013		0.9952	2.501
0.5 mM	3.071	0.026	****	2.236	9.502
1 mM	3.289	0.022	****	3.289	24.83
3 mM	2.930	0.023	****	3.746	34.26
5 mM	2.662	0.018	****	2.251	10.79

**** $p \leq 0.0001$, nonsignificant (ns) $p > 0.1234$; p-values generated using a One-Way ANOVA and Tukey's Multiple Comparisons Test.

Interestingly, we noticed a greater decrease in mean fluorescence at higher external NaF concentrations compared to sensors without RNAse present, which we hypothesized was due to slightly higher degrees of vesicle instability or membrane permeability from the addition of small amounts of glycerol in the RNAse buffer (**Figure 7.8**). Instability could lead to higher rates of vesicle lysis and therefore lower overall GFP fluorescence, while increased permeability could cause increased reaction poisoning with high fluoride concentrations. Nevertheless, all vesicle populations exhibited increased GFP expression in the presence of fluoride, demonstrating simultaneous permeation of fluoride into the vesicle interior and exclusion of RNAse A from the cell-free reaction.

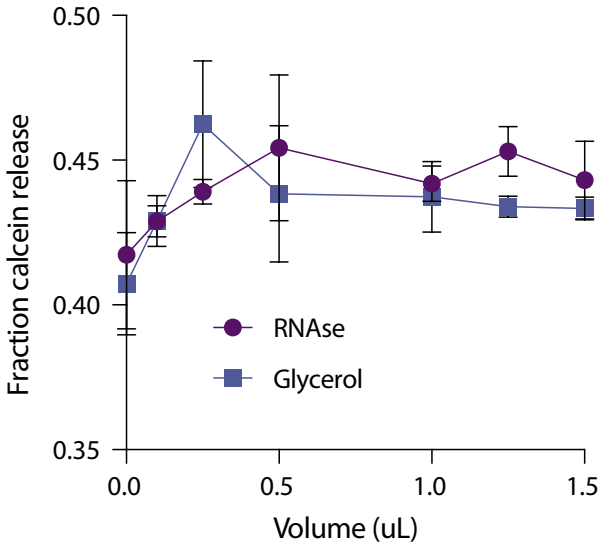

Figure 7.8 Glycerol addition increases membrane permeability. Lipid/cholesterol vesicles encapsulating calcein, a self-quenching fluorescent dye, show slightly increasing cargo leakage following glycerol addition to the surrounding buffer. In both the presence and absence of RNAse, addition of increasing volumes of 0.02% glycerol solutions (1.25 uL of which was added in vesicle studies) leads to slightly higher levels of calcein dye release from the vesicle interior, indicating increased membrane permeability to small molecules.

7.4.4 Vesicle-based sensors can incorporate a colorimetric readout and detect fluoride in real-world samples

Finally, we wondered if we could extend these results to conditions that would be more relevant for real-world environmental sensing. Although fluorescence is a common readout for many biological assays, GPF fluorescence in vesicles is difficult to monitor with common equipment, particularly in non-laboratory settings. To address this limitation, we coupled fluoride detection to an alternative reporter enzyme, catechol (2,3)-dioxygenase (C23DO).[150] In this system, the riboswitch "ON" state leads to the expression of C23DO, which catalyzes the conversion of its colorless substrate, catechol, to the yellow-colored 2-hydroxymuconate

semialdehyde to generate a colorimetric response (**Figure 7.9 A**). In bulk conditions this construct exhibits a fast and robust response to fluoride, and the colorimetric output generated is clearly distinguishable by eye for both laboratory and field-collected water samples.[150]

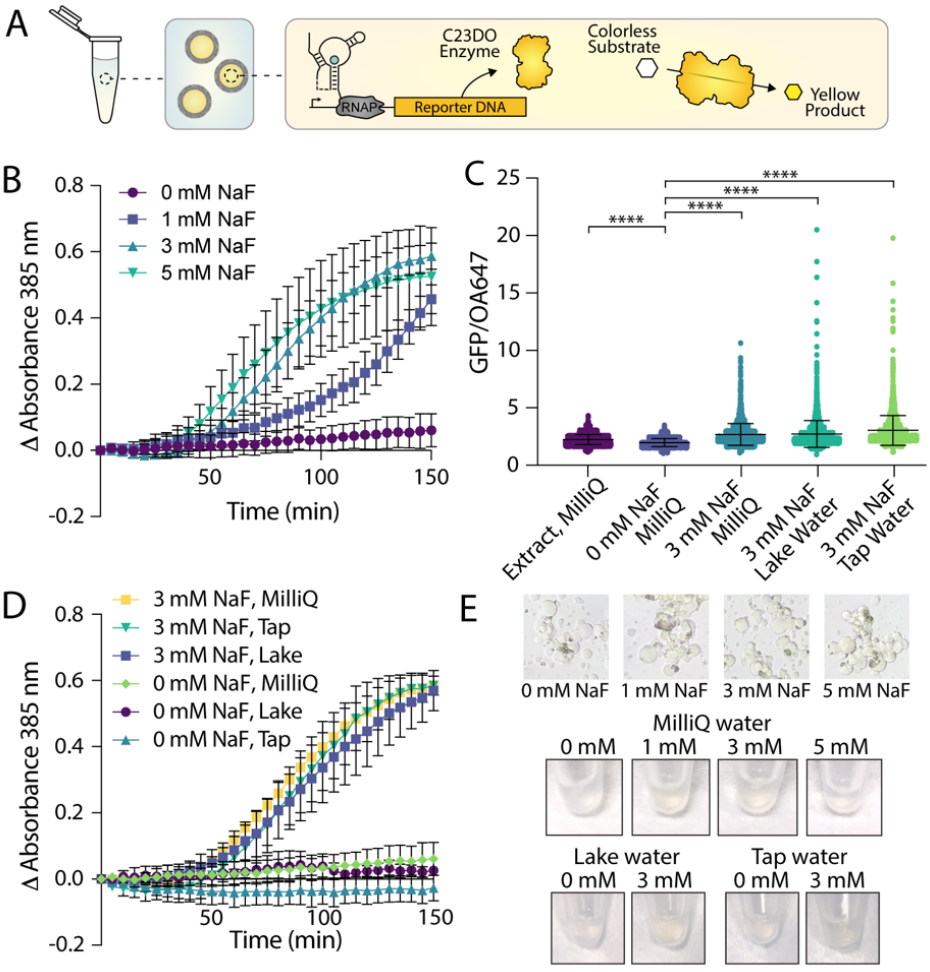

Figure 7.9 Enzymatic readout and detection of fluoride in real-world samples. A. Schematic of encapsulated enzymatic readout. Riboswitch activation inside vesicles leads to the expression of C23DO, resulting in the production of a yellow product that is localized to the vesicle interior. **B.** Absorbance over time inside of vesicles encapsulating a catecholase-based readout in response to external NaF. Output is reported as a change in absorbance to account for variations in final vesicle concentration between different vesicle preparations. N=3 independent vesicle preparations. **C**. GFP/OA647 fluorescence ratios observed in vesicles containing a GFP-based

readout after incubation in outer solutions from laboratory grade water (MilliQ), tap water, and lake water supplemented with NaF. **D.** Absorbance over time inside of vesicles incubated in samples derived from MilliQ water, tap water and lake water supplemented with either 0 mM NaF or 3 mM NaF. N=2 independent vesicle preparations. **E.** Colorimetric changes in vesicles as viewed through a microscope eyepiece and by eye in Eppendorf tubes. **** $p \leq 0.0001$, nonsignificant (ns) $p > 0.1234$; p-values generated using a One-Way ANOVA and Tukey's Multiple Comparisons Test.

To investigate whether this enzymatic reporter could function within our sensor vesicles, we encapsulated cell-free reactions with DNA coding for the riboswitch-C23DO construct and supplemented them with 1 mM catechol (**Figure 7.9 A**). We then titrated NaF into the outer solution and monitored color changes in each population of vesicles via changes in absorbance at 385 nm. In contrast to our GFP-based readout, signal amplification from the enzyme-regulated construct allowed us to assess absorbance changes in an entire population of vesicles rather than on a vesicle-by-vesicle basis. To control for variations in vesicle concentration across multiple vesicle preparations, output is reported as a change in absorbance over time. RNAse A was also added to the outer vesicle solution to control for any unencapsulated reactions caused by vesicle lysis. The response was significantly lower than that observed in bulk (**Figure 7.10 A**), but increases in absorption in response to increasing NaF concentrations were observed across multiple sample preparations (**Figure 7.9 B**). Readout time plays a key role in sensor response,[150] particularly for the 1 mM NaF condition, where amplified responses followed by signal decay make quantification difficult (**Figure 7.9 B, Figure 7.10 A**). Little expression was observed in 0 mM NaF samples in this time frame, however, which indicates potential for these sensors to serve as binary classifiers even in the presence of low fluoride concentrations.

Importantly, responses to fluoride could be detected within 2 hours of incubation compared to 6 hours for the GFP-based readout.

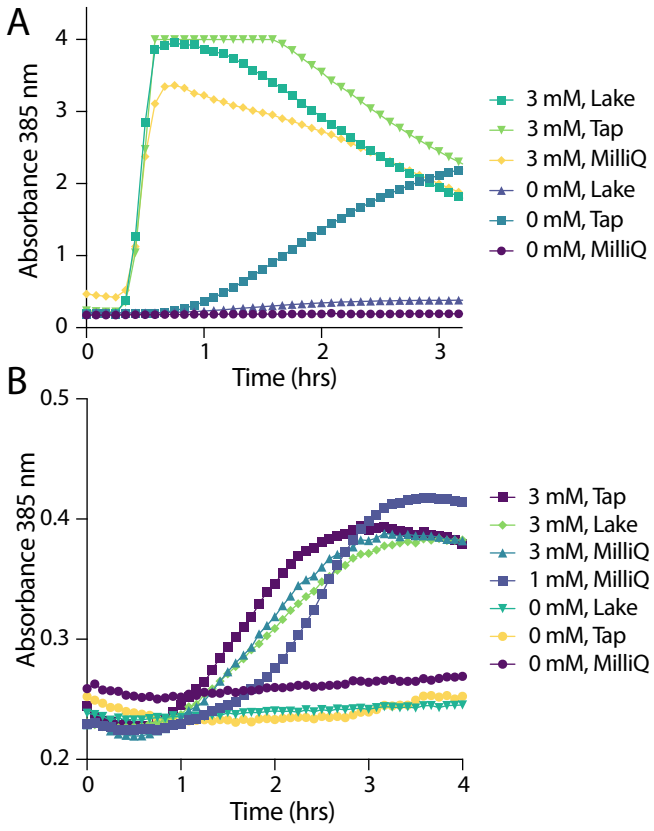

Figure 7.10 Raw absorbance values showing catecholase conversion in response to fluoride in bulk and inside of vesicles. A. Bulk reactions show slightly higher responses to 3 mM NaF supplemented in water samples taken from Lake and Tap water compared to laboratory-grade MilliQ water. Absorbance was also observed to increase in unsupplemented tap water, likely due to low levels of fluoride added to public drinking supply. **B**. In vesicles, absorbance increases specifically in the presence of supplemented NaF. Quantification is difficult, with 1 mM NaF exhibiting a slightly delayed response compared to 3 mM NaF but a similar expression profile and maximum absorbance. Responses are similar between all 3 mM samples regardless of water source, with a slight increase in expression in unsupplemented tap water at later timepoints (consistent with bulk data). (n=1 example vesicle preparation)

Having demonstrated the compatibility of our encapsulated sensors with multiple reporters and their ability to detect extravesicular fluoride, we finally set out to test whether these sensors could be used to monitor fluoride concentrations in real-world samples. We collected water samples from Lake Michigan and the Evanston municipal tap water supply and used each sample to prepare the vesicle outer solution. We supplemented these outer solutions with either 0 mM NaF or 3 mM NaF and added vesicles with either the GFP-coupled riboswitch readout or the colorimetric readout. We observed increased GFP expression in all populations of vesicles incubated with 3 mM NaF outside compared to no-fluoride controls, with a slightly higher level of GFP expression in both lake and tap water samples compared to those incubated with laboratory-grade Milli Q water (**Figure 7.9 C**). Similarly, vesicles encapsulating the enzymatic readout showed increasing absorption over time in the presence of 3 mM NaF, while all no-fluoride controls exhibited no significant changes in absorption (**Figure 7.9 D, Figure 7.10 B**). Slight color changes were visible by eye in tubes containing vesicles, and changes in color inside of vesicles could be observed on the microscope as imaged through the eyepiece (**Figure 7.9 E**). These results were consistent with raw absorbance values observed in bulk assays, which showed a slightly higher response to both tap and lake water and a significant difference between all 0 mM and 3 mM conditions (**Figure 7.10 A & B**). The results observed here highlight the feasibility of these vesicle-based sensors to detect environmentally relevant small molecules in real-world samples, a step toward encapsulation to generate deployable cell-free sensors.

7.5 Conclusions

To our knowledge, this work represents the first demonstrated function of a transcriptionally regulated riboswitch encapsulated in bilayer vesicles. We have demonstrated that this encapsulated riboswitch can detect exogenous fluoride through permeability-based sensing, generating both fluorescent and colorimetric outputs. Additionally, we have shown that responses to fluoride can be modulated by changing membrane composition, which provides a useful handle to control sensor stability and sensitivity. Looking ahead toward sensor deployment, this work establishes that encapsulation can protect cell-free sensors from degradative sample components while allowing analyte detection in real-world samples. While cell-free sensors have been previously used for the detection of environmental molecules of interest,[149-153,157,256-258] encapsulation of these systems may ultimately diversify the contexts within which cell-free sensors can operate.

Although encapsulation can provide powerful advantages to cell-free sensing, it also brings some limitations. The concentrations of fluoride assessed here are high compared to the Maximum Contaminant Limits set by the Environmental Protection Agency (0.5 mM vs 0.22 mM[282]), which were chosen based on the spread of responses observed in liposomes. The variability observed in the responses of individual liposomes within a vesicle population would likely serve as a hurdle for technological use of these sensors in future applications, which may necessitate alternative vesicle assembly techniques, such as microfluidics,[276] and a better understanding of the underlying biophysics of cell-free reactions inside membranes. While we explored protein-based outputs here, riboswitch expression could also be coupled to transcription-based reporting, such as aptamer-dye outputs,[150] to build a transcription-only sensor that would require encapsulation of fewer components and potentially operate on quicker

timescales. Finally, the reintroduction of a barrier between sample and sensor also requires strategies to transport specific analytes into the vesicle. Membrane compositional changes can enable permeability-based import for certain small analytes, with many natural and synthetic amphiphiles to choose from. Moving forward, we can gain even finer control of membrane permeability by incorporating transmembrane proteins to enhance sensing capabilities and introduce more advanced sensing or responsive functions. These strategies could ultimately allow new functions for these types of sensors, including conjugation-based capture methods, deployment and transport of cell-free reactions, controlled sensor degradation, or enhanced sensor biocompatibility.[12]

The diversity of existing cell-free sensors could ultimately lead to a new generation of encapsulated biosensors for a wide array of analytes. With the modularity of components in these systems, vesicle-based sensors could be engineered which use various membrane components, genetic circuits, and triggered responses to detect small molecules of interest.[36,84,283] As focus shifts toward sensor application, these platforms could offer additional handles with which to tune sensor characteristics to advance the types of contexts in which cell-free sensing can operate, allowing for detection in environments like soil, ground water, or biological samples. The incorporation of additional transcription-based cell-free systems, particularly those using riboswitch-based sensing, may ultimately allow the development of a family of encapsulated sensors that are fast, specific, and deployable.

Chapter 8: Conclusions and Future Directions

The work presented in this thesis demonstrates how model membranes can be harnessed to create sensors for nanoscale forces and small molecule signals. By engineering vesicle-based platforms with membrane-associated probes, membrane transporters and encapsulated sensor systems, we show the development of self-contained nano- and microscale sensors that use biological and bio-inspired molecules in new contexts. Here, we leverage the ability of membranes to incorporate both membrane-localized sensors as well as those encapsulated within the aqueous interior of vesicles and explore the ways in which membranes can serve as tunable, semipermeable barriers to convey molecular and physical information. This work demonstrates how membrane composition and the incorporation of amphiphilic biomolecules into the bilayer can impart new functionality onto these sensors, allowing bilayer membranes to not only serve as a container and spatial organizer of sensor components but to directly modulate sensing behaviors.

8.1 Membrane composition and biophysical properties

To better understand the features of model membrane systems, we began by considering the ways in which the membrane itself forms, the types of molecules that can be incorporated into membranes, and the resulting impact on physical properties of the membrane. For the development of membrane-based sensors, which must balance characteristics like stability, permeability, and cargo retention, it is key to first understand the basic principles of membrane biophysics which regulate these properties. Towards this goal, **Chapter 2** discusses the

thermodynamics of membrane formation and the ways in which membrane composition in particular can be harnessed to modulate membrane properties. With regard to sensor development, we expected that membrane robustness would be an important property for sensors which would be deployed into real-world samples and therefore encounter changing external conditions. A characteristic of particular interest in this circumstance is membrane elasticity, which plays a role in the ability of vesicle membranes to accommodate stretch-inducing forces caused by external solute imbalances. Expanding upon the work described in the literature, we used micropipette aspiration techniques to assess the area expansion moduli of specific membrane compositions of interest. Our results indicated that various types of membrane amphiphiles, including cholesterol and synthetic polymers, can be incorporated into the bilayer to change its force-responsive behaviors. In addition, we showed that membrane area expansion moduli are relatively robust to variations in vesicle formation methods and the presence of cell-free protein expression systems, even when membrane proteins are expressed into vesicle bilayers. The work described in this chapter ultimately served as a foundation upon which we sought to engineer specific membrane properties for sensor development in later studies.

8.2 Monitoring physical force using membrane-localized probes

We began our exploration of membranes for sensor development by focusing our attention on processes occurring within the bilayer membrane itself. In **Chapter 3**, we developed an optical method to monitor physical changes within the membrane in order to monitor force applied to the bilayer in the form of osmotic pressure. As assemblies of many amphiphilic monomers that associate together but remain dynamic, membranes can serve as a platform which

respond globally to applied forces through structural changes that occur locally. In particular, membranes exhibit responses to applied stretching forces through both increased inter-lipid distances as well as increased hydration within the membrane core. By incorporating specific optical probes which exist within localized regions of the bilayer, we demonstrated that lipid stretch and membrane hydration could be monitored in concert to report osmotically-induced membrane tension due to changing solute conditions. The combinatorial use of lipid headgroup-conjugated FRET probes and a hydration-sensitive Laurdan probe in the hydrophobic core allowed us to assess changes in area per lipid as well as subsequent permeation of water into the bilayer. We were then able to use this system to visualize membrane growth through lipid uptake through the external addition of fatty acid micelles. We found that not only do lipids take up micelles from the external environment, but this process also occurs faster and in overall greater amounts in membranes under tension. Together, the system of optical probes described in this chapter provided a method to optically monitor forces acting globally upon a population of membranes, serving as a nanoscale sensor of physical forces occurring on a molecular scale.

8.2.1 Future directions of membrane force sensors

Model membranes serve as a useful system with which to better characterize behaviors which membranes themselves exhibit, however physical force is a major stimulus in live cells that has wide-ranging implications in cellular behavior.[7] As a result, it would be of great interest to incorporate force-responsive probes into cellular systems to better establish global as well as local changes in membranes under force in live systems. Similar single-molecule probes have been explored specifically for this purpose, providing insights into the dynamics of cellular membranes.[284] The probes described in **Chapter 3** could similarly be incorporated into cellular

systems, and as a combination of spatially localized dyes may provide additional insights into a variety of changes occurring within the bilayer by teasing out contributions of lipid composition and polarity from tension-induced stretch and uptake.

8.3 Vesicle-based sensors for small molecules

Moving beyond forces within the membrane itself, we next set out to explore the incorporation of sensors into the vesicle interior with strategies to modulate cross-membrane transport. Bilayer vesicles can encapsulate a wide range of biological and synthetic molecules, ranging from ions and small molecule reactants to large proteins such as ribosomes. Importantly, these cargo molecules can exhibit dedicated sensing behaviors, which can be retained upon encapsulation within membranes. While encapsulation is feasible in these contexts, the effect of the membrane on molecular sensing must be considered as it introduces a semipermeable barrier through which target analytes must now pass. In addition, membrane permeability is bidirectional in that the transport of small molecules into the vesicle interior often also results in the leakage of other molecules out. For the development of sensors which exist in dynamic environments and those which interface with other cells, either live or artificial, the incorporation of strategies to control membrane features in order to balance analyte entry, reactant retention and sensor stability are imperative. **Chapter 4** discusses how these considerations have led to existing strategies to develop vesicle-based biosensors, with a specific focus on sensors which incorporate genetically encoded sensing mechanisms. These principles informed our later approaches to develop three types of encapsulated sensors for small molecule analytes.

Building upon our previous exploration of membrane-based sensors, we next sought to explore the ways in which the membrane can be engineered to modulate sensing by encapsulated aqueous systems. We assessed this idea through the development of three different types of vesicle-based sensors with increasing levels of complexity, ranging from a simple fluorescent indicator to a protein-expression-based cell-free sensor. Our results highlight the various ways in which membranes can be harnessed to not only contain aqueous sensors but protect them, improve their specificity, and modulate sensitivity to target analytes. Importantly, these studies also highlight tradeoffs that arise between compartmentalization, specificity of membrane transport, and sensor kinetics.

8.3.1 Improving specificity of indicators with membrane ionophores

As a first step toward the development of vesicle-based sensors with encapsulated cargo, **Chapter 5** describes the development of a nanosensor with an encapsulated fluorescent indicator for potassium combined with a membrane-based ionophore - a highly specific type of membrane transporter. In solution, the fluorescent indicator, PBFI, exhibits poor selectivity for potassium over the similarly monovalent cation sodium; we found that PBFI also responds nonspecifically to calcium, a biologically important divalent cation. To improve specificity by introducing an additional gating step, thereby controlling molecular access to the dye, we encapsulated PBFI in lipid vesicles and incorporated the potassium ionophore Valinomycin into the membrane. We observed that encapsulation and membrane gating significantly improved specificity of the indicator to potassium, even in the presence of other cations – a response which was reversible to a degree upon removal of potassium from the surrounding buffer. The observed improvement in sensor specificity did come at cost of reduced detection speed, consistent with the introduction of

a physical barrier which molecules must traverse before interacting with the compartmentalized indicator.

Although the time to detection was increased, the incorporation of such a highly specific transporter allowed analyte entry with relatively little cargo loss, a feature which diversifies the contexts within which such a sensor can operate. To demonstrate the utility of this approach, we deployed these sensors within cultures of live bacteria and monitored ion uptake in populations of *E. coli*. Here, encapsulation localized the small molecule dye to molecular "beacons," which could be detected via microscopy and which prevented the dye from interacting directly with bacterial cells. The improved specificity to potassium was retained, even in the complex environment surrounding living cells. We expect that this relatively simple platform consisting of a chemical indicator paired with a specific membrane transporter could ultimately be expanded to incorporate a number of existing dye-transporter pairs, which could monitor the presence of other ions and small molecules within self-contained, nanoscale sensors.

8.3.2 Membrane pores allow initiation of fluorescent aptamer transcription

Chemical indicators offer a relatively simple platform for encapsulated sensor development, however we next wanted to explore sensing strategies that would allow greater tunability. **Chapter 6** details our work to encapsulate a simple transcription system that produces a fluorescent, RNA-aptamer-based output upon the entry of an ionic target into the vesicle interior. By incorporating a nonspecific membrane pore, alpha-hemolysin, into lipid/cholesterol vesicles, we demonstrated spatial and temporal control over transcription reactions through the addition of magnesium, a cofactor for T7 polymerase. We assessed various types of transcriptionally regulated reporters, including strand displacement and aptamer-dye outputs, and

established variable levels of compatibility with bilayer membrane platforms. Finally, we observed that both pore concentration and the addition of magnesium regulated the magnitude of fluorescent output achieved, indicating that both the presence of the analyte as well as the degree of induced membrane permeability have a significant impact on overall sensor output. These results demonstrate that transcription can ultimately serve as a useful platform which harnesses simple genetically encoded sensing mechanisms within lipid vesicles to detect externally added molecules.

8.3.3 Membranes modulate sensing by an encapsulated cell-free riboswitch

Offering the most modularity but also the highest level of complexity, **Chapter 7** presents the development of an encapsulated, cell-free protein expression-based sensor for fluoride, an ion of significant technological and biological importance. Here, our focus was on the application of vesicle-based sensors for monitoring water quality, particularly in resource-limited settings. Encapsulated cell-free sensors may be especially well-suited for these types of applications, as a broad set of cell-free sensors exist and could be incorporated into the vesicle interior while the presence of the membrane serves to gate molecular transport from the environment and compartmentalize necessary reactants to protect them from sample components. We focused on a cell-free riboswitch for fluoride, which undergoes a conformational change in the presence of fluoride that allows transcription to occur. Importantly, this work is, to our knowledge, the first demonstration of a transcriptionally regulated riboswitch encapsulated in lipid vesicles. We first demonstrated that the riboswitch could function when encapsulated in vesicles and showed that fluoride can be added to the vesicle exterior to initiate the cell-free expression of a GFP reporter in the vesicle interior. We then explored the ways in

which membrane composition could modulate the sensitivity of the encapsulated sensor to fluoride and found that the composition of the membrane has a significant impact on the resulting sensing behaviors.

To highlight the feasibility of using these sensors in real-world applications, we showed how the presence of membranes prevents the degradation of cell-free sensors by nucleases present in the external sample while still allowing the sensor to receive permeable small molecules from the environment. Fluoride is relatively membrane permeable, so our strategy did not require the addition of membrane transporters. We then incorporated a colorimetric output into the vesicle sensors and showed that a color change was visible inside vesicles in the presence of fluoride. While fluorescence is a commonly used sensor output in lab-based assays, this shift to colorimetric output is critical for the translation of these sensors to resource-poor settings where their use would be most critical. Finally, we deployed sensors with both fluorescent and colorimetric outputs into real-world water samples and demonstrated that the sensors remain capable of detecting fluoride in these conditions.

8.4 Future directions of vesicle-based sensing

The studies discussed in this dissertation highlight strategies to incorporate bilayer membranes into nano- and microscale sensors in order to introduce new functionality and to diversify the contexts within which existing small molecule sensors can be used. We have demonstrated the detection of three different ions through three separate combinations of sensors and membrane transport strategies. This emphasizes a major benefit of membrane-based sensing:

the ability to incorporate a broader set of gating and sensing strategies within a single structure to alter the ways in which multiple types of sensors can function.

The combination of membrane engineering and aqueous sensors can provide specific benefits to sensing, as discussed above, however significant work remains to be done to improve these sensors to a point where they may become widely deployable. The tradeoffs of encapsulation must be considered, particularly the difficulty in encapsulating a large number of reactants and the effect of an additional physical barrier on reaction kinetics and maximum signal. Regarding encapsulation, microfluidics could be a useful strategy to reduce the impacts of low encapsulation efficiency and reduce variability between individual vesicles. Towards the limitations of the membrane barrier, the incorporation of membrane transporters and, most likely, functional membrane proteins could be a strategy to mitigate some of these drawbacks; cell-free systems have been demonstrated to directly express proteins into model membranes, but further work remains to be done in making this technique broadly applicable.[36,285] Alternatively, transporters like ionophores could be inserted into membranes through detergent-mediated methods, but a small subset of ionophores exist which can be selected from. Moving forward, further engineering of membrane gating strategies that allow analyte entry while retaining reactants will likely be a key focus to develop a more diverse set of encapsulated sensors.

In addition to membrane engineering strategies, future studies could include the encapsulation of different types of sensors. Cell-free sensors in particular offer a wealth of options for potential encapsulation, and a variety of cell-free sensors have been developed and characterized in recent years, as discussed in **Chapter 4**. Beyond analyte selection, cell-free

sensors can encode a variety of products that range from fluorescent or colorimetric readouts to pores and lytic enzymes that can initiate triggered responses from the sensor. These types of membrane-based platforms may ultimately serve as a scaffold for complex signal-and-response sensors which could enable complex behaviors like smart drug delivery or the direction of cell activity and proliferation. The incorporation of cell-free, transcription-only sensors may similarly offer an advantage for these encapsulated platforms due to their inherent improvements toward loading and reaction time, and further work could be done to implement transcription-based sensing with alternative analytes and readouts. We have demonstrated the detection of magnesium, however the diversification of this type of platform to detect more technologically relevant ions or other small molecules would be of significant interest.

Aside from genetically encoded sensors, there are a large set of chemical indicators that may also benefit from encapsulation in certain applications. A diverse range of chemical fluorescent indicators are commercially available, and encapsulation may serve to improve specificity, allow localization and capture, or reduce toxicity to cells depending on the sensing environment. These indicator-based sensors may be widely engineerable with a variety of membrane compositions and properties due to the relative ease of encapsulating small molecule dyes and the increased number of compatible vesicle formation methods to do so. Perhaps most importantly, these types of sensors do not require the capabilities of cell-free expression, which can be expensive and which is a fairly specialized technique, and may therefore be more accessible to a wider scientific audience.

While significant work remains to be done to improve the limitations described above, a growing number of advances in synthetic biology and membrane biophysics may offer further engineering strategies and additional handles by which the development of these sensors can be tuned. We expect that the applications of these sensors could be diverse due to the bioinspired and biocompatible nature of the membrane; these focuses might range from water quality monitoring to bloodstream-based detection of pathogens. It is similarly important to note that these sensors represent a step in increasing complexity toward the development of artificial cells, which may ultimately harness minimal genetic instructions and a bioinspired chassis to sense and respond to their environment in complex ways. Following our observations in the studies described in this dissertation, we expect that a wide array of aqueous sensors could ultimately be encapsulated in bilayer vesicles to generate vesicle-based nano- and microsensors.

REFERENCES

1 Anishkin, A., Loukin, S. H., Teng, J. & Kung, C. Feeling the hidden mechanical forces in lipid bilayer is an original sense. *Proc Natl Acad Sci U S A* **111**, 7898-7905, doi:10.1073/pnas.1313364111 (2014).

2 Harayama, T. & Riezman, H. Understanding the diversity of membrane lipid composition. *Nat Rev Mol Cell Biol* **19**, 281-296, doi:10.1038/nrm.2017.138 (2018).

3 Janmey, P. A. & Kinnunen, P. K. Biophysical properties of lipids and dynamic membranes. *Trends Cell Biol* **16**, 538-546, doi:10.1016/j.tcb.2006.08.009 (2006).

4 Singer, S. J. & Nicolson, G. L. The fluid mosaic model of the structure of cell membranes. *Science* **175**, 720-731, doi:10.1126/science.175.4023.720 (1972).

5 Lieber, A. D., Yehudai-Resheff, S., Barnhart, E. L., Theriot, J. A. & Keren, K. Membrane tension in rapidly moving cells is determined by cytoskeletal forces. *Curr Biol* **23**, 1409-1417, doi:10.1016/j.cub.2013.05.063 (2013).

6 Staykova, M., Holmes, D. P., Read, C. & Stone, H. A. Mechanics of surface area regulation in cells examined with confined lipid membranes. *Proc Natl Acad Sci U S A* **108**, 9084-9088, doi:10.1073/pnas.1102358108 (2011).

7 Keren, K. Membrane tension leads the way. *Proc Natl Acad Sci U S A* **108**, 14379-14380, doi:10.1073/pnas.1111671108 (2011).

8 Hamill, O. P. & Martinac, B. Molecular basis of mechanotransduction in living cells. *Physiol Rev* **81**, 685-740, doi:10.1152/physrev.2001.81.2.685 (2001).

9 Morris, C. E. & Homann, U. Cell surface area regulation and membrane tension. *J Membr Biol* **179**, 79-102, doi:10.1007/s002320010040 (2001).

10 Houk, A. R. *et al.* Membrane tension maintains cell polarity by confining signals to the leading edge during neutrophil migration. *Cell* **148**, 175-188, doi:10.1016/j.cell.2011.10.050 (2012).

11 Diz-Munoz, A., Fletcher, D. A. & Weiner, O. D. Use the force: membrane tension as an organizer of cell shape and motility. *Trends Cell Biol* **23**, 47-53, doi:10.1016/j.tcb.2012.09.006 (2013).

12 Boyd, M. A. & Kamat, N. P. Designing Artificial Cells towards a New Generation of Biosensors. *Trends Biotechnol* **39**, 927-939, doi:10.1016/j.tibtech.2020.12.002 (2021).

13 Sezgin, E., Levental, I., Mayor, S. & Eggeling, C. The mystery of membrane organization: composition, regulation and roles of lipid rafts. *Nat Rev Mol Cell Biol* **18**, 361-374, doi:10.1038/nrm.2017.16 (2017).

14 Casares, D., Escriba, P. V. & Rossello, C. A. Membrane Lipid Composition: Effect on Membrane and Organelle Structure, Function and Compartmentalization and Therapeutic Avenues. *Int J Mol Sci* **20**, doi:10.3390/ijms20092167 (2019).

15 van Meer, G., Voelker, D. R. & Feigenson, G. W. Membrane lipids: where they are and how they behave. *Nat Rev Mol Cell Biol* **9**, 112-124, doi:10.1038/nrm2330 (2008).

16 Gould, S. B. Membranes and evolution. *Curr Biol* **28**, R381-R385, doi:10.1016/j.cub.2018.01.086 (2018).

17 Chan, Y. H. & Boxer, S. G. Model membrane systems and their applications. *Curr Opin Chem Biol* **11**, 581-587, doi:10.1016/j.cbpa.2007.09.020 (2007).

18 Israelachvili, J. N., Mitchell, D. J. & Ninham, B. W. Theory of self-assembly of lipid bilayers and vesicles. *Biochim Biophys Acta* **470**, 185-201, doi:10.1016/0005-2736(77)90099-2 (1977).

19 Rideau, E., Dimova, R., Schwille, P., Wurm, F. R. & Landfester, K. Liposomes and polymersomes: a comparative review towards cell mimicking. *Chem Soc Rev* **47**, 8572-8610, doi:10.1039/c8cs00162f (2018).

20 Sackmann, E. Supported membranes: scientific and practical applications. *Science* **271**, 43-48, doi:10.1126/science.271.5245.43 (1996).

21 Winterhalter, M. Black lipid membranes. *Curr Opin Colloid In* **5**, 250-255, doi:Doi 10.1016/S1359-0294(00)00063-7 (2000).

22 Jacobs, M. L., Boyd, M. A. & Kamat, N. P. Diblock copolymers enhance folding of a mechanosensitive membrane protein during cell-free expression. *Proc Natl Acad Sci U S A* **116**, 4031-4036, doi:10.1073/pnas.1814775116 (2019).

23 Le Meins, J. F., Schatz, C., Lecommandoux, S. & Sandre, O. Hybrid polymer/lipid vesicles: state of the art and future perspectives. *Materials Today* **16**, 397-402, doi:10.1016/J.MATTOD.2013.09.002 (2013).

24 Meyer, C. E., Abram, S. L., Craciun, I. & Palivan, C. G. Biomolecule-polymer hybrid compartments: combining the best of both worlds. *Phys Chem Chem Phys* **22**, 11197-11218, doi:10.1039/d0cp00693a (2020).

25 Discher, B. M. *et al.* Polymersomes: tough vesicles made from diblock copolymers. *Science* **284**, 1143-1146, doi:10.1126/science.284.5417.1143 (1999).

26 Mahendra, A., James, H. P. & Jadhav, S. PEG-grafted phospholipids in vesicles: Effect of PEG chain length and concentration on mechanical properties. *Chem Phys Lipids* **218**, 47-56, doi:10.1016/j.chemphyslip.2018.12.001 (2019).

27 Choucair, A., Lavigueur, C. & Eisenberg, A. Polystyrene-b-poly(acrylic acid) vesicle size control using solution properties and hydrophilic block length. *Langmuir* **20**, 3894-3900, doi:10.1021/la035924p (2004).

28 Lim Soo, P. & Eisenberg, A. Preparation of block copolymer vesicles in solution. *Journal of Polymer Science Part B: Polymer Physics* **42**, 923-938, doi:10.1002/polb.10739 (2004).

29 Pattni, B. S., Chupin, V. V. & Torchilin, V. P. New Developments in Liposomal Drug Delivery. *Chem Rev* **115**, 10938-10966, doi:10.1021/acs.chemrev.5b00046 (2015).

30 Allen, T. M. & Cullis, P. R. Liposomal drug delivery systems: from concept to clinical applications. *Adv Drug Deliv Rev* **65**, 36-48, doi:10.1016/j.addr.2012.09.037 (2013).

31 Barenholz, Y. Doxil(R)--the first FDA-approved nano-drug: lessons learned. *J Control Release* **160**, 117-134, doi:10.1016/j.jconrel.2012.03.020 (2012).

32 Hou, X., Zaks, T., Langer, R. & Dong, Y. Lipid nanoparticles for mRNA delivery. *Nat Rev Mater* **6**, 1078-1094, doi:10.1038/s41578-021-00358-0 (2021).

33 Wang, H. & Huan, Y. Combination therapy based on nano codelivery for overcoming cancer drug resistance. *Medicine in Drug Discovery* **6**, 100024 (2020).

34 Silverman, A. D., Karim, A. S. & Jewett, M. C. Cell-free gene expression: an expanded repertoire of applications. *Nat Rev Genet* **21**, 151-170, doi:10.1038/s41576-019-0186-3 (2020).

35 Tinafar, A., Jaenes, K. & Pardee, K. Synthetic Biology Goes Cell-Free. *BMC Biol* **17**, 64, doi:10.1186/s12915-019-0685-x (2019).

36 Kruyer, N. S. *et al.* Membrane Augmented Cell-Free Systems: A New Frontier in Biotechnology. *ACS Synth Biol* **10**, 670-681, doi:10.1021/acssynbio.0c00625 (2021).

37 Elani, Y., Law, R. V. & Ces, O. Vesicle-based artificial cells as chemical microreactors with spatially segregated reaction pathways. *Nature Communications* **5**, 5305-5305, doi:10.1038/ncomms6305 (2014).

38 Adamala, K. P., Martin-Alarcon, D. A., Guthrie-Honea, K. R. & Boyden, E. S. Engineering genetic circuit interactions within and between synthetic minimal cells. *Nat Chem* **9**, 431-439, doi:10.1038/nchem.2644 (2017).

39 Hindley, J. W., Law, R. V. & Ces, O. Membrane functionalization in artificial cell engineering. *SN Applied Sciences* **2**, 1-10, doi:10.1007/s42452-020-2357-4 (2020).

40 Niwa, T. *et al.* Comprehensive study of liposome-assisted synthesis of membrane proteins using a reconstituted cell-free translation system. *Sci Rep* **5**, 18025, doi:10.1038/srep18025 (2015).

41 Mizutani, T. & Bergström, L. M. *Application of Thermodynamics to Biological and Materials Science*. 289-314 (IntechOpen, 2011).

42 Marsh, D. Thermodynamics of phospholipid self-assembly. *Biophys J* **102**, 1079-1087, doi:10.1016/j.bpj.2012.01.049 (2012).

43 Nagarajan, R. Molecular Packing Parameter and Surfactant Self-assembly: the Neglected Role of the Surfactant Tail. *Langmuir* **18**, 31-38 (2001).

44 Zhang, L. & Eisenberg, A. Thermodynamic vs Kinetic Aspects in the Formation and Morphological Transitions of Crew-Cut Aggregates Produced by Self-Assembly of Polystyrene-b-poly(acrylic acid) Block Copolymers in Dilute Solution. *Macromolecules* **32**, 2239-2249, doi:10.1021/ma981039f (1999).

45 Zhang, L. & Eisenberg, A. Multiple Morphologies and Characteristics of "Crew-Cut" Micelle-like Aggregates of Polystyrene-b-poly(acrylic acid) Diblock Copolymers in Aqueous Solutions. *Journal of the American Chemical Society* **118**, 3168-3181, doi:10.1021/ja953709s (1996).

46 Yu, Y. & Eisenberg, A. Control of Morphology through Polymer−Solvent Interactions in Crew-Cut Aggregates of Amphiphilic Block Copolymers. *Journal of the American Chemical Society* **119**, 8383-8384, doi:10.1021/ja9709740 (1997).

47 Yu, K. & Eisenberg, A. Multiple Morphologies in Aqueous Solutions of Aggregates of Polystyrene-block-poly(ethylene oxide) Diblock Copolymers. *Macromolecules* **29**, 6359-6361, doi:10.1021/ma960381u (1996).

48 Terreau, O., Bartels, C. & Eisenberg, A. Effect of poly(acrylic acid) block length distribution on polystyrene-b-poly(acrylic acid) block copolymer aggregates in solution. 2. A partial phase diagram. *Langmuir* **20**, 637-645, doi:10.1021/la035557h (2004).

49 Shen, H. & Eisenberg, A. Morphological Phase Diagram for a Ternary System of Block Copolymer PS310-b-PAA52/Dioxane/H2O. *The Journal of Physical Chemistry B* **103**, 9473-9487, doi:10.1021/jp991365c (1999).

50 Mai, Y. & Eisenberg, A. Self-assembly of block copolymers. *Chem Soc Rev* **41**, 5969-5985, doi:10.1039/c2cs35115c (2012).

51 Luo, L. & Eisenberg, A. Thermodynamic size control of block copolymer vesicles in solution. *Langmuir* **17**, 6804-6811, doi:10.1021/la0104370 (2001).

52 Chen, L., Shen, H. & Eisenberg, A. Kinetics and Mechanism of the Rod-to-Vesicle Transition of Block Copolymer Aggregates in Dilute Solution. *Journal of Physical Chemistry B* **103**, 9488-9497, doi:10.1021/jp9913665 (1999).

53 Israelachvili, J. N. Self-assembly in Two Dimensions: Surface Micelles and Domain Formation in Monolayers. *Langmuir* **10**, 3774-3781 (1994).

54 Discher, D. E. & Eisenberg, A. Polymer vesicles. *Science* **297**, 967-973, doi:10.1126/science.1074972 (2002).

55 Godbey, W. T. *Biotechnology and its applications : using cells to change the world*. 2. edn, (Elsevier, Inc, 2020).

56 Escriba, P. V. Membrane-lipid therapy: A historical perspective of membrane-targeted therapies - From lipid bilayer structure to the pathophysiological regulation of cells. *Biochim Biophys Acta Biomembr* **1859**, 1493-1506, doi:10.1016/j.bbamem.2017.05.017 (2017).

57 Holthuis, J. C. & Menon, A. K. Lipid landscapes and pipelines in membrane homeostasis. *Nature* **510**, 48-57, doi:10.1038/nature13474 (2014).

58 van der Koog, L., Gandek, T. B. & Nagelkerke, A. Liposomes and Extracellular Vesicles as Drug Delivery Systems: A Comparison of Composition, Pharmacokinetics, and

Functionalization. *Adv Healthc Mater* **11**, e2100639, doi:10.1002/adhm.202100639 (2022).

59 Simons, K. & Ikonen, E. Functional rafts in cell membranes. *Nature* **387**, 569-572, doi:10.1038/42408 (1997).

60 Lingwood, D. & Simons, K. Lipid rafts as a membrane-organizing principle. *Science* **327**, 46-50, doi:10.1126/science.1174621 (2010).

61 Helms, J. B. & Zurzolo, C. Lipids as targeting signals: lipid rafts and intracellular trafficking. *Traffic* **5**, 247-254, doi:10.1111/j.1600-0854.2004.0181.x (2004).

62 Ohvo-Rekila, H., Ramstedt, B., Leppimaki, P. & Slotte, J. P. Cholesterol interactions with phospholipids in membranes. *Prog Lipid Res* **41**, 66-97, doi:10.1016/s0163-7827(01)00020-0 (2002).

63 Deamer, D. W. & Bramhall, J. Permeability of lipid bilayers to water and ionic solutes. *Chem Phys Lipids* **40**, 167-188, doi:10.1016/0009-3084(86)90069-1 (1986).

64 Lopez, M. *et al.* Effects of Acyl Chain Unsaturation on Activation Energy of Water Permeability across Droplet Bilayers of Homologous Monoglycerides: Role of Cholesterol. *Langmuir* **34**, 2147-2157, doi:10.1021/acs.langmuir.7b03590 (2018).

65 Arouri, A., Lauritsen, K. E., Nielsen, H. L. & Mouritsen, O. G. Effect of fatty acids on the permeability barrier of model and biological membranes. *Chem Phys Lipids* **200**, 139-146, doi:10.1016/j.chemphyslip.2016.10.001 (2016).

66 Jespersen, H., Andersen, J. H., Ditzel, H. J. & Mouritsen, O. G. Lipids, curvature stress, and the action of lipid prodrugs: free fatty acids and lysolipid enhancement of drug transport across liposomal membranes. *Biochimie* **94**, 2-10, doi:10.1016/j.biochi.2011.07.029 (2012).

67 Mckersie, B. D., Crowe, J. H. & Crowe, L. M. Free fatty acid effects on leakage, phase properties and fusion of fully hydrated model membranes. *Biochimica et Biophysica Acta (BBA) - Biomembranes* **982**, 156-160 (1989).

68 Zhang, X., Barraza, K. M. & Beauchamp, J. L. Cholesterol provides nonsacrificial protection of membrane lipids from chemical damage at air-water interface. *Proc Natl Acad Sci U S A* **115**, 3255-3260, doi:10.1073/pnas.1722323115 (2018).

69 Shinoda, W. Permeability across lipid membranes. *Biochim Biophys Acta* **1858**, 2254-2265, doi:10.1016/j.bbamem.2016.03.032 (2016).

70 Apodaca, G. Modulation of membrane traffic by mechanical stimuli. *Am J Physiol Renal Physiol* **282**, F179-190, doi:10.1152/ajprenal.2002.282.2.F179 (2002).

71 Evans, E. & Needham, D. Physical Properties of Surfactant Bilayer Membranes: Thermal Transitions, Elasticity, Rigidity, Cohesion, and Colloidal Interactions. *J Phys Chem-Us* **91**, 4219-4228 (1987).

72 Evans, E. & Rawicz, W. Entropy-driven tension and bending elasticity in condensed-fluid membranes. *Phys Rev Lett* **64**, 2094-2097, doi:10.1103/PhysRevLett.64.2094 (1990).

73 Rawicz, W., Olbrich, K. C., McIntosh, T., Needham, D. & Evans, E. Effect of chain length and unsaturation on elasticity of lipid bilayers. *Biophys J* **79**, 328-339, doi:10.1016/S0006-3495(00)76295-3 (2000).

74 Evans, E., Ritchie, K. & Merkel, R. Sensitive force technique to probe molecular adhesion and structural linkages at biological interfaces. *Biophysical Journal* **68**, 2580-2587, doi:10.1016/s0006-3495(95)80441-8 (1995).

75 Evans, E. A., Waugh, R. & Melnik, L. Elastic area compressibility modulus of red cell membrane. *Biophys J* **16**, 585-595, doi:10.1016/S0006-3495(76)85713-X (1976).

76 Schindelin, J. *et al.* Fiji: an open-source platform for biological-image analysis. *Nat Methods* **9**, 676-682, doi:10.1038/nmeth.2019 (2012).

77 Bermudez, H., Brannan, A. K., Hammer, D. A., Bates, F. S. & Discher, D. E. Molecular weight dependence of polymersome membrane structure, elasticity, and stability. *Macromolecules* **35**, 8203-8208, doi:10.1021/ma020669l (2002).

78 Pautot, S., Frisken, B. J. & Weitz, D. A. Production of Unilamellar Vesicles Using an Inverted Emulsion. *Langmuir* **19**, 2870-2879, doi:10.1021/la026100v (2003).

79 Deshpande, S., Caspi, Y., Meijering, A. E. & Dekker, C. Octanol-assisted liposome assembly on chip. *Nat Commun* **7**, 10447, doi:10.1038/ncomms10447 (2016).

80 Kamat, N. P., Lee, M. H., Lee, D. & Hammer, D. A. Micropipette aspiration of double emulsion-templated polymersomes. *Soft Matter* **7**, 9863-9866, doi:10.1039/c1sm06282d (2011).

81 Stockbridge, R. B., Robertson, J. L., Kolmakova-Partensky, L. & Miller, C. A family of fluoride-specific ion channels with dual-topology architecture. *Elife* **2**, e01084, doi:10.7554/eLife.01084 (2013).

82 Lentini, R. *et al.* Integrating artificial with natural cells to translate chemical messages that direct E. coli behaviour. *Nat Commun* **5**, 4012, doi:10.1038/ncomms5012 (2014).

83 Martini, L. & Mansy, S. S. Cell-like systems with riboswitch controlled gene expression. *Chemical Communications* **47**, 10734-10736, doi:10.1039/c1cc13930d (2011).

84 Dwidar, M. *et al.* Programmable Artificial Cells Using Histamine-Responsive Synthetic Riboswitch. *J Am Chem Soc* **141**, 11103-11114, doi:10.1021/jacs.9b03300 (2019).

85 Nishimura, K. *et al.* Cell-Free Protein Synthesis inside Giant Unilamellar Vesicles Analyzed by Flow Cytometry. *Langmuir* **28**, 8426-8432, doi:10.1021/la3001703 (2012).

86 Martinac, B., Buechner, M., Delcour, A. H., Adler, J. & Kung, C. Pressure-sensitive ion channel in Escherichia coli. *Proc Natl Acad Sci U S A* **84**, 2297-2301, doi:10.1073/pnas.84.8.2297 (1987).

87 Ranade, S. S., Syeda, R. & Patapoutian, A. Mechanically Activated Ion Channels. *Neuron* **87**, 1162-1179, doi:10.1016/j.neuron.2015.08.032 (2015).

88 Chen, D. & Santore, M. M. Large effect of membrane tension on the fluid-solid phase transitions of two-component phosphatidylcholine vesicles. *Proc Natl Acad Sci U S A* **111**, 179-184, doi:10.1073/pnas.1314993111 (2014).

89 Oglecka, K., Rangamani, P., Liedberg, B., Kraut, R. S. & Parikh, A. N. Oscillatory phase separation in giant lipid vesicles induced by transmembrane osmotic differentials. *Elife* **3**, e03695, doi:10.7554/eLife.03695 (2014).

90 Portet, T., Gordon, S. E. & Keller, S. L. Increasing membrane tension decreases miscibility temperatures; an experimental demonstration via micropipette aspiration. *Biophys J* **103**, L35-37, doi:10.1016/j.bpj.2012.08.061 (2012).

91 Uline, M. J., Schick, M. & Szleifer, I. Phase behavior of lipid bilayers under tension. *Biophys J* **102**, 517-522, doi:10.1016/j.bpj.2011.12.050 (2012).

92 Veatch, S. L. & Keller, S. L. Organization in lipid membranes containing cholesterol. *Phys Rev Lett* **89**, 268101, doi:10.1103/PhysRevLett.89.268101 (2002).

93 Boulant, S., Kural, C., Zeeh, J. C., Ubelmann, F. & Kirchhausen, T. Actin dynamics counteract membrane tension during clathrin-mediated endocytosis. *Nat Cell Biol* **13**, 1124-1131, doi:10.1038/ncb2307 (2011).

94 Gauthier, N. C., Fardin, M. A., Roca-Cusachs, P. & Sheetz, M. P. Temporary increase in plasma membrane tension coordinates the activation of exocytosis and contraction during cell spreading. *Proceedings of the National Academy of Sciences* **108**, 14467-14472, doi:10.1073/pnas.1105845108 (2011).

95 Raucher, D. & Sheetz, M. P. Cell spreading and lamellipodial extension rate is regulated by membrane tension. *J Cell Biol* **148**, 127-136, doi:10.1083/jcb.148.1.127 (2000).

96 Weber, G. F., Bjerke, M. A. & DeSimone, D. W. A mechanoresponsive cadherin-keratin complex directs polarized protrusive behavior and collective cell migration. *Dev Cell* **22**, 104-115, doi:10.1016/j.devcel.2011.10.013 (2012).

97 Gauthier, N. C., Masters, T. A. & Sheetz, M. P. Mechanical feedback between membrane tension and dynamics. *Trends Cell Biol* **22**, 527-535, doi:10.1016/j.tcb.2012.07.005 (2012).

98 Vlahakis, N. E. & Hubmayr, R. D. Invited review: plasma membrane stress failure in alveolar epithelial cells. *J Appl Physiol (1985)* **89**, 2490-2496;discussion 2497, doi:10.1152/jappl.2000.89.6.2490 (2000).

99 Kliesch, T. T. *et al.* Membrane tension increases fusion efficiency of model membranes in the presence of SNAREs. *Sci Rep* **7**, 12070, doi:10.1038/s41598-017-12348-w (2017).

100 Wen, P. J. *et al.* Actin dynamics provides membrane tension to merge fusing vesicles into the plasma membrane. *Nat Commun* **7**, 12604, doi:10.1038/ncomms12604 (2016).

101 Dai, J. & Sheetz, M. P. Mechanical properties of neuronal growth cone membranes studied by tether formation with laser optical tweezers. *Biophys J* **68**, 988-996, doi:10.1016/S0006-3495(95)80274-2 (1995).

102 Hochmuth, R. M. Micropipette aspiration of living cells. *J Biomech* **33**, 15-22, doi:10.1016/s0021-9290(99)00175-x (2000).

103 Shao, J. Y. & Hochmuth, R. M. Micropipette suction for measuring piconewton forces of adhesion and tether formation from neutrophil membranes. *Biophys J* **71**, 2892-2901, doi:10.1016/S0006-3495(96)79486-9 (1996).

104 Solon, J. *et al.* Negative tension induced by lipid uptake. *Phys Rev Lett* **97**, 098103, doi:10.1103/PhysRevLett.97.098103 (2006).

105 Zhang, H. & Liu, K. K. Optical tweezers for single cells. *J R Soc Interface* **5**, 671-690, doi:10.1098/rsif.2008.0052 (2008).

106 Lay, A. *et al.* Upconverting Nanoparticles as Optical Sensors of Nano- to Micro-Newton Forces. *Nano Lett* **17**, 4172-4177, doi:10.1021/acs.nanolett.7b00963 (2017).

107 Sezgin, E. & Schwille, P. Fluorescence techniques to study lipid dynamics. *Cold Spring Harb Perspect Biol* **3**, a009803, doi:10.1101/cshperspect.a009803 (2011).

108 Choi, C. L., Koski, K. J., Olson, A. C. & Alivisatos, A. P. Luminescent nanocrystal stress gauge. *Proc Natl Acad Sci U S A* **107**, 21306-21310, doi:10.1073/pnas.1016022107 (2010).

109 Hickenboth, C. R. *et al.* Biasing reaction pathways with mechanical force. *Nature* **446**, 423-427, doi:10.1038/nature05681 (2007).

110 Kamat, N. P. *et al.* Sensing membrane stress with near IR-emissive porphyrins. *Proc Natl Acad Sci U S A* **108**, 13984-13989, doi:10.1073/pnas.1102125108 (2011).

111 Parasassi, T., De Stasio, G., Ravagnan, G., Rusch, R. M. & Gratton, E. Quantitation of lipid phases in phospholipid vesicles by the generalized polarization of Laurdan fluorescence. *Biophys J* **60**, 179-189, doi:10.1016/S0006-3495(91)82041-0 (1991).

112 Lee, J. C. M., Law, R. J. & Discher, D. E. Bending Contributions to Hydration of Phospholipid and Block Copolymer Membranes: Unifying Correlations between Probe Fluorescence and Vesicle Thermoelasticity. *Langmuir* **17**, 3592-3597, doi:10.1021/la001678v (2001).

113 Zhang, Y. L., Frangos, J. A. & Chachisvilis, M. Laurdan fluorescence senses mechanical strain in the lipid bilayer membrane. *Biochem Biophys Res Commun* **347**, 838-841, doi:10.1016/j.bbrc.2006.06.152 (2006).

114 Owen, D. M., Rentero, C., Magenau, A., Abu-Siniyeh, A. & Gaus, K. Quantitative imaging of membrane lipid order in cells and organisms. *Nat Protoc* **7**, 24-35, doi:10.1038/nprot.2011.419 (2011).

115 Mayer, L. D., Hope, M. J. & Cullis, P. R. Vesicles of variable sizes produced by a rapid extrusion procedure. *Biochim Biophys Acta* **858**, 161-168, doi:10.1016/0005-2736(86)90302-0 (1986).

116 Hof, M., Hutterer, R., Perez, N., Ruf, H. & Schneider, F. W. Influence of vesicle curvature on fluorescence relaxation kinetics of fluorophores. *Biophys Chem* **52**, 165-172, doi:10.1016/0301-4622(94)00093-x (1994).

117 Olbrich, K., Rawicz, W., Needham, D. & Evans, E. Water permeability and mechanical strength of polyunsaturated lipid bilayers. *Biophys J* **79**, 321-327, doi:10.1016/S0006-3495(00)76294-1 (2000).

118 Chabanon, M., Ho, J. C. S., Liedberg, B., Parikh, A. N. & Rangamani, P. Pulsatile Lipid Vesicles under Osmotic Stress. *Biophys J* **112**, 1682-1691, doi:10.1016/j.bpj.2017.03.018 (2017).

119 Mui, B. L., Cullis, P. R., Evans, E. A. & Madden, T. D. Osmotic properties of large unilamellar vesicles prepared by extrusion. *Biophysical Journal* **64**, 443-453, doi:10.1016/S0006-3495(93)81385-7 (1993).

120 Su, W. C., Gettel, D. L., Chabanon, M., Rangamani, P. & Parikh, A. N. Pulsatile Gating of Giant Vesicles Containing Macromolecular Crowding Agents Induced by Colligative Nonideality. *J Am Chem Soc* **140**, 691-699, doi:10.1021/jacs.7b10192 (2018).

121 Förster, T. Zwischenmolekulare Energiewanderung und Fluoreszenz. *Annalen der Physik* **437**, 55-75, doi:10.1002/andp.19484370105 (2006).

122 Jares-Erijman, E. A. & Jovin, T. M. FRET imaging. *Nat Biotechnol* **21**, 1387-1395, doi:10.1038/nbt896 (2003).

123 Chirio-Lebrun, M.-C. & Prats, M. Fluorescence resonance energy transfer (FRET): theory and experiments. *Biochemical Education* **26**, 320-323, doi:10.1016/s0307-4412(98)80010-1 (1998).

124 Fa, N. *et al.* Decrease of elastic moduli of DOPC bilayers induced by a macrolide antibiotic, azithromycin. *Biochim Biophys Acta* **1768**, 1830-1838, doi:10.1016/j.bbamem.2007.04.013 (2007).

125 Rutkowski, C. A., Williams, L. M., Haines, T. H. & Cummins, H. Z. The elasticity of synthetic phospholipid vesicles obtained by photon correlation spectroscopy. *Biochemistry* **30**, 5688-5696, doi:10.1021/bi00237a008 (1991).

126 Kamp, F., Zakim, D., Zhang, F., Noy, N. & Hamilton, J. A. Fatty acid flip-flop in phospholipid bilayers is extremely fast. *Biochemistry* **34**, 11928-11937, doi:10.1021/bi00037a034 (1995).

127 Chen, I. A., Roberts, R. W. & Szostak, J. W. The emergence of competition between model protocells. *Science* **305**, 1474-1476, doi:10.1126/science.1100757 (2004).

128 Kemp-O'Brien, K. & Parsons, M. Using FRET to analyse signals controlling cell adhesion and migration. *J Microsc* **251**, 270-278, doi:10.1111/j.1365-2818.2012.03686.x (2013).

129 Nordenfelt, P., Elliott, H. L. & Springer, T. A. Coordinated integrin activation by actin-dependent force during T-cell migration. *Nat Commun* **7**, 13119, doi:10.1038/ncomms13119 (2016).

130 Rothenberg, K. E., Scott, D. W., Christoforou, N. & Hoffman, B. D. Vinculin Force-Sensitive Dynamics at Focal Adhesions Enable Effective Directed Cell Migration. *Biophys J* **114**, 1680-1694, doi:10.1016/j.bpj.2018.02.019 (2018).

131 Shaner, N. C., Patterson, G. H. & Davidson, M. W. Advances in fluorescent protein technology. *J Cell Sci* **120**, 4247-4260, doi:10.1242/jcs.005801 (2007).

132 Shi, S., Ang, E. L. & Zhao, H. In vivo biosensors: mechanisms, development, and applications. *J Ind Microbiol Biotechnol* **45**, 491-516, doi:10.1007/s10295-018-2004-x (2018).

133 Morales-Narvaez, E. & Dincer, C. The impact of biosensing in a pandemic outbreak: COVID-19. *Biosens Bioelectron* **163**, 112274, doi:10.1016/j.bios.2020.112274 (2020).

134 Mollarasouli, F., Kurbanoglu, S. & Ozkan, S. A. The role of electrochemical immunosensors in clinical analysis. *Biosensors* **9**, doi:10.3390/bios9030086 (2019).

135 Dai, Y. & Liu, C. C. Recent Advances on Electrochemical Biosensing Strategies toward Universal Point-of-Care Systems. *Angew Chem Int Ed Engl* **58**, 12355-12368, doi:10.1002/anie.201901879 (2019).

136 Slomovic, S., Pardee, K. & Collins, J. J. Synthetic biology devices for in vitro and in vivo diagnostics. *Proc Natl Acad Sci U S A* **112**, 14429-14435, doi:10.1073/pnas.1508521112 (2015).

137 Pardee, K. *et al.* Paper-based synthetic gene networks. *Cell* **159**, 940-954, doi:10.1016/j.cell.2014.10.004 (2014).

138 Pardee, K. *et al.* Rapid, Low-Cost Detection of Zika Virus Using Programmable Biomolecular Components. *Cell* **165**, 1255-1266, doi:10.1016/j.cell.2016.04.059 (2016).

139 Riangrungroj, P., Bever, C. S., Hammock, B. D. & Polizzi, K. M. A label-free optical whole-cell Escherichia coli biosensor for the detection of pyrethroid insecticide exposure. *Sci Rep* **9**, 12466, doi:10.1038/s41598-019-48907-6 (2019).

140 Miller, R. A. *et al.* Development of a paper-immobilized yeast biosensor for the detection of physiological concentrations of doxycycline in technology-limited settings. *Analytical Methods* **12**, 2123-2132, doi:10.1039/d0ay00001a (2020).

141 Jia, X., Bu, R., Zhao, T. & Wu, K. Sensitive and Specific Whole-Cell Biosensor for Arsenic Detection. *Appl Environ Microbiol* **85**, AEM.00694-00619, doi:10.1128/AEM.00694-19 (2019).

142 Lin, C., Zhang, Q.-X. & Yeh, Y.-C. Development of a whole-cell biosensor for the determination of tyrosine in urine for point-of-care diagnostics. *Analytical Methods* **11**, 1400-1404, doi:10.1039/c9ay00070d (2019).

143 Mimee, M. *et al.* An ingestible bacterial-electronic system to monitor gastrointestinal health. *Science* **360**, 915-918, doi:10.1126/science.aas9315 (2018).

144 Jia, X., Zhao, T., Liu, Y., Bu, R. & Wu, K. Gene circuit engineering to improve the performance of a whole-cell lead biosensor. *FEMS Microbiol Lett* **365**, doi:10.1093/femsle/fny157 (2018).

145 Watstein, D. M. & Styczynski, M. P. Development of a Pigment-Based Whole-Cell Zinc Biosensor for Human Serum. *ACS Synth Biol* **7**, 267-275, doi:10.1021/acssynbio.7b00292 (2018).

146 Mao, N., Cubillos-Ruiz, A., Cameron, D. E. & Collins, J. J. Probiotic strains detect and suppress cholera in mice. *Sci Transl Med* **10**, eaao2586-eaao2586, doi:10.1126/scitranslmed.aao2586 (2018).

147 Ma, D., Shen, L., Wu, K., Diehnelt, C. W. & Green, A. A. Low-cost detection of norovirus using paper-based cell-free systems and synbody-based viral enrichment. *Synth Biol (Oxf)* **3**, ysy018, doi:10.1093/synbio/ysy018 (2018).

148 Verosloff, M., Chappell, J., Perry, K. L., Thompson, J. R. & Lucks, J. B. PLANT-Dx: A Molecular Diagnostic for Point-of-Use Detection of Plant Pathogens. *ACS Synth Biol* **8**, 902-905, doi:10.1021/acssynbio.8b00526 (2019).

149 Gräwe, A. *et al.* A paper-based, cell-free biosensor system for the detection of heavy metals and date rape drugs. *PLOS ONE* **14**, e0210940-e0210940, doi:10.1371/journal.pone.0210940 (2019).

150 Thavarajah, W. *et al.* Point-of-Use Detection of Environmental Fluoride via a Cell-Free Riboswitch-Based Biosensor. *ACS Synth Biol* **9**, 10-18, doi:10.1021/acssynbio.9b00347 (2020).

151 Zhang, P. *et al.* Detection of inorganic ions and organic molecules with cell-free biosensing systems. *J Biotechnol* **300**, 78-86, doi:10.1016/j.jbiotec.2019.05.011 (2019).

152 Liu, X. *et al.* Design of a Transcriptional Biosensor for the Portable, On-Demand Detection of Cyanuric Acid. *ACS Synth Biol* **9**, 84-94, doi:10.1021/acssynbio.9b00348 (2020).

153 Silverman, A. D., Akova, U., Alam, K. K., Jewett, M. C. & Lucks, J. B. Design and Optimization of a Cell-Free Atrazine Biosensor. *ACS Synth Biol* **9**, 671-677, doi:10.1021/acssynbio.9b00388 (2020).

154 Wen, K. Y. *et al.* A Cell-Free Biosensor for Detecting Quorum Sensing Molecules in P. aeruginosa-Infected Respiratory Samples. *ACS Synth Biol* **6**, 2293-2301, doi:10.1021/acssynbio.7b00219 (2017).

155 Takahashi, M. K. *et al.* A low-cost paper-based synthetic biology platform for analyzing gut microbiota and host biomarkers. *Nat Commun* **9**, 3347, doi:10.1038/s41467-018-05864-4 (2018).

156 McNerney, M. P. *et al.* Point-of-care biomarker quantification enabled by sample-specific calibration. *Sci Adv* **5**, eaax4473, doi:10.1126/sciadv.aax4473 (2019).

157 Voyvodic, P. L. *et al.* Plug-and-play metabolic transducers expand the chemical detection space of cell-free biosensors. *Nat Commun* **10**, 1697, doi:10.1038/s41467-019-09722-9 (2019).

158 Hindley, J. W. *et al.* Light-triggered enzymatic reactions in nested vesicle reactors. *Nat Commun* **9**, 1093, doi:10.1038/s41467-018-03491-7 (2018).

159 Joesaar, A. *et al.* DNA-based communication in populations of synthetic protocells. *Nat Nanotechnol* **14**, 369-378, doi:10.1038/s41565-019-0399-9 (2019).

160 Peng, R. *et al.* DNA-based artificial molecular signaling system that mimics basic elements of reception and response. *Nat Commun* **11**, 978, doi:10.1038/s41467-020-14739-6 (2020).

161 Tian, L., Li, M., Patil, A. J., Drinkwater, B. W. & Mann, S. Artificial morphogen-mediated differentiation in synthetic protocells. *Nat Commun* **10**, 3321, doi:10.1038/s41467-019-11316-4 (2019).

162 Lai, S. N. *et al.* Artificial Cells Capable of Long-Lived Protein Synthesis by Using Aptamer Grafted Polymer Hydrogel. *ACS Synth Biol* **9**, 76-83, doi:10.1021/acssynbio.9b00338 (2020).

163 Niederholtmeyer, H., Chaggan, C. & Devaraj, N. K. Communication and quorum sensing in non-living mimics of eukaryotic cells. *Nat Commun* **9**, 5027, doi:10.1038/s41467-018-07473-7 (2018).

164 Tang, T. D. *et al.* Gene-Mediated Chemical Communication in Synthetic Protocell Communities. *ACS Synth Biol* **7**, 339-346, doi:10.1021/acssynbio.7b00306 (2018).

165 Stano, P. Gene Expression Inside Liposomes: From Early Studies to Current Protocols. *Chemistry* **25**, 7798-7814, doi:10.1002/chem.201806445 (2019).

166 Spencer, A. C., Torre, P. & Mansy, S. S. The encapsulation of cell-free transcription and translation machinery in vesicles for the construction of cellular mimics. *J Vis Exp*, e51304, doi:10.3791/51304 (2013).

167 Nele, V. *et al.* Effect of Formulation Method, Lipid Composition, and PEGylation on Vesicle Lamellarity: A Small-Angle Neutron Scattering Study. *Langmuir* **35**, 6064-6074, doi:10.1021/acs.langmuir.8b04256 (2019).

168 Sakamoto, R., Noireaux, V. & Maeda, Y. T. Anomalous Scaling of Gene Expression in Confined Cell-Free Reactions. *Sci Rep* **8**, 7364, doi:10.1038/s41598-018-25532-3 (2018).

169 Garenne, D. & Noireaux, V. Membrane functions genetically programmed in synthetic cells: A barrier to conquer. *Current Opinion in Systems Biology* **24**, 9-17, doi:10.1016/j.coisb.2020.09.006 (2020).

170 Monnard, P. A. & Deamer, D. W. Membrane self-assembly processes: steps toward the first cellular life. *Anat Rec* **268**, 196-207, doi:10.1002/ar.10154 (2002).

171 Dupin, A. & Simmel, F. C. Signalling and differentiation in emulsion-based multi-compartmentalized in vitro gene circuits. *Nat Chem* **11**, 32-39, doi:10.1038/s41557-018-0174-9 (2019).

172 Monnard, P. A., Luptak, A. & Deamer, D. W. Models of primitive cellular life: polymerases and templates in liposomes. *Philos Trans R Soc Lond B Biol Sci* **362**, 1741-1750, doi:10.1098/rstb.2007.2066 (2007).

173 Mansy, S. S. *et al.* Template-directed synthesis of a genetic polymer in a model protocell. *Nature* **454**, 122-125, doi:10.1038/nature07018 (2008).

174 Zocher, F., van der Spoel, D., Pohl, P. & Hub, J. S. Local partition coefficients govern solute permeability of cholesterol-containing membranes. *Biophys J* **105**, 2760-2770, doi:10.1016/j.bpj.2013.11.003 (2013).

175 Kowal, J., Wu, D., Mikhalevich, V., Palivan, C. G. & Meier, W. Hybrid polymer-lipid films as platforms for directed membrane protein insertion. *Langmuir* **31**, 4868-4877, doi:10.1021/acs.langmuir.5b00388 (2015).

176 Petit, J. *et al.* A modular approach for multifunctional polymersomes with controlled adhesive properties. *Soft Matter* **14**, 894-900, doi:10.1039/c7sm01885a (2018).

177 Garenne, D. & Noireaux, V. Analysis of Cytoplasmic and Membrane Molecular Crowding in Genetically Programmed Synthetic Cells. *Biomacromolecules* **21**, 2808-2817, doi:10.1021/acs.biomac.0c00513 (2020).

178 Garenne, D., Libchaber, A. & Noireaux, V. Membrane molecular crowding enhances MreB polymerization to shape synthetic cells from spheres to rods. *Proc Natl Acad Sci U S A* **117**, 1902-1909, doi:10.1073/pnas.1914656117 (2020).

179 Noireaux, V. & Libchaber, A. A vesicle bioreactor as a step toward an artificial cell assembly. *PNAS* **101**, 17669 –17674-17669 –17674 (2004).

180 Hilburger, C. E., Jacobs, M. L., Lewis, K. R., Peruzzi, J. A. & Kamat, N. P. Controlling Secretion in Artificial Cells with a Membrane AND Gate. *ACS Synth Biol* **8**, 1224-1230, doi:10.1021/acssynbio.8b00435 (2019).

181 Henrich, E., Hein, C., Dotsch, V. & Bernhard, F. Membrane protein production in Escherichia coli cell-free lysates. *FEBS Lett* **589**, 1713-1722, doi:10.1016/j.febslet.2015.04.045 (2015).

182 Hovijitra, N. T., Wuu, J. J., Peaker, B. & Swartz, J. R. Cell-free synthesis of functional aquaporin Z in synthetic liposomes. *Biotechnol Bioeng* **104**, 40-49, doi:10.1002/bit.22385 (2009).

183 Uyeda, A., Nakayama, S., Kato, Y., Watanabe, H. & Matsuura, T. Construction of an in Vitro Gene Screening System of the E. coli EmrE Transporter Using Liposome Display. *Anal Chem* **88**, 12028-12035, doi:10.1021/acs.analchem.6b02308 (2016).

184 Matthies, D. *et al.* Cell-free expression and assembly of ATP synthase. *J Mol Biol* **413**, 593-603, doi:10.1016/j.jmb.2011.08.055 (2011).

185 Fenz, S. F., Sachse, R., Schmidt, T. & Kubick, S. Cell-free synthesis of membrane proteins: tailored cell models out of microsomes. *Biochim Biophys Acta* **1838**, 1382-1388, doi:10.1016/j.bbamem.2013.12.009 (2014).

186 Hamada, S. *et al.* Giant vesicles functionally expressing membrane receptors for an insect pheromone. *Chem Commun (Camb)* **50**, 2958-2961, doi:10.1039/c3cc48216b (2014).

187 Sonnabend, A. *et al.* Production of G protein-coupled receptors in an insect-based cell-free system. *Biotechnol Bioeng* **114**, 2328-2338, doi:10.1002/bit.26346 (2017).

188 Hindley, J. W. *et al.* Building a synthetic mechanosensitive signaling pathway in compartmentalized artificial cells. *Proc Natl Acad Sci U S A* **116**, 16711-16716, doi:10.1073/pnas.1903500116 (2019).

189 Peruzzi, J. A., Jacobs, M. L., Vu, T. Q., Wang, K. S. & Kamat, N. P. Barcoding Biological Reactions with DNA-Functionalized Vesicles. *Angew Chem Int Ed Engl* **58**, 18683-18690, doi:10.1002/anie.201911544 (2019).

190 Majumder, S. *et al.* Cell-sized mechanosensitive and biosensing compartment programmed with DNA. *Chem Commun (Camb)* **53**, 7349-7352, doi:10.1039/c7cc03455e (2017).

191 Garamella, J., Majumder, S., Liu, A. P. & Noireaux, V. An Adaptive Synthetic Cell Based on Mechanosensing, Biosensing, and Inducible Gene Circuits. *ACS Synthetic Biology* **8**, 1913-1920, doi:10.1021/acssynbio.9b00204 (2019).

192 Schroeder, A. *et al.* Remotely activated protein-producing nanoparticles. *Nano Lett* **12**, 2685-2689, doi:10.1021/nl2036047 (2012).

193 Berhanu, S., Ueda, T. & Kuruma, Y. Artificial photosynthetic cell producing energy for protein synthesis. *Nat Commun* **10**, 1325, doi:10.1038/s41467-019-09147-4 (2019).

194 Schwarz-Schilling, M., Aufinger, L., Muckl, A. & Simmel, F. C. Chemical communication between bacteria and cell-free gene expression systems within linear chains of emulsion droplets. *Integr Biol (Camb)* **8**, 564-570, doi:10.1039/c5ib00301f (2016).

195 Lentini, R. *et al.* Two-Way Chemical Communication between Artificial and Natural Cells. *ACS Cent Sci* **3**, 117-123, doi:10.1021/acscentsci.6b00330 (2017).

196 Ding, Y., Contreras-Llano, L. E., Morris, E., Mao, M. & Tan, C. Minimizing Context Dependency of Gene Networks Using Artificial Cells. *ACS Applied Materials and Interfaces* **10**, 30137-30146, doi:10.1021/acsami.8b10029 (2018).

197 Toparlak, O. D. *et al.* Artificial cells drive neural differentiation. *Sci Adv* **6**, eabb4920-eabb4920, doi:10.1126/sciadv.abb4920 (2020).

198 Miller, M. B. & Bassler, B. L. Quorum sensing in bacteria. *Annu Rev Microbiol* **55**, 165-199, doi:10.1146/annurev.micro.55.1.165 (2001).

199 Krinsky, N. *et al.* Synthetic Cells Synthesize Therapeutic Proteins inside Tumors. *Adv Healthc Mater* **7**, e1701163, doi:10.1002/adhm.201701163 (2018).

200 Panganiban, B. *et al.* Random heteropolymers preserve protein function in foreign environments. *Science* **359**, 1239-1243, doi:10.1126/science.aao0335 (2018).

201 Halperin, M. L. & Kamel, K. S. Potassium. *Lancet* **352**, 135-140, doi:10.1016/S0140-6736(98)85044-7 (1998).

202 Palmer, B. F. Regulation of Potassium Homeostasis. *Clin J Am Soc Nephrol* **10**, 1050-1060, doi:10.2215/CJN.08580813 (2015).

203 Prindle, A. *et al.* Ion channels enable electrical communication in bacterial communities. *Nature* **527**, 59-63, doi:10.1038/nature15709 (2015).

204 Yellen, G. The voltage-gated potassium channels and their relatives. *Nature* **419**, 35-42, doi:10.1038/nature00978 (2002).

205 Cheng, C. J., Kuo, E. & Huang, C. L. Extracellular potassium homeostasis: insights from hypokalemic periodic paralysis. *Semin Nephrol* **33**, 237-247, doi:10.1016/j.semnephrol.2013.04.004 (2013).

206 Eil, R. *et al.* Ionic immune suppression within the tumour microenvironment limits T cell effector function. *Nature* **537**, 539-543, doi:10.1038/nature19364 (2016).

207 Filosa, J. A. *et al.* Local potassium signaling couples neuronal activity to vasodilation in the brain. *Nat Neurosci* **9**, 1397-1403, doi:10.1038/nn1779 (2006).

208 Newsom-Davis, J. *et al.* Autoimmune disorders of neuronal potassium channels. *Ann N Y Acad Sci* **998**, 202-210, doi:10.1196/annals.1254.022 (2003).

209 Sica, D. A. *et al.* Importance of potassium in cardiovascular disease. *J Clin Hypertens (Greenwich)* **4**, 198-206, doi:10.1111/j.1524-6175.2002.01728.x (2002).

210 Bazzigaluppi, P., Dufour, S. & Carlen, P. L. Wide field fluorescent imaging of extracellular spatiotemporal potassium dynamics in vivo. *Neuroimage* **104**, 110-116, doi:10.1016/j.neuroimage.2014.10.012 (2015).

211 Bischof, H. *et al.* Novel genetically encoded fluorescent probes enable real-time detection of potassium in vitro and in vivo. *Nat Commun* **8**, 1422, doi:10.1038/s41467-017-01615-z (2017).

212 van de Velde, L., d'Angremont, E. & Olthuis, W. Solid contact potassium selective electrodes for biomedical applications - a review. *Talanta* **160**, 56-65, doi:10.1016/j.talanta.2016.06.050 (2016).

213 He, H., Mortellaro, M. A., Leiner, M. J., Fraatz, R. J. & Tusa, J. K. A fluorescent sensor with high selectivity and sensitivity for potassium in water. *J Am Chem Soc* **125**, 1468-1469, doi:10.1021/ja0284761 (2003).

214 Minta, A. & Tsien, R. Y. Fluorescent indicators for cytosolic sodium. *J Biol Chem* **264**, 19449-19457, doi:10.1016/s0021-9258(19)47321-3 (1989).

215 Padmawar, P., Yao, X., Bloch, O., Manley, G. T. & Verkman, A. S. K+ waves in brain cortex visualized using a long-wavelength K+-sensing fluorescent indicator. *Nat Methods* **2**, 825-827, doi:10.1038/nmeth801 (2005).

216 Rimmele, T. S. & Chatton, J. Y. A novel optical intracellular imaging approach for potassium dynamics in astrocytes. *PLoS One* **9**, e109243, doi:10.1371/journal.pone.0109243 (2014).

217 Zhou, X. *et al.* A new highly selective fluorescent K+ sensor. *J Am Chem Soc* **133**, 18530-18533, doi:10.1021/ja207345s (2011).

218 Meuwis, K., Boens, N., De Schryver, F. C., Gallay, J. & Vincent, M. Photophysics of the fluorescent K+ indicator PBFI. *Biophys J* **68**, 2469-2473, doi:10.1016/S0006-3495(95)80428-5 (1995).

219 Rana, P. S. *et al.* Calibration and characterization of intracellular Asante Potassium Green probes, APG-2 and APG-4. *Anal Biochem* **567**, 8-13, doi:10.1016/j.ab.2018.11.024 (2019).

220 Li, C., Law, G. L. & Wong, W. T. Luminescent Tb3+ complex with pendant crown ether showing dual-component recognition of H+ and K+ at multiple pH windows. *Org Lett* **6**, 4841-4844, doi:10.1021/ol048261r (2004).

221 Liu, J. *et al.* A sensitive and specific nanosensor for monitoring extracellular potassium levels in the brain. *Nat Nanotechnol* **15**, 321-330, doi:10.1038/s41565-020-0634-4 (2020).

222 Dufour, S., Dufour, P., Chever, O., Vallee, R. & Amzica, F. In vivo simultaneous intra- and extracellular potassium recordings using a micro-optrode. *J Neurosci Methods* **194**, 206-217, doi:10.1016/j.jneumeth.2010.10.004 (2011).

223 Kasner, S. E. & Ganz, M. B. Regulation of intracellular potassium in mesangial cells: A fluorescence analysis using the dye, PBFI. *American Journal of Physiology - Renal Fluid and Electrolyte Physiology* **262**, doi:10.1152/ajprenal.1992.262.3.f462 (1992).

224 Kozoriz, M. G., Church, J., Ozog, M. A., Naus, C. C. & Krebs, C. Temporary sequestration of potassium by mitochondria in astrocytes. *J Biol Chem* **285**, 31107-31119, doi:10.1074/jbc.M109.082073 (2010).

225 Liu, J. *et al.* A highly sensitive and selective nanosensor for near-infrared potassium imaging. *Sci Adv* **6**, eaax9757, doi:10.1126/sciadv.aax9757 (2020).

226 Lomora, M., Itel, F., Dinu, I. A. & Palivan, C. G. Selective ion-permeable membranes by insertion of biopores into polymersomes. *Phys Chem Chem Phys* **17**, 15538-15546, doi:10.1039/c4cp05879h (2015).

227 Steller, L., Kreir, M. & Salzer, R. Natural and artificial ion channels for biosensing platforms. *Anal Bioanal Chem* **402**, 209-230, doi:10.1007/s00216-011-5517-y (2012).

228 Mueller, P. & Rudin, D. O. Development of K+-Na+ discrimination in experimental bimolecular lipid membranes by macrocyclic antibiotics. *Biochem Biophys Res Commun* **26**, 398-404, doi:10.1016/0006-291x(67)90559-1 (1967).

229 Su, Z. *et al.* How Valinomycin Ionophores Enter and Transport K(+) across Model Lipid Bilayer Membranes. *Langmuir* **35**, 16935-16943, doi:10.1021/acs.langmuir.9b03064 (2019).

230 Boyd, M. A. & Kamat, N. P. Visualizing Tension and Growth in Model Membranes Using Optical Dyes. *Biophys J* **115**, 1307-1315, doi:10.1016/j.bpj.2018.08.021 (2018).

231 Cayley, S. & Record, M. T., Jr. Roles of cytoplasmic osmolytes, water, and crowding in the response of Escherichia coli to osmotic stress: biophysical basis of osmoprotection by glycine betaine. *Biochemistry* **42**, 12596-12609, doi:10.1021/bi0347297 (2003).

232 Dinnbier, U., Limpinsel, E., Schmid, R. & Bakker, E. P. Transient accumulation of potassium glutamate and its replacement by trehalose during adaptation of growing cells of Escherichia coli K-12 to elevated sodium chloride concentrations. *Arch Microbiol* **150**, 348-357, doi:10.1007/BF00408306 (1988).

233 McLaggan, D., Naprstek, J., Buurman, E. T. & Epstein, W. Interdependence of K+ and glutamate accumulation during osmotic adaptation of Escherichia coli. *J Biol Chem* **269**, 1911-1917 (1994).

234 Meury, J., Robin, A. & Monnier-Champiex, P. Turgor-controlled K+ fluxes and their pathways in Escherichia coli. *Eur. J. Biochem* **151**, 613-619 (1985).

235 Szatmari, D. *et al.* Intracellular ion concentrations and cation-dependent remodelling of bacterial MreB assemblies. *Sci Rep* **10**, 12002, doi:10.1038/s41598-020-68960-w (2020).

236 Kubitschek, H. E., Freedman, M. L. & Silver, S. Potassium uptake in synchronous and synchronized cultures of Escherichia coli. *Biophys J* **11**, 787-797, doi:10.1016/S0006-3495(71)86254-9 (1971).

237 Schaferling, M. The art of fluorescence imaging with chemical sensors. *Angew Chem Int Ed Engl* **51**, 3532-3554, doi:10.1002/anie.201105459 (2012).

238 Sun, Z., Nguyen, T., McAuliffe, K. & You, M. Intracellular Imaging with Genetically Encoded RNA-based Molecular Sensors. *Nanomaterials (Basel)* **9**, doi:10.3390/nano9020233 (2019).

239 Zhang, L., Guo, W. & Lu, Y. Advances in Cell-Free Biosensors: Principle, Mechanism, and Applications. *Biotechnol J* **15**, e2000187, doi:10.1002/biot.202000187 (2020).

240 Palmer, A. E., Qin, Y., Park, J. G. & McCombs, J. E. Design and application of genetically encoded biosensors. *Trends Biotechnol* **29**, 144-152, doi:10.1016/j.tibtech.2010.12.004 (2011).

241 Hancock, J. T. *Cell signalling*. (Oxford University Press, 2021).

242 Buddingh, B. C. & van Hest, J. C. M. Artificial Cells: Synthetic Compartments with Life-like Functionality and Adaptivity. *Acc Chem Res* **50**, 769-777, doi:10.1021/acs.accounts.6b00512 (2017).

243 Yim, G., Wang, H. H. & Davies, J. Antibiotics as signalling molecules. *Philos Trans R Soc Lond B Biol Sci* **362**, 1195-1200, doi:10.1098/rstb.2007.2044 (2007).

244 Bereza-Malcolm, L. T., Mann, G. & Franks, A. E. Environmental sensing of heavy metals through whole cell microbial biosensors: a synthetic biology approach. *ACS Synth Biol* **4**, 535-546, doi:10.1021/sb500286r (2015).

245 Jung, J. K. *et al.* Cell-free biosensors for rapid detection of water contaminants. *Nat Biotechnol* **38**, 1451-1459, doi:10.1038/s41587-020-0571-7 (2020).

246 Cho, E. J., Lee, J. W. & Ellington, A. D. Applications of aptamers as sensors. *Annu Rev Anal Chem (Palo Alto Calif)* **2**, 241-264, doi:10.1146/annurev.anchem.1.031207.112851 (2009).

247 Swetha, P., Fan, Z., Wang, F. & Jiang, J. H. Genetically encoded light-up RNA aptamers and their applications for imaging and biosensing. *J Mater Chem B* **8**, 3382-3392, doi:10.1039/c9tb02668a (2020).

248 Famulok, M. & Mayer, G. Aptamer modules as sensors and detectors. *Acc Chem Res* **44**, 1349-1358, doi:10.1021/ar2000293 (2011).

249 Lucks, J. B., Qi, L., Mutalik, V. K., Wang, D. & Arkin, A. P. Versatile RNA-sensing transcriptional regulators for engineering genetic networks. *Proc Natl Acad Sci U S A* **108**, 8617-8622, doi:10.1073/pnas.1015741108 (2011).

250 Houseley, J. & Tollervey, D. The many pathways of RNA degradation. *Cell* **136**, 763-776, doi:10.1016/j.cell.2009.01.019 (2009).

251 Thomen, P. *et al.* T7 RNA polymerase studied by force measurements varying cofactor concentration. *Biophys J* **95**, 2423-2433, doi:10.1529/biophysj.107.125096 (2008).

252 Jung, J. K., Archuleta, C. M., Alam, K. K. & Lucks, J. B. Programming cell-free biosensors with DNA strand displacement circuits. *Nat Chem Biol* **18**, 385-393, doi:10.1038/s41589-021-00962-9 (2022).

253 Mitra, J. & Ha, T. Nanomechanics and co-transcriptional folding of Spinach and Mango. *Nat Commun* **10**, 4318, doi:10.1038/s41467-019-12299-y (2019).

254 Janas, T., Janas, T. & Yarus, M. Specific RNA binding to ordered phospholipid bilayers. *Nucleic Acids Research* **34**, 2128-2136, doi:10.1093/NAR/GKL220 (2006).

255 Czerniak, T. & Saenz, J. P. Lipid membranes modulate the activity of RNA through sequence-dependent interactions. *Proc Natl Acad Sci U S A* **119**, doi:10.1073/pnas.2119235119 (2022).

256 Duyen, T. T. M. *et al.* Paper-based colorimetric biosensor for antibiotics inhibiting bacterial protein synthesis. *Journal of Bioscience and Bioengineering* **123**, 96-100, doi:10.1016/J.JBIOSC.2016.07.015 (2017).

257 Pellinen, T., Huovinen, T. & Karp, M. A cell-free biosensor for the detection of transcriptional inducers using firefly luciferase as a reporter. *Analytical Biochemistry* **330**, 52-57, doi:10.1016/j.ab.2004.03.064 (2004).

258 Gupta, S., Sarkar, S., Katranidis, A. & Bhattacharya, J. Development of a Cell-Free Optical Biosensor for Detection of a Broad Range of Mercury Contaminants in Water: A

Plasmid DNA-Based Approach. *ACS Omega* **4**, 9480-9487, doi:10.1021/acsomega.9b00205 (2019).

259 Hunt, J. P. *et al.* Rapid sensing of clinically relevant glutamine concentrations in human serum with metabolically engineered E. coli-based cell-free protein synthesis. *Journal of Biotechnology* **325**, 389-394, doi:10.1016/J.JBIOTEC.2020.09.011 (2021).

260 Hunt, J. P. *et al.* Towards detection of SARS-CoV-2 RNA in human saliva: A paper-based cell-free toehold switch biosensor with a visual bioluminescent output. *New Biotechnology* **66**, 53-60, doi:10.1016/J.NBT.2021.09.002 (2022).

261 Salehi, A. S. *et al.* Cell-Free Protein Synthesis Approach to Biosensing hTRbeta-Specific Endocrine Disruptors. *Anal Chem* **89**, 3395-3401, doi:10.1021/acs.analchem.6b04034 (2017).

262 Soltani, M., Hunt, J. P. & Bundy, B. C. Rapid RNase inhibitor production to enable low-cost, on-demand cell-free protein synthesis biosensor use in human body fluids. *Biotechnol Bioeng* **118**, 3973-3983, doi:10.1002/bit.27874 (2021).

263 Tan, C., Saurabh, S., Bruchez, M. P., Schwartz, R. & Leduc, P. Molecular crowding shapes gene expression in synthetic cellular nanosystems. *Nat Nanotechnol* **8**, 602-608, doi:10.1038/nnano.2013.132 (2013).

264 Nourian, Z. & Danelon, C. Linking genotype and phenotype in protein synthesizing liposomes with external supply of resources. *ACS Synthetic Biology* **2**, 186-193, doi:10.1021/sb300125z (2013).

265 de Souza, T. P., Stano, P. & Luisi, P. L. The Minimal Size of Liposome-Based Model Cells Brings about a Remarkably Enhanced Entrapment and Protein Synthesis. *ChemBioChem* **10**, 1056-1063, doi:10.1002/CBIC.200800810 (2009).

266 Strobel, E. J., Cheng, L., Berman, K. E., Carlson, P. D. & Lucks, J. B. A ligand-gated strand displacement mechanism for ZTP riboswitch transcription control. *Nat Chem Biol* **15**, 1067-1076, doi:10.1038/s41589-019-0382-7 (2019).

267 (UNICEF), U. N. C. s. F. & Organization, W. H. Progress on drinking water, sanitation and hygiene 2000–2017. Special focus on inequalities. (New York, 2019).

268 Damania, R., Desbureaux, S. b., Rodella, A.-S., Russ, J. & Zaveri, E. *Quality unknown : the invisible water crisis*. (World Bank Group, 2020).

269 Fuge, R. Fluorine in the environment, a review of its sources and geochemistry. *Applied Geochemistry* **100**, 393-406, doi:10.1016/J.APGEOCHEM.2018.12.016 (2019).

270 McMahon, P. B., Brown, C. J., Johnson, T. D., Belitz, K. & Lindsey, B. D. Fluoride occurrence in United States groundwater. *Science of The Total Environment* **732**, 139217-139217, doi:10.1016/J.SCITOTENV.2020.139217 (2020).

271 Silverman, A. D., Kelley-Loughnane, N., Lucks, J. B. & Jewett, M. C. Deconstructing Cell-Free Extract Preparation for in Vitro Activation of Transcriptional Genetic Circuitry. *ACS Synth Biol* **8**, 403-414, doi:10.1021/acssynbio.8b00430 (2019).

272 NIS-Elements Advanced Research (Nikon Instruments, Inc.).

273 Prism v. 9 (GraphPad).

274 Watters, K. E., Strobel, E. J., Yu, A. M., Lis, J. T. & Lucks, J. B. Cotranscriptional folding of a riboswitch at nucleotide resolution. *Nat Struct Mol Biol* **23**, 1124-1131, doi:10.1038/nsmb.3316 (2016).

275 Barbier, O., Arreola-Mendoza, L. & Del Razo, L. M. Molecular mechanisms of fluoride toxicity. *Chem Biol Interact* **188**, 319-333, doi:10.1016/j.cbi.2010.07.011 (2010).

276 Gonzales, D. T., Yandrapalli, N., Robinson, T., Zechner, C. & Tang, T. D. Cell-Free Gene Expression Dynamics in Synthetic Cell Populations. *ACS Synth Biol* **11**, 205-215, doi:10.1021/acssynbio.1c00376 (2022).

277 Nishimura, K., Tsuru, S., Suzuki, H. & Yomo, T. Stochasticity in Gene Expression in a Cell-Sized Compartment. *ACS Synthetic Biology* **4**, 566-576, doi:10.1021/SB500249G (2014).

278 Nourian, Z., Roelofsen, W. & Danelon, C. Triggered Gene Expression in Fed-Vesicle Microreactors with a Multifunctional Membrane. *Angewandte Chemie International Edition* **51**, 3114-3118, doi:10.1002/anie.201107123 (2012).

279 Saito, H. *et al.* Time-resolved tracking of a minimum gene expression system reconstituted in giant liposomes. *Chembiochem* **10**, 1640-1643, doi:10.1002/cbic.200900205 (2009).

280 Gutknecht, J. & Walter, A. Hydrofluoric and nitric acid transport through lipid bilayer membranes. *Biochim Biophys Acta* **644**, 153-156, doi:10.1016/0005-2736(81)90071-7 (1981).

281 Papahadjopoulos, D., Nir, S. & Oki, S. Permeability properties of phospholipid membranes: effect of cholesterol and temperature. *Biochim Biophys Acta* **266**, 561-583, doi:10.1016/0006-3002(72)90001-7 (1972).

282 EPA. National Primary Drinking Water Regulations. (Environmental Protection Agency, 2009).

283 Lazar, J. T. & Tabor, J. J. Bacterial two-component systems as sensors for synthetic biology applications. *Curr Opin Syst Biol* **28**, doi:10.1016/j.coisb.2021.100398 (2021).

284 Colom, A. *et al.* A fluorescent membrane tension probe. *Nat Chem* **10**, 1118-1125, doi:10.1038/s41557-018-0127-3 (2018).

285 Kuruma, Y. & Ueda, T. The PURE system for the cell-free synthesis of membrane proteins. *Nature Protocols* **10**, 1328-1344, doi:10.1038/nprot.2015.082 (2015).